Implementing point merge system based arrival management at Amsterdam Airport Schiphol

J.M. de Wilde

Technische Universiteit Delft

TU Delft

Implementing point merge system based arrival management at Amsterdam Airport Schiphol

by

J.M. de Wilde

to obtain the degree of Master of Science
at the Delft University of Technology,
to be defended publicly on Monday August 27, 2018 at 12:00 PM.

Student number: 4087372

Thesis committee:	Prof. dr. ir. H. G. Visser,	TU Delft, supervisor
	Ir. P. C. Roling,	TU Delft
	Ir. J. A. Melkert,	TU Delft

This thesis is confidential and cannot be made public until August 27, 2018.

TU Delft

Summary

The continued growth in air transport for the past thirty years, led to the congestion of the currently available airspace. The Terminal Area (TMA) of Amsterdam Airport Schiphol (AAS) is no exception. Aircraft arriving at the TMA need to be directed towards the runway. Currently, radar vectoring is used by the Air Traffic Control (ATC) to direct aircraft towards the runway. Radar vectoring is an open-loop system allowing for flexibility. However, a significant amount of communication is required between the pilot and the controller. During dense traffic periods a loss of situational awareness can arise. By using radar vectoring, unnecessary noise, emission and a non-continuous descent is created.

Since, the introduction of Performance Based Navigation (PBN), alternative ways of sequencing inbound aircraft are investigated. One such alternative is called the Point Merge System (PMS). The PMS arrival routes are designed to absorb delays in the arrival phase on a sequence leg, which is an equidistant arc from the merging point. As the PMS provides better predictability, it can potentially offer significant fuel and environmental benefits as well as a considerable reduction of inbound delays, by permitting Continuous Descent Approaches (CDAs) even under high traffic conditions. Currently, the PMS is successfully implemented at ten airports around the world, but not at AAS. This study focusses on the implementation of point merge arrival management in the TMA of AAS and assess the advantages and drawbacks. Due to the better predictability inside the PMS, the project also includes the design and demonstration of an optimal PMS scheduler based on a Mixed Integer Linear Programming (MILP) approach. The following research objective is identified:

The objective of the research is to explore the potential benefits and drawbacks (environmental impact, capacity, delay, fuel efficiency and safety) of implementing point merge system based arrival management for one single and one dual runway configuration at AAS by the design and evaluation of a point merge air traffic sequencing system at AAS. Including the design and demonstration of an optimal point merge system scheduler using Mixed Integer Linear Programming.

Before the actual research is started, the principles of the PMS are investigated. The PMS is possible due to the improved accuracy of the Area Navigation (RNAV). The PMS concept is based on a merge point and a sequencing legs at iso-distance. The aim of the sequencing leg is to create spacing. The aircraft fly over the sequencing leg until enough spacing is obtained and then turn towards the merge point. The PMS can be adjusted to fit in any TMA. Depending on the number of inbound sectors, the number of sequencing legs increases. Different design parameters are investigated. The size of the sequencing leg can be increased to absorb delays. The height of the sequencing leg can be adjusted to increase the flight performance. The distance to the merge point can be increase to enable a increase CDA segment. Beside these parameters, multiple PMSs can be combined if required. The research performed on the scheduling in the PMS, is found limited. The currently existing MILP formulation use assumptions as constant speed and a limited set of aircraft.

At AAS, a complex runway system of five runways exists. Based on a preference list, traffic loads and wind directions numerous runway combinations can be used. The most used runway combination for landing is 18R during off-peak hours and both 18C and 18R during peak hours. Aircraft enter the TMA at three Initial Approach Fixed (IAFs) which is the entry point of the TMA. The IAFs are the waypoints SUGOL, RIVER and ARTIP. Due to a high population around AAS, noise limits have to be followed.

A model able to schedule and sequence the aircraft using a PMS is required to be developed. In order to develop such a model, multiple methodologies are explained. The first being the design of the route network of the PMS. The PMS arrival routes are designed between the three IAFs and the runway configuration used. It is designed for the most used runway configurations at AAS. One design for inbound flights during off-peak times to single runway 18R. Another design for the inbound flights during peak-hours to the dual runway configuration for runway 18R and 18C. The design of the PMS is made in such a way that switching between peak time and off-peak time is possible. A multi-system is designed consisting of an east and west PMS. The west PMS consists of two sequencing legs, for flights from SUGOL and RIVER. The sequencing legs are at a distance of 17 and 18 NM, respectively of

merge point NIRSI. At an altitude of 10,000 and 9,000 ft. The east PMS consist of a single sequencing leg for flight coming from ARTIP. The sequencing leg is identical to the 10,000 ft sequencing leg of the west system. For a realistic simulation of the aircraft performance, calculations are needed. For both the initial segment and the sequencing segment of the PMS, the velocity of the aircraft can be varied. Therefore, the method for calculating the feasible velocity range is explained. For the fuel-usage, the method for calculating the fuel flow is explained. The final segment of the PMS is an CDA. For each aircraft type, a method of calculating the optimal CDA profile and fuel-used is showed. The output of the scheduling model is used to make a noise contour map. The computations for noise of a single flight and cumulative flights are explained.

The scheduling model, as the PMS scheduler is called, is optimised using MILP approach. The linear programming concept is explained. The mathematical problem of scheduling and sequencing aircraft in the TMA has been transformed to a Mixed Integer Linear Programming form. To decrease the computational time, two exact algorithms are introduced. Constrained Position Shift (CPS) reduces the possible number of position shifts in the sequence. An event-based rolling horizon limits the set of aircraft solved at once. The objective function of the MILP formulation optimised the makespan or minimises the fuel-used. The formulation takes into account the minimum vortex separation standards and the aircraft performance calculations.

The scheduling model is able to schedule flights and sequence inbound aircraft over the designed PMS towards the runway. Optimising for minimum makespan or minimum fuel used. It is programmed using the Python language and optimised using IBM cplex. The scheduling model is applicable for the single runway configuration and the dual runway configuration. Also, the maximum number of position shifts in the sequence can be adjusted in the range from First-Come-First-Served (FCFS) to up to 2 position shifts. The output of the model are the optimised flight schedule and flight trajectories of each optimised aircraft. These trajectories are used to model the noise produced by the aircraft in the schedule. To visualize the noise a noise contour map is made.

A case study is performed to compare the introduced PMSs to the current situation of radar vectoring. Actual flight data of AAS is used and divided into three cases. Two are during peak hours and one for off-peak hours. During peak hours about 97 aircraft are scheduled in each case and during off-peak hours 50 aircraft. A dual runway configuration is used during peak hours and a single runway configuration during off-peak hours. For each of the cases the flight schedule, ground track, height profile and noise contour map are compared.

Implementing the PMS at AAS showed to have a positive impact over the current situation. The main research question to be answered is: What are the advantages and disadvantages of implementing point merge system based arrival management for one single and one dual runway configuration at AAS in terms of environmental impact, capacity, delay, fuel efficiency and safety?

The advantages of the environmental impact found are that by design, the aircraft sequenced at a higher altitude and follow a CDA towards the runway. The CDA caused the aircraft to decent without level segments after the sequencing leg unlike the stepped approach employed in the current situation. Therefore, the aircraft are higher compared to the aircraft during the current situation and fly more efficient. This resulted in noise contour levels higher than 48dB relatively close to runway. Limiting the noise impact in the vicinity of AAS. The aircraft routes in the PMS are fixed and therefore the noise contour map are situated around the PMS route structure, reducing the noise footprint.

The fuel efficiency improved by implementing the PMS. Due to the CDA, the PMS saves fuel in every case compared to the current situation. The fuel-used savings range from 14.30% up to a saving of 33.07%. Also, the sequencing at higher altitude where aircraft performance is more efficient contributes to the fuel savings. However, when less aircraft are in the sequence the fuel savings decrease. By allowing the aircraft to switch up to two positions in the sequence, a total of 4.74% of fuel can be reduced compared to the FCFS case however, at the cost of a slight increase in makespan. Depending on the amount of traffic, the distance flown increased or decreased compared to the current situation. The maximum improvement found is 7.28%, while the maximum increase in distance was found to be 8.24%. The increase is caused by the fixed route structure of the PMS instead of the flexible radar vectoring routes.

Implementing the PMS had advantages in terms of throughput capacity. However, the improvements are small. The improvement ranged from 1.73% to a maximum of 9.29%. The improvements are due to the sequencing at a higher level where speeds are faster, but also by the CDA, which is faster than a stepped descent. A larger improvement is reached when the aircraft stream consists of

more heavy aircraft types. The average travel time per aircraft is reduced in the PMS, improving the throughput capacity of the system and reducing the delay. The average travel time improvement from the IAF to the final Approach Fix (FAF) ranges from 5.77% to 14.3%. This is caused by the sequencing at higher altitude.

By design, the PMS route structure is clearer and more intuitive, increasing safety. Currently, using radar vectoring the area of flight tracks covers a larger area. The PMS has a predefined horizontal and vertical envelop, due to the wedge to the merge point. This results in easier deconfliction of objects compared to vectoring aircraft. The PMS is a closed-loop intervention. Compared to the current situation at AAS, closed-loop interventions provides that aircraft are kept on lateral navigation, even during periods of dense traffic. This means that the PMS potentially reduces the number of tactical interventions. However, there is less flexibility for ATC as the aircraft have to follow the fixed route structure of the PMS.

Preface

This thesis completes the two year master track of air transport and operations. At the faculty of aerospace engineering of the university of technology Delft. It has been an intense journey, with long days, to come up with the end result. I learned a lot during the past year this thesis took. The result could not be obtained without the help of so many people for which I am very grateful.
First and foremost, I would like to thank Dries Visser. As daily supervisor, his input proved very valuable and helped me a lot. I felt always welcome when having any questions. We had a lot of good discussions. I would also like to thank Paul Roling. During the kick-off meeting and mid-term meeting, he always provided me with good advice.
Making long, intense days of programming it is very import to have some laughs during the day. I would like to thank my fellow graduate students in the room 3.15 for the good times we had.
Last but not least, I would like to thank my family, friends and especially my girlfriend for the intense support and unconditional support during this thesis. Keeping me motivated during the entire project.

J.M. de Wilde
Delft, August 2018

Contents

List of Figures

List of Tables

List of Acronyms

AAS	Amsterdam Airport Schiphol
APP	Approach
ASP	Aircraft Scheduling Problem
ATC	Air Traffic Control
ATM	Air Traffic Management
BADA	Base of Aircraft Data
BCIA	Beijing Capital International Airport
B-RNAV	Basic Area Navigation
CAS	Calibrated Airspeed
CBS	Centraal Bureau van de Statistiek
CCO	Continuous Climb Operations
CDA	Continuous Decent Approach
CNS	Communication, Navigation and Surveillance
CPS	Constrained Position Shift
CTA	Control Area
CTR	Control Tower Region
DME	Distance Measuring Equipment
FAF	Final Approach Fix
FCFS	First-Come-First-Served
FL	Flight Level
FMS	Flight Management System
GNSS	Global Navigation Satellite System
IAF	Initial Approach Fix
ICAO	International Civil Authority Organisation
IF	Intermediate Fix
ILS	Instrument Landing System
INM	Integrated Noise Model
IRS	Inertial Reference System
LAS	Lower Airspace
LVNL	Air Traffic Control the Netherlands

MILP Mixed Integer Linear Programming

ML-PM Multi-layer Point Merge

MPS Maximum Position Shift

MTOW Maximum Take-off Weight

MUAC Maastrich Upper Airspace Control

NADP Noise Abatement Departure Procedure

NDB Non Directional Beacon

NextGen Next Generation Air Transportation System

NOMOS Noise Monitoring System

PBN Performance Based Navigation

PMS Point Merge System

P-RNAV Precision Area Navigation

RHC Receding Horizon Control

RNAV Area Navigation

RPS Relative Position Shift

SEL Sound Exposure Level

SESAR Single European Sky ATM Research

SID Standard Instrument Departure

STAR Standard Terminal Arrival Route

TCAS Traffic Collision Avoidance System

TAS True Airspeed

TEM Total Energy Model

TMA Terminal Control Area

UAS Upper Airspace

VOR VHF Omni-directional Range

List of Symbols

Thr	thrust acting parallel to the aircraft velocity vector	$[N]$
D	aerodynamic drag	$[N]$
m	aircraft mass	$[kg]$
h	geodetic altitude	$[m]$
g_0	gravitational acceleration	$[m/s^2]$
V_{TAS}	true airspeed	$[m/s]$
$\frac{d}{dt}$	time derivative	$[s^{-1}]$
C_D	drag coefficient	$[-]$
ρ	air density	$[kg/m^3]$
S	reference wing surface area	$[m^2]$
ϕ	bank angle	$[rad]$
p	atmospheric pressure	$[Pa]$
p_0	atmospheric pressure at sea level	$[Pa]$
ρ_0	air density at sea level	$[kg/m^3]$
V_{CAS}	calibrated airspeed	$[m/s]$
$V_{TAS_{stall}}$	true stall airspeed	$[m/s]$
$C_{L_{max}}$	maximum lift coefficient	$[-]$
T_{idle}	Idle thrust	$[N]$
γ	flight path angle	$[rad]$
κ	adiabatic index	$[-]$
L_{AE}	sound exposure level	$[dB]$
L_A	instantaneous A-weighted sound level	$[dB]$
L_{DEN}	day–evening–night noise level	$[dB]$

1 Introduction

There has been a continued growth in air transport for the past thirty years with an average growth of five percent [8]. This results in the congestion of the currently available airspace. In fact, congestion is considered as one of the bottlenecks of future growth in the air transport industry [50]. There is a need to optimise the available airspace and aim for greater flight efficiency. Both the United States and Europe have started initiatives to research solutions to cope with the increasing air transport introducing NextGen and SESAR, respectively[41]. The optimisation of available airspace is achieved by improved Air Transport Management and by using technological improvements in the Communication, Navigation and Surveillance (CNS) environment. This led to the introduction of the Performance Based Navigation (PBN) concept which focuses on the improvement of the navigation part of CNS[23]. Today in the Terminal Control Area (TMA) of airport, to enhance efficiency and safety, Standard Instrument Departures (SIDs) and Standard Terminal Arrival Routes (STARs) are defined for arriving and departing aircraft. These routes are flown by aircraft using the Flight Management System (FMS), which is a closed-loop system. However, during peak hours the Air Traffic Control (ATC) uses radar vectoring to sequence and space aircraft before landing, which is an open-loop system. The advantage of radar vectoring is flexibility for the ATC, but this causes a higher workload as a large amount of radio communication between the controller and the pilot is required to direct the aircraft to the right position. For both the pilot and the controller a loss of situational awareness arises due to complexity and difficulty to predict and optimise the vertical profiles. This causes aircraft flying at lower altitudes and creating unnecessary noise, emissions and a non-continuous descent. EUROCONTROL designed a special technique as part of the PBN concept, which is called point merge or the Point Merge System (PMS) [33]. The PMS is designed to cope with high traffic loads without radar vectoring with as goal to improve safety, environment and capacity using existing technology. Due to the standardisation of operations, it is possible to optimise and automate the scheduling and sequencing of aircraft using Mixed Integer Linear Programming. The PMS is already successfully implemented in the TMA at ten airports around the world, however, not yet at Amsterdam Airport Schiphol (AAS). It is interesting to research if the proposed advantages of the PMS are applicable to AAS and if it is possible to automate the scheduling and sequencing using the PMS based on an actual case study. As the PMS provides better predictability, it can potentially offer significant fuel and environmental benefits as well as a considerable reduction of inbound delays at AAS, by permitting Continuous Descent Approach (CDA) even under dense traffic conditions. This translates to the following main research question for this thesis:

What are the advantages and disadvantages of implementing point merge system based arrival management for one single and one dual runway configuration at Amsterdam Airport Schiphol in terms of environmental impact, capacity, delay, fuel efficiency and safety?

In the following sections of this chapter the project plan will be discussed. First, the research objective, questions and scope are identified. Second, the way the research is performed in the methodology section and third, the exponential set-up is discussed. The chapter ends with an explanation of the structure of this thesis.

1.1. Research Objective, Questions and Scope

The objective of the research is to explore the potential benefits and drawbacks (environmental impact, capacity, delay, fuel efficiency and safety) of implementing point merge system based arrival management for one single and one dual runway configuration at AAS by the design and evaluation of a point merge air traffic sequencing system at AAS. Including the design and demonstration of an optimal point merge system scheduler using Mixed Integer Linear Programming. Multiple core-questions and sub-questions have been identified to answer the research question and to reach the research objective. Three core-questions have been identified:

1. How is the design of the PMS with regard to the relevant assessment criteria for designing a PMS system?
   (a) What is the effect of the PMS design on the current SID situation?
   (b) What is the effect of the PMS design on the future continuous climb operations?
2. How is the design of the scheduler with regard to the relevant assessment criteria for designing a scheduler?
   (a) What is the maximum capacity of the scheduler in the current design?
   (b) What is the effect of aircraft mix to the results?
   (c) What is the effect of minimum separation distance to the design?
   (d) What is the effect of continuous descent approach?
   (e) What is the performance of the algorithm in terms of computational time?
3. What are the influences of the designed PMS on the design of the scheduler and vice versa?
   (a) Is the design able to cope with the arrival peaks at schiphol airport?
   (b) What is the effect of PMS on the noise contour map?
   (c) What is the effect of PMS on fuel efficiency and emissions?
   (d) What is the effect of PMS on safety of the airspace?

The research is limited to one single and one dual runway configuration. For each configuration, only arrivals are investigated. The advantages and disadvantages of the environmental impact, capacity, delay, fuel efficiency and safety are based on the aircraft performance only. An extensive literature study has been performed prior to this thesis during which the following gaps where found:

- The PMS has never been implemented at AAS.
- The noise impact of the PMS has never been identified.
- The possible effect on the capacity at AAS has never been calculated.
- The available models for scheduling aircraft in a PMS are limited by assumptions as constant speed, two entry points and small case studies [16].

1.2. Theoretical Content

First the design of the PMS has to be done, prior to the scheduling model. This includes finding the most used runway configuration at AAS. Using a combination of arrival route design constraints and PMS design criteria, a PMS can be designed in the TMA around AAS. Second step is the design of the scheduling model to test advantages and drawbacks of the PMS. The following hypothesis from literature are to be tested. Based on the available literature, the following hypothesis are to be tested; implementing a PMS at AAS will:

- Save fuel due to continuous descent approach (environmental impact)
- Decrease Workload for pilot and Air Traffic control by design (safety)

- Result in a higher vertical profile for approaching aircraft (noise, environmental impact)
- Decrease distance and time in terminal control area (capacity, environmental impact, delay)

The theoretical basis, used for the scheduling model, is based on the Mixed Integer Linear Programming model of Capozzi [14], however applied to the PMS as seen in the paper of Hong [34]. The goal is to optimise the schedule of arriving aircraft in the PMS. The objective of the scheduling model is to minimise the makespan, which is the sum of the arrival times for all aircraft. To see the potential fuel savings a second objective is introduced to minimise the total fuel-used. Compared to current scheduling models for scheduling inside the PMS, this model will allow speed changes in the initial segment, sequencing leg segment and final segment.

The inputs of the model will be the PMS design, the time of entry at the IAF, point of entry at the IAF, aircraft size, aircraft type, aircraft flight number and scheduled landing time. The output of the model will be the time at which the aircraft reaches the runway, the path travelled, the total time travelled, the number of position shifts, the separation between aircraft and the total fuel-consumed. Based on the trajectories flown a noise analysis is performed by calculating the noise levels at grid-points creating noise contours.

When the scheduler model is verified actual flight data for AAS airport is used for a case study. The results will be discussed and analysed. At the end a conclusion is drawn which answers the main research question.

1.3. Experimental Set-up

The project that is studied during this research is completely based on a numerical analysis. Operational research and computer modelling are the main tools for analysing the performance of the PMS. This section explains the set-up used for this research.

1.3.1. Scheduling model

This model will be the main tool and tailor made for this research. The model is based on the algorithm of Capozzi and the design parameters of the developed PMS at AAS. The goal of this model is to optimise the makespan or fuel-used by sequencing the aircraft in such a way that the separation constraints are maintained during the complete manoeuvre from IAF to the runway. Due to the complexity of the algorithm and computational time, heuristics can be applied such as a maximum position shift.

1.3.2. Integrated Noise Model (INM)

This model is designed by the Federal Aviation Authority (FAA) in the United States and used for the calculation of the impact of noise in the vicinity of the airport. The input of the model is the flight path, speed, thrust and type of aircraft. There are multiple noise observer locations defined and the model calculates the noise at each point which results in a noise contour map.

1.3.3. Base of Aircraft Data (BADA)

The BADA model is made by EUROCONTROL in Brussels, Belgium. It consists of an aircraft performance model designed to model aircraft trajectories using datasets containing aircraft-specific information. In light of this research BADA is used to find the average fuel flow to evaluate both the fuel consumption, to find the speed limits of aircraft and calculate the CDA for each aircraft type.

1.3.4. Modeling Environment

Python 2.7 is used as the modelling language for this research, as it is widely used in the technical domain. Python is used to input and configure the flight data. Because the computational speed of the Python optimiser is relatively slow, the IBM commercial optimisation software CPLEX is used for the optimisation. In Python the objective function, constraints and decision variables are written and sent to the CPLEX environment which solves the optimisation problem. The output of CPLEX is transferred back to Python where it can be modified into the outputs needed for the analysis.

1.4. Structure of this thesis

The focus of this thesis is the implementation of the PMS at AAS and assess the advantages and disadvantages in relation to the current situation. The thesis starts with an introduction of the PMS in chapter 2, where the PMS is explained in detail. In chapter 3, the AAS situation is identified and the rules and regulations are shown to know how the PMS can be implemented in the TMA of AAS. After the requirements and characteristics, the detailed methodology of this thesis is shown in chapter 4 and chapter 5. Where it is explained how the PMS design, aircraft performance and noise calculations are performed. A separate chapter is introduced to explain the Mixed Integer Linear Programming formulation of the scheduling model. Using all methodology components, the scheduling model is designed in chapter 6. After the methodology and the scheduling model the actual cases are performed. First, the cases and reference scenarios are introduced where-after, the results are shown and discussed in chapter 7. The verification and validation are an important aspect in building the scheduling model and are discussed in chapter 8. The thesis ends with the conclusions and recommendations chapter which is in chapter 9.

2

The Point Merge System

This chapter explains the concept of point merge arrival management. The chapter begins with a brief history about the PMS followed by the principles of the PMS. After this, the design options are identified and the different airports where PMS is already implemented are shown. This chapter ends with the current state-of-art of scheduling inside the PMS.

2.1. History of the Point Merge System

Since the introduction of Area Navigation (RNAV), EUROCONTROL is proposing new options for merging traffic in the TMA. RNAV is defined as: "*a method of navigation which permits aircraft operation on any desired flight path within the coverage of the station-referenced navigation aids or within the limits of the capability of self-contained aids, or a combination of these*"[38]. Before RNAV, aerial navigation was performed by ground-based navigation aids such as VHF Omni-directional Range (VOR), Non Directional Beacon (NDB) and Distance Measuring Equipment (DME). The aircraft flew directly towards the navigation aid and then selected the next one to follow a predefined path in the Flight Management System (FMS). The RNAV system is able to get a position fix for the aircraft at every point in time. To accurately get a position fix of the aircraft, the RNAV system combines the best available set of information from different aircraft sensors. The RNAV system is primary based on ground-based navigation aids such as two or more DMEs or, less accurately, a VOR and DME. This made it possible for the aircraft to deviate from the constraint ground-based conventional route and enable point-to-point navigation along a set of waypoints. Where a waypoint is identified as "*A specified geographical location used to define an area navigation route or the flight path of an aircraft employing area navigation*"[38] .

Two types of RNAV exist, namely Basic Area Navigation (B-RNAV) and Precision Area Navigation (P-RNAV) [19]. The difference is the accuracy of the RNAV. B-RNAV has a navigation performance equal to or better than a track keeping accuracy of $\pm$ 5 Nautical Miles (NM) for 95% of the flight time and was the standard from 1998. As the demand of RNAV operations increased there was a need for an improvement in the accuracy and P-RNAV was introduced in 2006[31]. P-RNAV has an accuracy of $\pm$ 1 NM for 95% of the flight time. This makes P-RNAV suitable to be used in the TMA of an airport which can provide Air Traffic Control (ATC) interesting possibilities for the control of approaching aircraft. Instead of one arrival track, several tracks can be added alongside this one track. This gives the ATC more options for sequencing aircraft. In this way ATC does not have to vector each aircraft individually, but can send them on different tracks instead. Resulting in a reduced workload and decreases the risk of ATC error. However, there are two disadvantages: first, if there are many optional routes in the navigational charts, the readability will decrease and, second, during peak hours the ATC uses heading instructions for merging aircraft flows in the TMA in order to maximise capacity, an open-loop system [13]. To provide a solution for these disadvantages without changes in the phraseology and FMS modifications to speed up the implementation process, EUROCONTROL started to investigate a special method for merging the flows in the TMA denoted as the PMS. The following goals are defined for the PMS: maintain the possibility of guidance by the FMS and make CDA possible, even under peak traffic loads.

2.2. Point Merge Principle

An example of the PMS structure is shown in figure 2.1. The PMS consists of a merging point where different arrival flows merge to a single flight path. Additionally, there are so called ”sequencing legs”. These legs are predefined by waypoints and are at iso-distance from the merge point. The sequencing leg can be seen as an arc on a circle with a distance to the merge point equal to the radius of the circle. The length of the sequencing path determines the envelope of possible paths. The aim of the PMS is to integrate the inbound arrival flows and comprises of two phases: first, create spacing and, second, maintain spacing. Spacing is achieved by letting the aircraft fly over the sequencing legs until enough spacing is achieved after-which the ATC instructs a ”direct-to” command to the merging point. The aircraft will turn towards the merge point and fly towards it in a direct line. When the aircraft is flying towards the merging point the spacing is maintained using speed control, namely a constant speed [28]. Using the PMS the ATC only requires one intervention, namely the direct-to command.

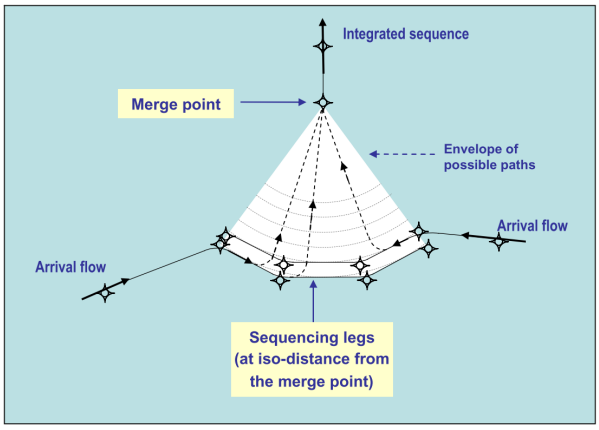

Figure 2.1: Example of the PMS with two inbound flows [28].

The following differences and advantages are identified between the PMS and the current situation:

The PMS route structure is based on a wedge shape with the purpose of converging traffic to a single point. The advantages are: a clearer and more intuitive route structure. The PMS has a predefined horizontal and vertical envelop due to the wedge shape pointed to the merge point. This results in easier deconfliction of objects compared to vectoring aircraft.

Current procedures encompass sequencing, metering and separation aspects, while PMS splits this into sequencing and spacing. Sequencing is the order in which the direct-to command is given to aircraft in the PMS and spacing depends on the interval between the direct-to order. The principal advantage of the PMS is the method involves a closed loop intervention keeping aircraft on lateral navigation even in dense airspace scenarios. The PMS also results in fewer tactical interventions. However, a closed-loop intervention leads to less flexibility for the ATC.

On a tactical level ATC has two main objectives, convergence in all dimensions and separation in at least one dimension. Convergence is obtained in the PMS when the aircraft directs to the merge point. The main advantage is that convergence in lateral and vertical plane requires only one instruction each; direct-to and descent, respectively. Separation is obtained by path stretching on the sequencing leg, requiring only one intervention; delaying the direct-to command.

The following advantages to other performance areas are identified. The principal advantage of the PMS is the possibility of a CDA from the sequence leg to the final point in the system. An example CDA is illustrated in figure 2.2. Compared to a step down approach, CDA eliminates level segments to keep aircraft at a higher altitude and minimise the need of additional thrust during descent. The benefits of CDA are noise reduction, decrease in noise contour areas, reduction of emissions and fuel savings. Another advantage of the PMS is the predefined and contained trajectory dispersion [51].

2.3. Point Merge System design options

The PMS shown in figure 2.1 consists of one system with two arrival flows. However, the design can be adjusted to suit different airport situations. This section first discusses the key dimensions, second,

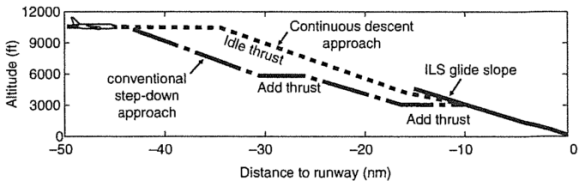

Figure 2.2: An example of a CDA procedure [50].

the angles and, third, the vertical separation of the PMS. Lastly, multi-system options are discussed.

2.3.1. Key Dimensions of the PMS

The route structure of the PMS is shown in figure 2.3. The following parameters can vary: length of the sequencing legs, distance between sequencing legs and merge point and the height of the sequencing legs. An increase in length of the sequencing legs can absorb the delay, but this will be more sensitive to wind and covers a larger area in the TMA. Increasing the distance from the sequencing legs to the point merge system will result in better spacing ability and applicability of speed control. Also, the sequence is more predictable as it is made early. However, this can make it difficult, resequencing aircraft during a missed approach. If the height of the sequencing leg is increased, the environmental impact decreases and the flight efficiency increases. Also, if combined with the stretching of the length to the merge point, the CDA can be started from a higher altitude. The downside of this is that the aircraft needs to increase speed at higher altitudes which decreases delay absorption. The main constraints influencing the design of a PMS are:

- The size of the airspace available including environmental constraints of AAS.
- The requirements as a result of CDA to cope with a mix of different aircraft types and the difference in performance.
- The number of entry points, the runway(s) in use and the complexity of the arrival and departure routes.

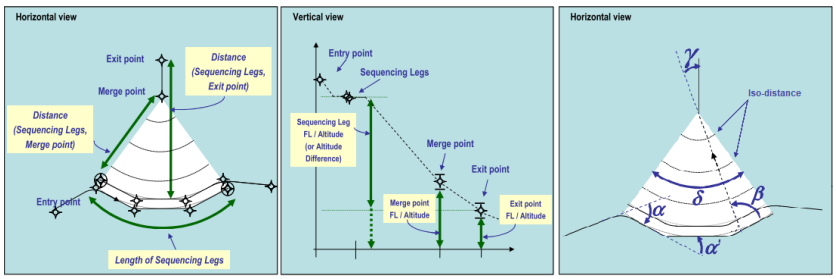

Figure 2.3: Route structure and angles in the design of a PMS [28].

2.3.2. Angles of the Point Merge System

In addition to the lengths, the angles in the design of the PMS can be varied to get the right dimension. The angles of the PMS are shown in figure 2.3. The following angles are defined: the track angle (α), which is the angle at the first waypoint between the entry flow and the sequencing leg. The angles at the following waypoints of the sequencing legs are identified as α', α'', etc. The angle between the sequencing leg and the merge point is called β, which is the angle the aircraft has to turn when the direct-to instruction is given. The angle δ is the central angle and γ is the angle between the track the aircraft flies and the leg between the merge point and the exit point.

Symmetry is an important requirement for the design of the PMS [28]. The goal is to keep the design as simple and intuitive as possible. Two important properties are identified: iso-distance and equidistance. Iso-distance is defined as: *"the shape of each sequencing leg shall be such that aircraft are kept (approximately) at the same distance from the merge point while flying along the leg (i.e. it is close*

to an arc of circle)"[28]. Equidistance is defined as: *"distinct sequencing legs shall be (approximately) located at the same distance from the merge point"[28].*

As an illustration, iso-distant lines are shown in figure 2.3. However, these lines are not equidistant as the distance to the merge point is different for each iso-distant line. Ideally, the sequencing legs needs to be both iso-distance from the merge point and equidistant from the merge point meaning both sequencing legs are at an equal distance from the merge point. These two properties cause better predictability of the trajectories flown.

In order to respect the symmetry guidelines, the track angle at each waypoint needs to be constant. For the same reason angle β is almost constant at every point on the sequencing leg and approximately equal to 90 degrees. If angle δ is increased the sequencing leg length is increased and vice versa. In the worst-case scenario, angle δ is 180 degrees which means that if two aircraft coming from opposing entry points and both take their shortest path to the merge point, both aircraft fly a head-on course. This causes less flexibility in case of issues and errors. As a baseline angle δ is chosen in such a way that the sequencing leg is at least 20 nautical miles.

2.3.3. Vertical separation sequencing legs

By the symmetrical design it is desired to have the sequencing legs as close as possible (at equidistance). This is favourable as the aircraft have to reach the same merge point and to keep the PMS possible for every aircraft class. The main general requirement is: *"Parallel sequencing legs shall be vertically separated e.g. each assigned with a different published level/altitude (i.e. at least 1,000ft apart), using appropriate vertical restrictions"* [20].

Vertical separation is required because of two reasons: first, due to the equidistant property the main goal of the design is not lateral separation and second, aircraft on the sequencing leg located furthest from the merge point have to cross the sequencing legs closer to the merge point which can cause loss of separation. In order to reduce the risk of loss of separation it is favourable to have the outer leg at a lower altitude than the inner leg. In that case the aircraft in the outer leg crosses the inner leg at least 1,000 ft below.

2.3.4. Multi-system Point Merge

The system shown in figure 2.1 concerns a single PMS with two arrival flows. However, more arrival flows can occur at other airport, requiring more sequencing legs. The PMS design can be adjusted to suit different airport situations. In figure 2.4 two different options are shown for an airport with four arrival routes. First option is a single PMS containing four sequencing legs. However, due to the constraint of at least 1,000 ft of vertical separation between the sequencing legs, the difference between the highest and lowest sequencing leg is 4,000 ft which influences the CDA performance. Additionally, the aircraft come from different sectors, some requiring additional travel distance from the Initial Approach Fix (IAF) to the entry point of the PMS. To overcome these issues, two identical PMSs can be created, both with two sequencing legs merging at one point. Note in figure 2.4 the offset between the merge points of the multi system which reduces the risk of a head-on encounter.

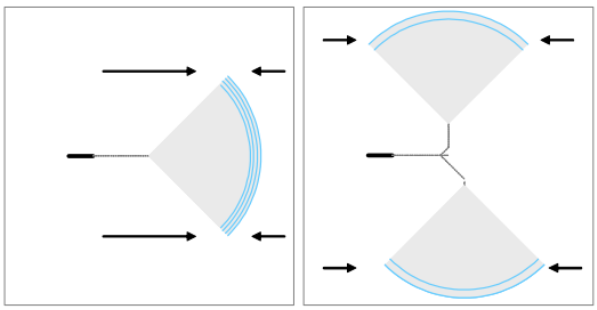

Figure 2.4: Two design options for four entry points, 1 runway [27].

2.4. Current applications of the point merge concept

In total ten airports have implemented the PMS in Europe, Asia and Africa, as shown in figure 2.5. The implementation of the PMS was an improvement over the old situation for each airport. For example, at Dublin the implementation of PMS resulted in 127kg of fuel-saved per flight while the total length of the flight was on average 11.3 miles shorter [33].

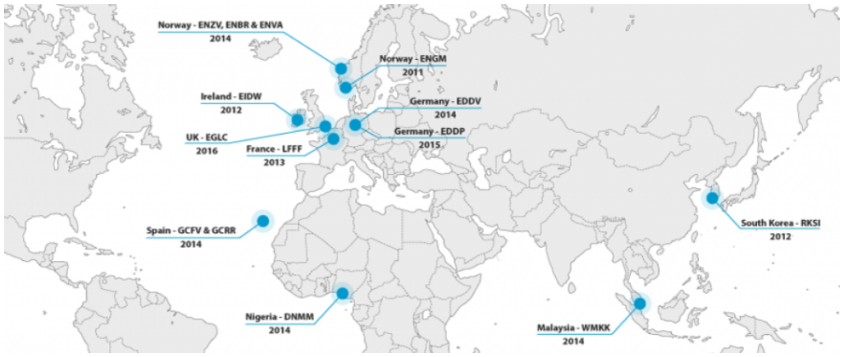

Figure 2.5: Airports where the PMS is currently implemented [33].

2.5. Current state-of-art of the Point Merge System Scheduling

In order to optimise and schedule the flight operations for arriving aircraft, a PMS scheduler has to be designed. Effective and efficient scheduling of aircraft take-offs and landings is an important subject to deal with the increase in congestion in the TMA. This is referred to as the Aircraft Scheduling Problem (ASP) [7]. The PMS can be scheduled as the ASP, but aircraft routing has to be included. As the PMS is a closed-loop intervention the aircraft are constrained by the design of the route structure.

The first to introduce an algorithm for the scheduling of aircraft in the PMS was Hong [35]. This research is performed based on Jeju International Airport in Korea. The PMS has two arrival flows from the same direction. The method used is based on the scheduling of aircraft in the metroplex area adjusted for the PMS[14] using Mixed Integer Linear Programming (MILP). The objective is defined as the minimisation of the total transit time. Using the following two decision variables: the time an aircraft takes to reach the first point (entry point) of the system, which is the first point of the sequencing leg and the time it takes to reach the final point. The sequencing legs of the PMS are divided into six and twelve discrete segments and multiple simulations are performed using four aircraft. Major assumptions are constant separation distance and constant speed. The paper concludes that the proposed scheduling algorithm is able to schedule the four aircraft in the PMS. However, the paper recommends the implementation of a continuous sequencing leg instead of a discretised version. It mentions that if the number of flights, routes and points increase heuristics might be necessary to keep the computational time contained.

The follow-up paper continues with the same formulation, but extends it by the integration of holding patterns at the end of the sequencing legs in the PMS [42]. Also Jeju international airport is used as case study. The algorithm proved to be successful in situations where the PMS is not able to absorb the delay without holding patterns. However, the paper concludes that multiple aircraft types should be incorporated in the algorithm.

Different aircraft classes are added in the follow-up paper of Hong [34]. The main difference is in the separation constraint, now requiring different minimum separation distances dependent on aircraft size and order. The travel time from the sequencing leg to the merge point is introduced as the CDA time. However, similar to the other papers aircraft speed is constant and therefore the CDA travel time is constant. Due to the constant speed, the sequencing legs can be continuous instead of discretised. Two exact algorithms are proposed, first the First-Come-First-Served (FCFS) and second the Constrained Position Shift (CPS) algorithm. A maximum position shift 1, 2 and 3 position in the sequence are simulated. A numerical simulation is performed using a random set of 7 aircraft. Using Monte-Carlo simulations, 100 test cases have been designed using 7 aircraft. The paper concludes that an increase in allowed position shifts results in a decrease of the makespan. The paper proposes that the model can be extended to deal with uncertainties as variable speed of aircraft in the operation.

3

Amsterdam Airport Schiphol

The principles and design options of the PMS have been identified. As the application of the PMS has to be tested on AAS, the basic constraints of AAS have to be identified. This chapter elaborates these constraints by first explaining the runway layout, second, the current route structure and last, the noise restrictions.

3.1. Runway Configuration and Combinations

Figure 3.1 shows the six runway layout of AAS. Runway 04-22 ”Schiphol-Oostbaan” is used mainly for general aviation, the rest of the runways are used for commercial traffic. The crosses in the figure show the two runways that can only be used in one direction. Runways 18R and 36R are restricted to landing aircraft only, while runways 36L and 18L are for take-off only.

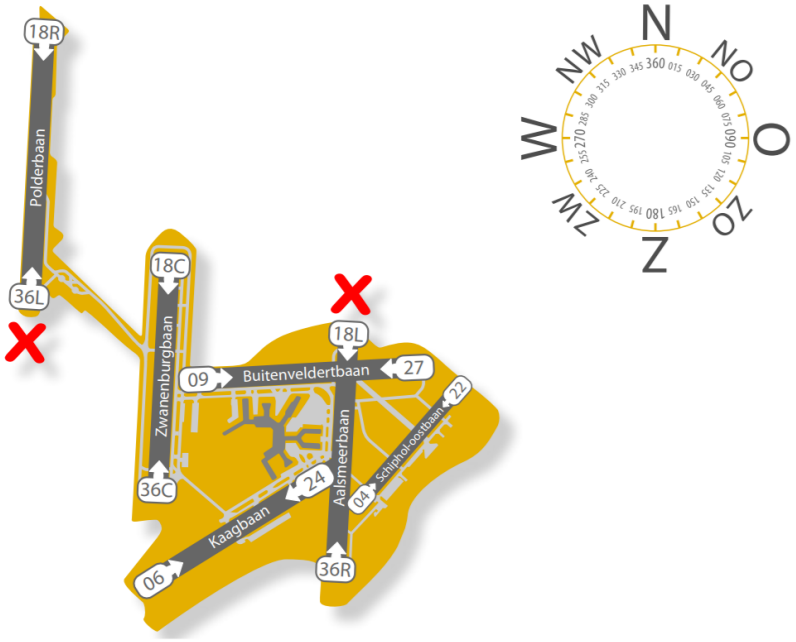

Figure 3.1: The runway configuration of AAS [56].

The runways are never used all at the same time. The number of runways that is used is based on the demand of air traffic, which changes during the day. Different runway modes are used for different situations. An example is shown in figure 3.2, where four different modes of operation can be seen. During off-peak periods there is one runway for aircraft taking-off and one for landing aircraft. During the departure peak there is one additional departure runway and during the arrival peak there is one

additional runway for landing. When there is a double peak, an extra departure runway and extra arrival runway are both in operation.

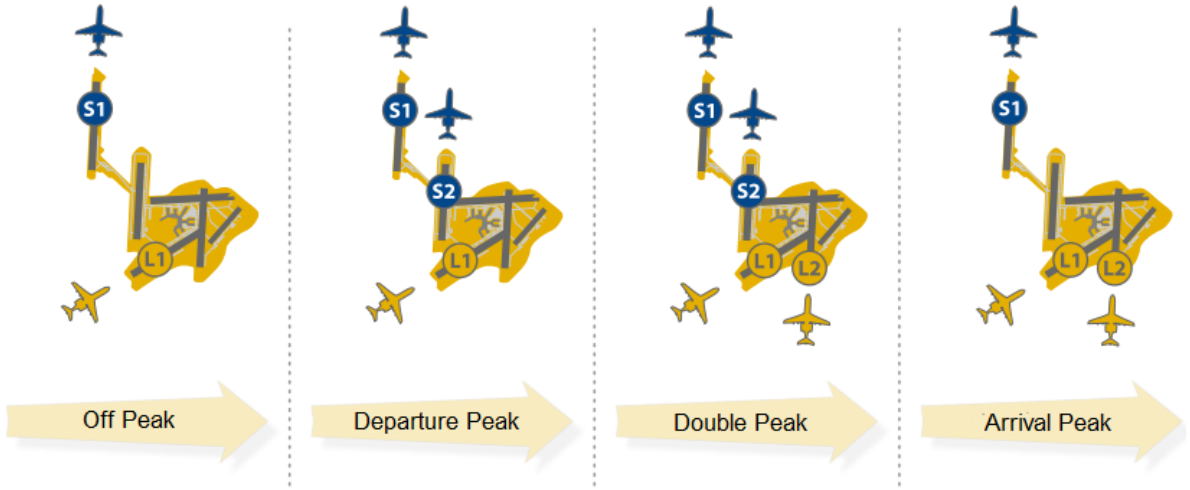

Figure 3.2: Different modes of operation at AAS [56].

The combination of runways used depends on the weather but also on the current supply of traffic and environmental rules. A list of ”runway preferences” has been put in place to determine the runways to be used. The preference was decided based on the agreement of the ”Alders table” which is an agreement between different stakeholders: AAS, Air Traffic Control the Netherlands (LVNL), local residents, administrators and the Dutch government [56]. Two different lists of preferences exist and depend on the hour of operation. The preference list during daytime can be seen in table 3.1 and for night time in table 3.2. The abbreviations L and S stand for landing runway and take-off runway, respectively. It can be seen that during day time the first preference for landing is runway 06 and if there is an arrival peak, 36R as additional runway. For take-off, runway 36L is the most preferred runway and if there is a departure peak, 36C is the second runway used.

Table 3.1: Runway preferences valid from 06-23 hours local time.

Required visibility and daylight conditions	Preference	Runway combinations				Expected use 2018
		L1	L2	S1	S2	
Good visibility within UDP	1	06	36R	36L	36C	24%
	2	18R	18C	24	18L	40%
	3	06	36R	09	36L	4%
	4	27	18R	24	18L	6%
Good visibility	5a	36R	36C	36L	36C	12%
	5b	18R	18C	18L	18C	
Marginal visibility	6a	36R	36C	36L	09	1%
	6b	18R	18C	18L	24	

During night time one runway for take-off and one for landing is sufficient, as shown in table 3.2. During night time the preference list is the same for both good and marginal visibility.

Table 3.2: Runway preference valid from 23-06 hours local time

Required visibility and daylight conditions	Preference	Runway combinations				Expected use 2018
		L1	L2	S1	S2	
Good or marginal visibility	1	06	-	36L	-	36%
	2	18R	-	24	-	43%
	3	36C	-	36L	-	5%
	4	18R	-	18C	-	6%

In both tables also the expected use in 2018 can be seen in the last column [56]. The configuration expected to be used most is preference 2. This can be explained by the dependency on the weather, especially caused by the average wind direction.

3.2. Route structure Amsterdam Airport Schiphol

In this section the route structure at AAS is explained. First, the airspace around AAS is discussed, second, the arrival routes are explained and, last, the separation requirements during arrival are identified.

3.2.1. Amsterdam Airport Schiphol Airspace

The airspace around AAS is vertically divided into the three sections: Upper Airspace (UAS), Lower Airspace (LAS) and Approach (APP) airspace. The flights above FL245 in the UAS, which is the airspace above FL095, are the responsibility of Maastrich Upper Airspace Control (MUAC) while below FL245 the flights are the responsibility of the LVNL. Below the UAS, the LAS is present which starts from FL095 to FL195 and is called the Control Area (CTA). Last section is the APP airspace, which is in the vicinity of the airport from ground level up to FL095. The APP airspace is split up in the TMA and the Control Tower Region (CTR). The last two sections are visualised in figure 3.3.

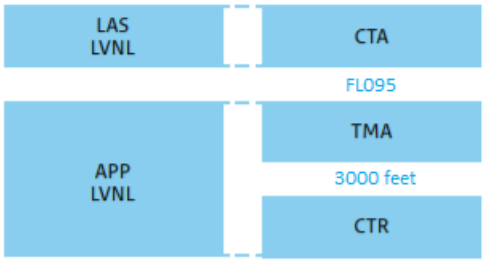

Figure 3.3: Airspace blocks at AAS and the responsible controller [46].

3.2.2. Arrival Routes and procedure

For safety AAS uses a fixed route structure to separate arrival and departing aircraft. This route structure can be seen in figure 3.4. There are three arrival sectors and five departure sectors. Each arrival sector has an entry point called the IAF. Arriving aircraft merge to one of the three IAFs, which are named SUGOL, ARTIP and RIVER. To transfer the aircraft from Air Traffic Service routes to the one of the three IAFs, a Standard Terminal Arrival Route (STAR) is used, which is completely situated inside the CTA. The actual flight chart can be seen in figure B.1 of Appendix B, containing the STARs for each of the three IAFs. The IAFs are the entry points of the aircraft into the TMA and the start of the approach segment of aircraft. From each runway towards each of the five departure sectors, a Standard Instrument Departure (SID) is defined. In figure 3.4 it is shown that most flights are expected to merge at ARTIP and come from the east. Most routes are departing towards sector 2 in south-east direction towards Frankfurt.

When an aircraft arrives at one of the IAFs, the navigation in the initial and intermediate approach segment is primarily based on radar vectors provided by ATC. However, for 36R from ARTIP an RNAV transition route exists in order the avoid noise-sensitive areas. In normal situations the aircraft decents to 2,000 ft or 3,000 ft and the final approach is started 12 or 17 km before the runway depending on the height the aircraft travels. When parallel runways 18R and 18C are in use the approach of 18R will be from 2,000 ft and for 18C 3,000 ft to keep the flows separated. During night operations special RNAV approach are used between 23:00 and 06:00 hours local time when low noise landing procedures are required. This is achieved by firstly apply CDA for runway 06 and runway 18R and secondly by requiring aircraft to fly a specific RNAV ground track which is shown in figure B.2a and B.2b of Appendix B. At AAS CDA implies that after waypoints NIRSI, NARIX or SOKSI a continuously descending flight path without level segments is to be flown in a low power and low drag configuration[47].

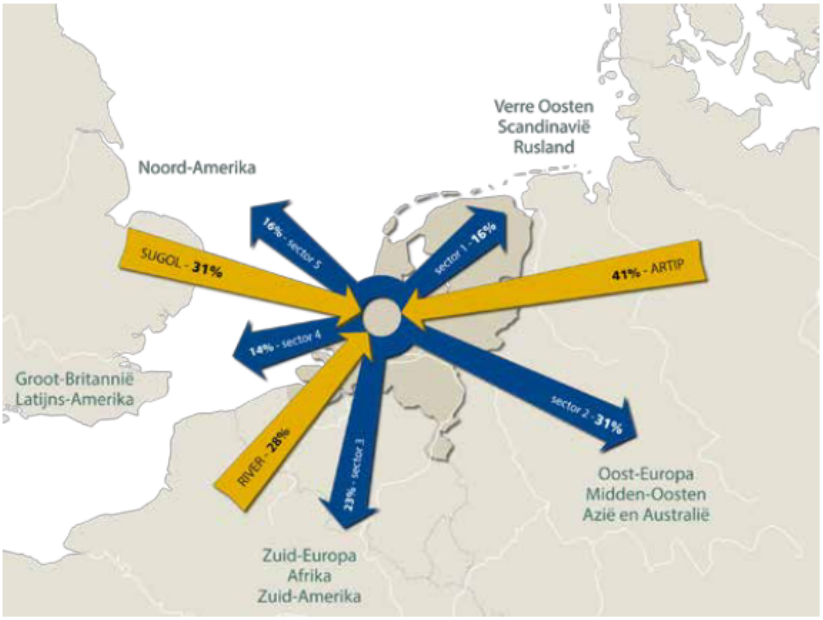

Figure 3.4: Route structure for arriving an departing aircraft at AAS [56].

3.2.3. Vortex separation requirements

The main task of the ATC is to ensure horizontal and vertical separation between aircraft. The vertical separation is set by International Civil Authority Organisation (ICAO) and is a minimum of 1,000 feet in controlled airspace. The horizontal separation required mainly depends on the position, aircraft weight and aircraft speed. When creating lift, aircraft generate wake vortices. This turbulent air can be a safety hazard for the aircraft flying behind it which can, in a worst-case scenario, lead to a crash [11]. The wake vortices are greater for heavier aircraft types, which results in a larger separation for smaller aircraft following heavier aircraft. As a result of this ICAO has specified minimum horizontal wake vortex separation standards dependent on the aircraft classes during approach using Instrument Flight Rules. ICAO identifies four separate aircraft classes according to their Maximum Take-off Weight (MTOW), shown in table 3.3. Since the introduction of the Airbus A380-800 an extra category is introduced, namely super heavy for aircraft above 560 tons.

Table 3.3: Aircraft classes according to ICAO classification ([8])

Aircraft Class	MTOW
Super Heavy	MTOW greater than 560 tons
Heavy (H)	MTOW greater than 136 tons
Large (L)	MTOW between 7 tons and 136 tons
Small (S)	MTOW under 7 tons

Based on these aircraft classes the horizontal separation requirements are listed in table 3.4. Thus, if the leading aircraft is a heavy aircraft and the trailing aircraft is a small aircraft a minimum separation of 6 nm is required. During most research the minimum permitted separation distances are converted to minimum permitted separation times. This can be done by dividing the separation distance by the approach speed [54].

Currently, for scheduling aircraft before landing, the FCFS strategy is widely used, where the ATC sequences the aircraft in the order that they arrive[5]. The longitudinal time based separation depends on the difference in approach speed and on the horizontal minimum wake-vortex separation distance between the aircraft weight classes. Making the time based separation a variable, which makes it possible to find a more efficient use of the runway compared to the currently used FCFS strategy. Two other 'sequencing' strategies are identified: weight-class sequencing and speed-class sequencing [59]. The effect of the weight-class sequencing strategy compared to the FCFS strategy is shown in figure

Table 3.4: Minimum wake vortex separation requirements for final approach according to ICAO in nautical miles (nm)([8]).

		Trailing Aircraft			
		Super Heavy	Heavy	Large	Small
Leading Aircraft	Super Heavy	3	6	7	8
	Heavy	3	4	5	6
	Large	3	3	3	4
	Small	3	3	3	3

3.5a. It can be seen that sequencing the aircraft according to weight-class increases the throughput capacity. In figure 3.5b, the effect of speed-class sequencing compared to the FCFS sequencing strategy are shown. Also, this results in an increase in capacity. Using operational research methods for scheduling aircraft the sequence can be optimised based on the two sequencing strategies maximising the throughput capacity.

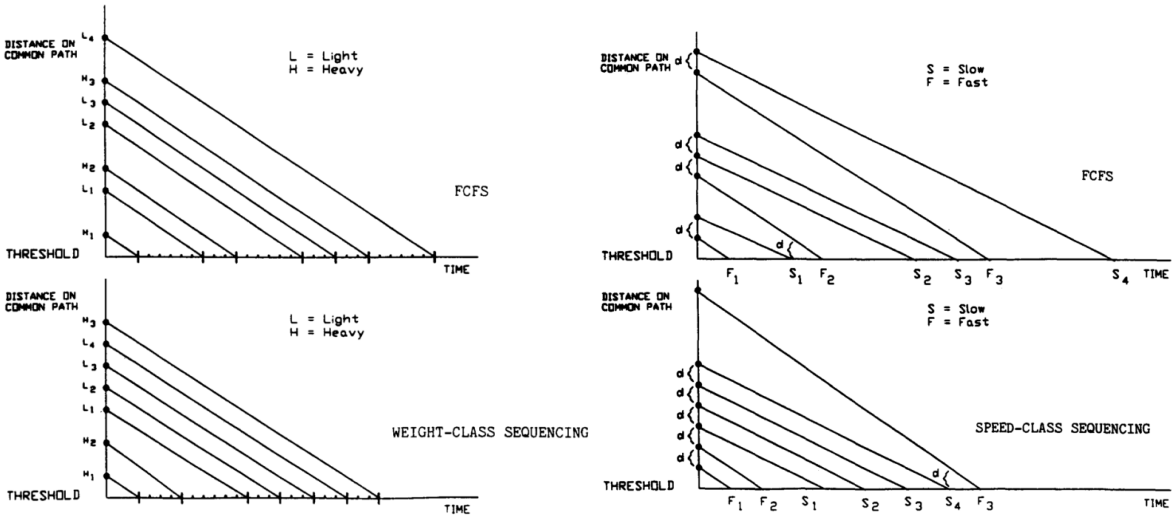

(a) Weight-class sequencing

(b) Speed-class sequencing

Figure 3.5: A comparison of sequencing strategies and FCFS strategy for sequencing aircraft prior to landing. (a) for weight-class sequencing and (b) for speed-class sequencing[59].

3.3. Noise at Amsterdam Airport Schiphol.

Noise has an impact on the health of people, causes annoyance and can result in a devaluation of property. As a result it is important to measure, analyse and monitor aircraft noise in the vicinity of an airport. This section explains how AAS deals with noise. First ,the noise measurements are explained, second the rules and restrictions are identified and lastly the monitoring and modelling of noise at AAS is discussed.

3.3.1. Measuring Noise

When an aircraft flies overhead, the noise observed increases until a maximum level of noise is reached and then the noise decreases again. This maximum level of noise is called the maximum A-weighted sound level expressed in decibel (dB) [55]. Not only the maximum sound level is important but also the total time exposed is relevant in determine the impact of the noise. The maximum A-weighted sound level is normalised to a time period of one second to get the Sound Exposure Level (SEL). The maximum A-weighted sound level and the SEL are measurements to calculate the noise for a single event. In order to calculate the noise impact around an airport cumulative noise measurements are used. At AAS the day-evening-night average level (L_{DEN}) is used. This is the SEL integrated over a 24 hour period or a year. Where a flight during night operations (23:00-07:00) counts for 10 flights during daytime operations and evening (19:00-23:00) flights count for 3 flights during daytime operations. At

AAS also night average level (L_{night}) is used to calculate the noise based on the operations between 23:00 and 07:00 hours.

3.3.2. Noise Rules and Regulations

To reduce the impact of AAS in the vicinity of the airport, rules and requirement have been established at the Alders table. Beside the preference list and night routes discussed before, a limit on the number of flights is agreed upon the stakeholders. This resulted in a maximum of 580,000 commercial flight a year in the Netherlands where 510,000 flights are assigned to AAS and 70,000 flights to other airports until 2020 and a maximum number of night flights set at 32,000. Also a limit is set to the maximum number of houses exposed to a given L_{DEN}/L_{night} contour and the maximum amount of people highly annoyed and sleep disturbances. The limits are:

- Maximum of 12,200 houses exposed to a L_{DEN} equal or higher than 58 dB(A).
- Maximum of 180,000 persons highly annoyed caused by a L_{DEN} equal or higher than 48 dB(A).
- Maximum of 11,100 houses exposed to a L_{night} equal or higher than 48 dB(A).
- maximum of 49,500 persons experiencing sleep disturbance caused by a L_{night} equal or higher than 48 dB(A).

Furthermore, discussed at the Alders Table it was decided that AAS is required to invest in noise insulation improvements in areas with high noise impact. Also, AAS has to develop and implement new annoyance reduction measures as CDA and Continuous Climb Operations (CCO).

4

Methodology

In the previous chapters, the PMS is discussed and the rules and regulations at AAS are identified. This chapter discussed the actions which have to be performed to design the scheduling model. It begins by showing the methodology overview used to built the scheduling model in section 4.1. The methodology is divided into components which are discussed in the subsequent sections. Section 4.2 describes the PMS design, section 4.3 explains the aircraft performance calculations and section 4.4 presents the aircraft noise calculations.

4.1. Methodology overview

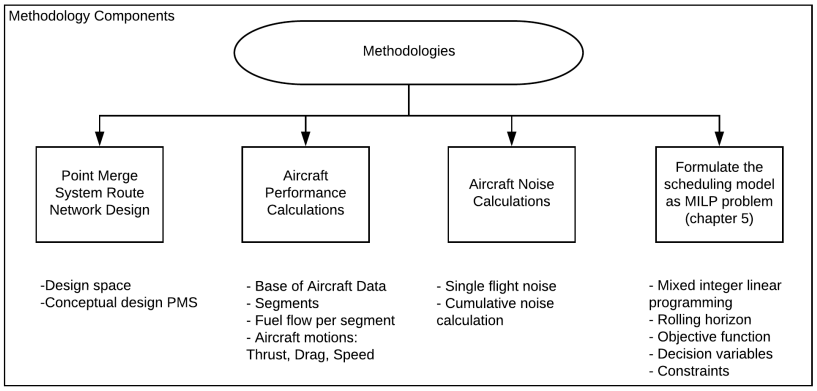

Figure 4.1: Methodology components overview.

In figure 4.1, the methodology overview for application in this research is shown. The methodology is divided into the following four components:

1. **Point Merge System Route Network Design**: Before the scheduling model can be built, the route network of the PMS has to be designed. The PMS route network has to be designed in collaboration with the rules and regulations and layout for AAS. The design of the PMS is performed in section 4.2.

2. **Aircraft Performance Calculations**: To calculate realistic 4D trajectories inside the PMS and calculate the aircraft motions. The performance calculations are explained in section 4.3.

3. **Aircraft Noise Calculations**: To build a noise contour map to calculate the total noise impact, the noise generated by each aircraft has to be calculated. The cumulative noise of all aircraft is plotted in a noise contour map. The method for calculating noise is shown in section 4.4.

4. **Formulate the scheduling model as MILP problem**: To optimise the flights entering the TMA at AAS the scheduling model is formulated as MILP problem. This is discussed in a separate chapter, in chapter 6

These components provide a basis of the scheduling model discussed in chapter 6.

4.2. Point Merge System Route Network Design

The first component is the design of the PMS route network in the airspace around AAS. In figure 4.2 the design methodology for TMA design in accordance with the EUROCONTROL manual for airspace planning is shown. The design methodology consists of a reference scenario, design guidelines and the conceptual design. The reference scenario marks the starting point of the new design. Starting from there, adjustments are performed to create the a new design concept in accordance with the design guidelines. The same design methodology is followed for the design of the PMS at AAS, but first the design space and requirements are identified.

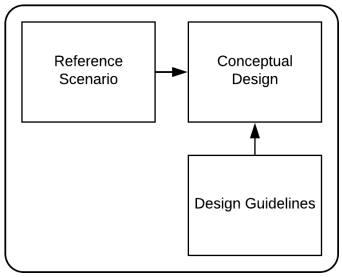

Figure 4.2: Design methodology of new arrival routes [22].

4.2.1. Design Space and Requirements.

The design space is the available airspace for the implementation of the PMS. Not the entire airspace is available. The airspace is limited by restricted military airspace and the size of the TMA. For this research, only one single and one dual runway configuration are tested. As shown in table 3.1, the runway combination of preference 2 is expected to be used 40% of the time. The PMS is designed for the runway combinations of preference 2, because of the highest expected use in 2018 and a parallel second runway during peak hours. Two configurations are used during preference 2. First, runway 18R as single runway configuration. Second, both runway 18R and 18C as dual runway configuration. The PMS is designed for both configurations.

Figure 4.3 shows the design space around AAS, within which the PMS is to be implemented. The design space is the current TMA at AAS. The aircraft enters the TMA at one of the three IAFs: SUGOL, RIVER and ARTIP. At an altitude of 10,000 ft. The IAFs are the starting points of the PMS design. The final point of the PMS design is the beginning of runway 18C or 18R. All airspace in between can be used for the design. However, the departure routes of runway 24 should be taken into account.

As AAS is a noise sensitive airport, the PMS needs to be designed such that aircraft do not fly over heavily populated areas. The population in the vicinity of AAS is shown in figure 4.4. The graph is based on the population density data of the Centraal Bureau van de Statistiek (CBS). Each cell in the figure represents the population of an area of 500 m^2.

Besides the design space and the population, the following set of requirements of the design are identified by EUROCONTROL [28]. These requirements are used for the design of the PMS at AAS.

- The design shall begin at all three IAFs and shall start at an altitude of 10,000ft.
- The full approach in the PMS shall fit in the current TMA, not interfering with the restricted airspaces and making implementation possible without major airspace changes.
- A three degrees glide slope has to be obtained at least 10 NM before the runway threshold in order to intercept the Instrument Landing System (ILS).

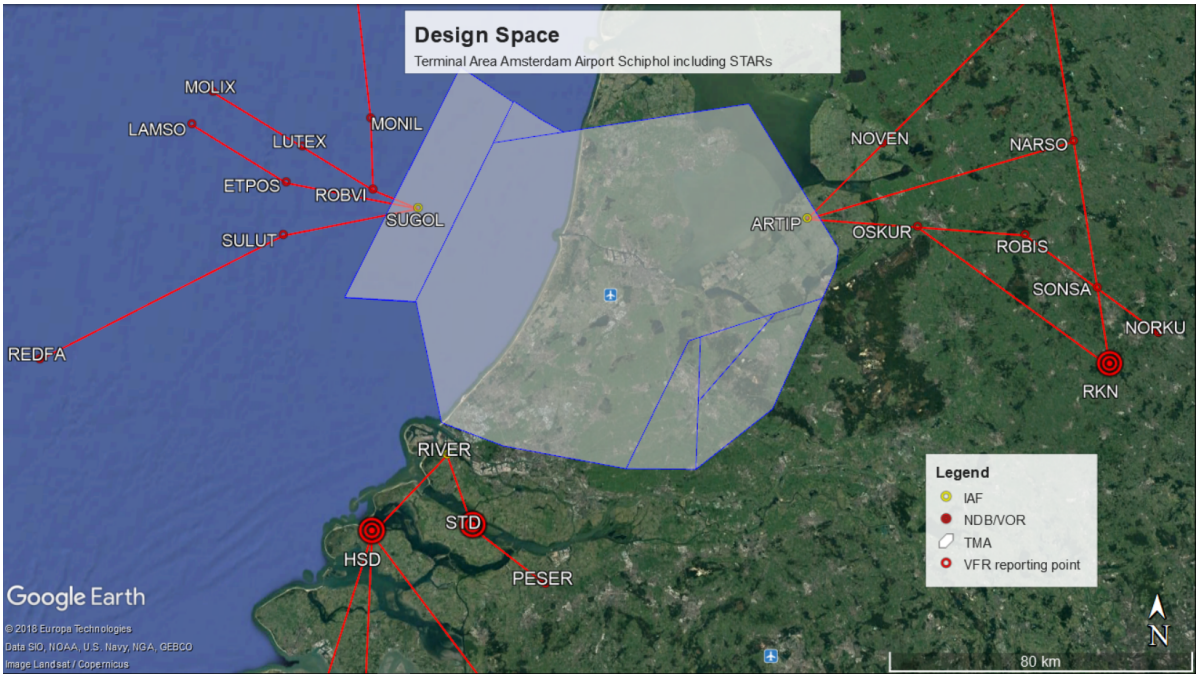

Figure 4.3: The design space where the PMS can be implemented.

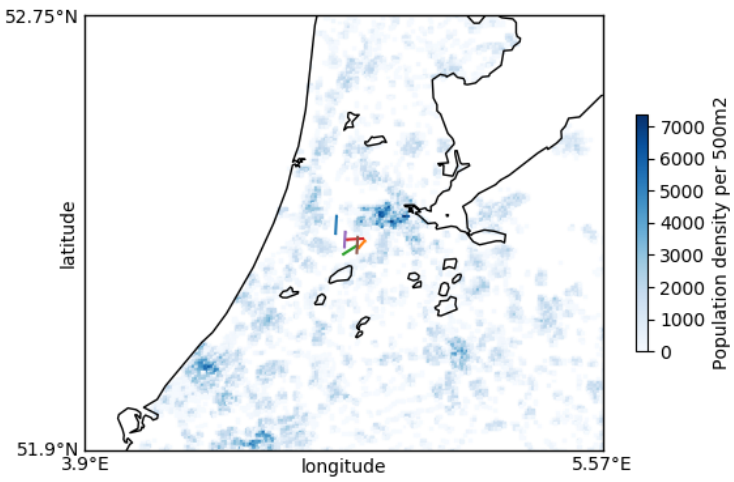

Figure 4.4: Population density in the vicinity of AAS.

- The sequencing legs will be level and at least 20 NM long, such as to have sufficient capacity to absorb delay.
- The leg between the sequencing leg and the Final Approach Fix (FAF) shall not have level segments, such as to the goal of the PMS is to implement CDAs which requires no level sections.
- To the extent possible, the route design should exhibit an overall symmetry. To keep the operating method simple and intuitive.
- When multiple point merge systems are combined there must be a lateral offset between merge points to avoid the risk of head-on collisions.

- To the extent possible, the sequencing legs shall be approximately equidistant from the merge point, so that the sequencing legs are at the same distance of the merge point.
- The sequencing leg shall be at iso-distance from the merge point, so that at each point on the sequencing leg the distance to the merge point is equal.
- Parallel sequencing legs shall have a vertical separation of at least 1,000 ft, such as to have procedural separation, separating aircraft by the design of the sequencing legs.
- The Parallel sequencing legs shall have at least a 1 NM lateral separation to avoid ATC display cluttering.
- The design shall be in accordance with terminal airspace design guidelines.
- The route structure shall not directly fly over heavily populated areas.
- The PMS design shall be designed for both the single and dual runway configurations without major changes. This to make the PMS applicable for both peak and non-peak hour operations and the opportunity to easily switch between single and dual runway configurations.

4.2.2. Conceptual Design

First, the PMS design of the single runway configuration is explained. This configuration uses runway 18R as arrival runway. Two design options are considered and illustrated in figure 4.5. Option 1: a single PMS. Option 2: a multi-system of two combined PMSs. Aircraft arrive at AAS from three sectors as shown in figure 3.4, requiring a total of three sequencing legs. Design option 1 has all three sequencing legs in one system. Design option 2 divides the sequencing legs over two systems.

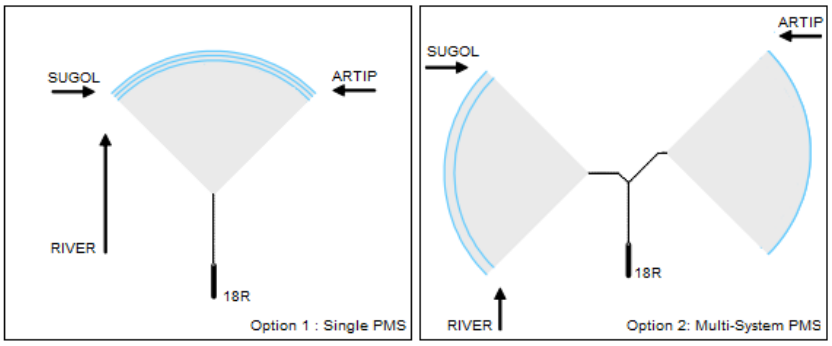

Figure 4.5: Two possible design options for a PMS at AAS.

Design option 2 is chosen for the design of the PMS at AAS. Compared to design option 2, design option 1 has the following drawbacks:

- The airspace north of the runway 18R is limited due to military airspace [1]. This limits the distance from the sequencing leg to the runway for design option 1. Requiring the sequencing legs to be at a lower height.
- It is difficult to design a single PMS which is able to easily switch from a single runway configuration to a dual runway configuration, while still respecting the symmetry requirements.
- Aircraft travelling from RIVER are required to fly a longer distance to get into the PMS, resulting in extra fuel-burn.

To distinct both PMSs of design option 2, the system for flights arriving from SUGOL and RIVER is called ”the west PMS”. The PMS for flight arriving from ARTIP is called ”the east PMS”.

As shown before, the concept design must be based on a reference scenario. An assessment has been made of the current arrival routes in the TMA of AAS and the PMSs at other airports, where PMS is already implemented. The information found during the assessment is shown in table 4.1 and is used as reference scenario data. The theoretical PMS is based on the example PMS proposed by

EUROCONTROL [28]. In the theoretical PMS, the sequencing leg is at an altitude of 12,000 ft and the merge point is at a height of 6,000 ft. The distance between the sequencing leg and the merge point is 20 NM, causing a descent rate of 300 ft/nm. At AAS no PMS arrival is currently implemented, however during the night hours a CDA approach is performed. For the CDA approach at AAS, the descent rate is approximately 260 ft/nm. At all other airports shown in table 4.1, the PMS is implemented.

Table 4.1: The PMS at other airports and night approach of AAS.

Airport Name	Initial Height (ft)	Final Height (ft)	Distance (NM)	Descent Rate (ft/nm)	Runway
Theoretical PMS [28]	12000	6000	20	300.00	
Amsterdam Airport Schiphol [1]	5500	2000	13.5	259.26	18R
Dublin Airport [40]	8000	3000	19	263.16	28
London City Airport [49]	10000	6000	15	266.67	27
Oslo Gardemoen Airport [4]	10000	5000	18.1	276.24	19L
Seoul incheon Airport [52]	9000	5000	13	307.69	16

In figure 4.6 the RNAV approach chart for runway 18R during night hours is shown. This particular CDA procedure is used as reference scenario for the segment between the merge point and runway 18R of the PMS design at AAS for the following reasons:

- The approach is currently flown at night hours, proving that aircraft can perform this CDA approach.
- The approach is designed to avoid noise sensitive areas [56].
- The approach is designed to avoid high objects in the vicinity of the airport.
- The approach is designed to intercept the ILS at a glide slope of three degrees.

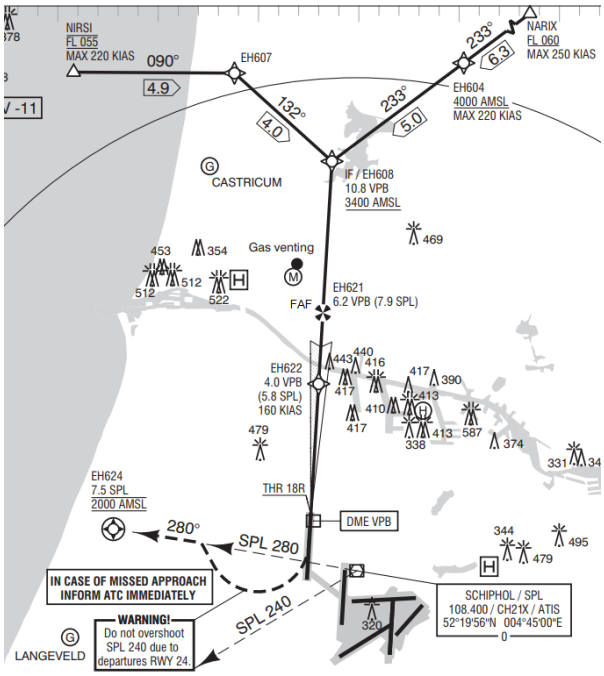

Figure 4.6: Night hours Instrument Approach Chart for runway 18R[1].

Based on the design requirements provided in section 4.2.1, the night hours approach at AAS and the reference data provided in table 4.1, the PMSs shown in figure 4.7 is designed. The ground track of the conceptual PMS is explained first. The vertical profile of the PMS is discussed second.

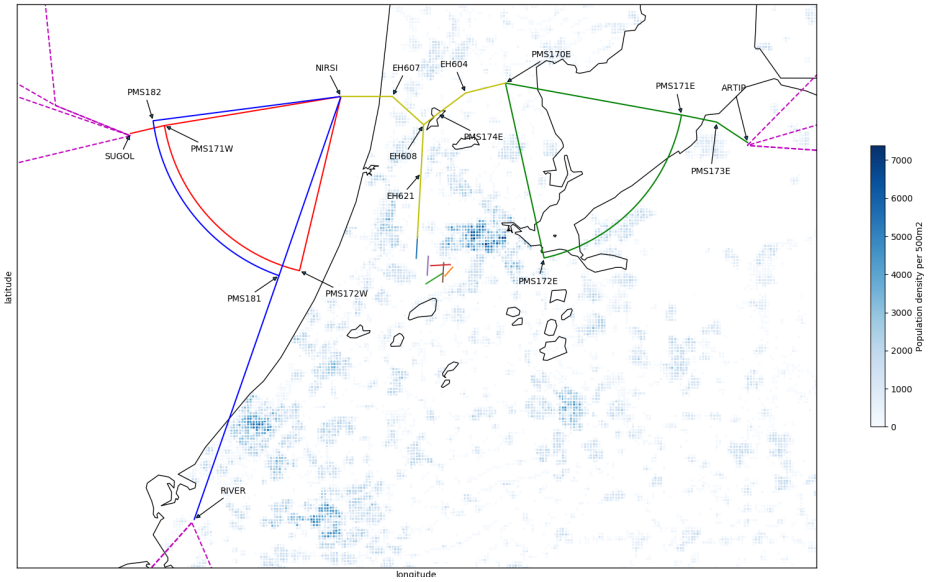

Figure 4.7: Point Merge System STAR design concept for AAS runway 18R.

Ground Track

First, the ground track between the merge points of the east and west PMSs are discussed. Due to the convenient location above the water, waypoint NIRSI is set as merge point of the west PMS. From the merge point NIRSI to runway 18R, the same night hours approach route network shown in figure 4.6 is used. Waypoint EH621 is used as FAF, at an altitude of 2000ft, and waypoint EH608 as initial fix. The waypoint EH608 is the point where the east and west PMSs merge. The distance between merge point NIRSI and the FAF, EH621 is 13.5 NM.

The symmetry constraint requires the segments between the merge points of the east and west PMS and runway 18R to be equal in length. For the east PMS, the night approach from runway 18R to waypoint EH604 is used, however this segment has a distance of 9.6 NM. By introducing waypoint PMS17E as merge point for the east PMS, a distance to waypoint EH621 of 13.5 NM is obtained.

Second, the dimensions of the PMS are explained, starting with the west PMS. The west PMS requires two sequencing legs to be designed. It is decided that the highest sequencing leg is set at an altitude of 10,000 ft to keep the sequencing leg as high as possible. As a result of the requirements set in subsection 4.2.1, the second sequencing leg is positioned at an altitude of 9,000 ft.

A CDA is performed from the sequencing leg to the FAF, requiring a vertical descent of 8,000 ft from the highest sequencing leg. A sequencing leg with a radius 17 NM was chosen in order to get a total distance from the sequencing leg to the FAF of 30.5 NM. Descending 8,000 ft within 30.5 NM requires a descent rate of 262.3 ft/NM, comparable to the descent rates provided in table 4.1. For the second sequencing leg, a radius of 18 NM was selected for two reasons. First, to avoid ATC display cluttering the sequencing legs should have a lateral separation of 1NM. Second, the inner sequencing leg should be at a higher altitude than the outer sequencing leg. Reducing the risk of separation infringement in case an aircraft descends immediately after the direct to instruction is given.

The inner, and highest sequencing leg is connected to SUGOL, since SUGOL is closest to the sequencing leg. limiting the distance available to descent. As a result, the outer sequencing leg is connected to RIVER. The entry waypoints PMS171W and PMS181 are defined in such a way that it is the most direct route towards merge point NIRSI, when no path stretching is required.

The east PMS is designed symmetrical to the inner system of the west PMS with a radius of 17 NM (figure 4.7). The entry waypoint PMS171E is not on the direct route between ARTIP and the merge point PMS170E. Waypoint PMS173E is introduced, to prevent the end of the sequencing leg to be positioned above heavily populated areas.

In figure 4.8, the PMS concept for the dual runway configuration is shown. It can be seen that the PMSs are similar in shape and location compared to the single runway design to make it possible to easily switch from a single to a dual runway configuration. However, the east PMS is uncoupled from the west PMS, by the newly introduced waypoint PMS174E. From that waypoint, the aircraft will be

directed via waypoints EH630 and EH262 to runway 18C, where waypoint EH630 serves as FAF at 2,000 ft. Note that it is assumed that no runway switches are performed and flights from ARTIP always land on runway 18C and from SUGOL and RIVER on runway 18R.

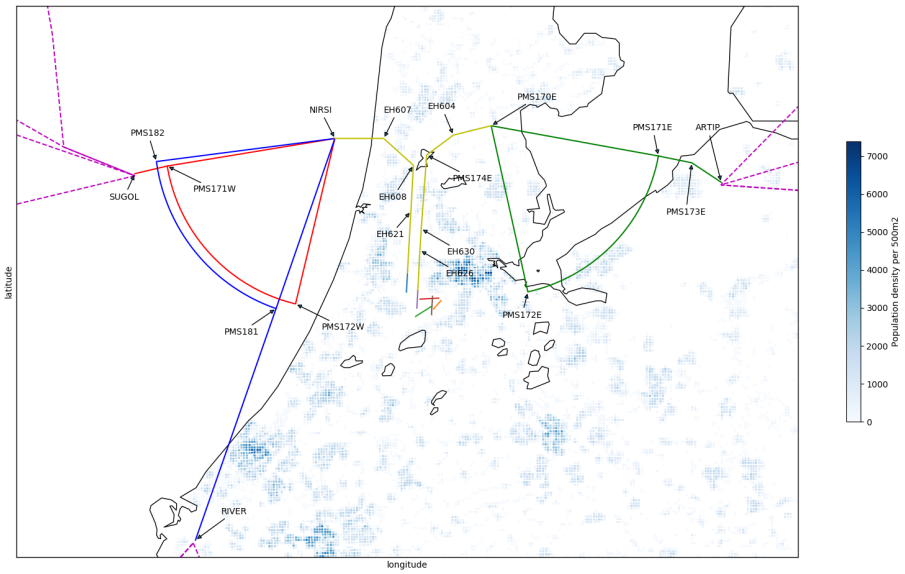

Figure 4.8: Point Merge System STAR design concept for AAS runway 18R and 18C.

Vertical Profile

In the west PMS, flights arriving from SUGOL enter the TMA and the sequencing leg at an altitude of 10,000 ft. Flights arriving from RIVER, enter the TMA at an altitude of 10,000 ft and the sequencing leg at an altitude of 9,000 ft. After the direct-to instruction is given on the sequencing leg, a CDA profile is performed towards waypoint EH621. The height profile of the CDA depends on the aircraft performance. However, a lower altitude limit is appointed to waypoints in order to enable departing aircraft to fly below the waypoints. The altitude limit also enables the aircraft, to intercept the ILS at the required height. At NIRSI, the minimum height is 5,500 ft. At waypoint EH608, the minimum height is set to 3,400 ft. At FAF EH621 the altitude is set to 2,000 ft.

For the east PMS, a similar setup is applied. Flights arrive at ARTIP at an altitude of 10,000 ft and enter the sequencing leg is at an altitude of 10,000 ft. The minimum height of merge point PMS170E is set at an altitude of 5,500 ft. For the dual runway configuration, the FAF for the east PMS is changed to EH630 with altitude limit set at 2,000 ft. The coordinates of the waypoints for both PMSs are shown in Appendix A.

4.3. Aircraft Performance Calculations

In the previous section, the PMSs are designed. The methodology continues with the performance calculations of aircraft inside the PMS. The calculations simulate the performance and limits of aircraft, serving as inputs for the scheduling model. The BADA is used to simulate the performance of different aircraft inside the PMS. Developed by EUROCONTROL, the BADA is an aircraft performance model with as goal to simulate and predict aircraft trajectories. The BADA is not a software itself, however, it contains the model specifications and the aircraft datasets containing the aircraft specific coefficients [24]. The model used in BADA is the Total Energy Model (TEM) [25], which ”*equates the rate of work done by forces acting on the aircraft with the rate of increase in potential and kinetic energy*” [24]. The model is based on a reduced point mass system, which is shown in figure 4.9. Assuming the angle between the thrust vector and the velocity vector (α_T) is small and no wind exists, the equation for the TEM is expressed as in equation 4.1.

$$(Thr - D) \cdot V_{TAS} = mg_0 \frac{dh}{dt} + mV_{TAS} \frac{dV_{TAS}}{dt} \tag{4.1}$$

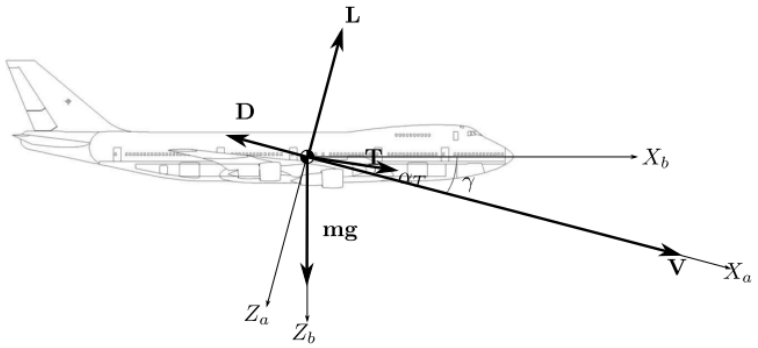

Figure 4.9: Free body diagram of aircraft motions expressed in a body frame [57].

Four forces act on the aircraft which are Thrust (T), Weight (W), Lift (L) and Drag (D). Depending on the situation, acceleration in the vertical or in the horizontal plane is obtained.

In comparison to the currently existing scheduling models, the scheduling model in this research allows speed changes as an additional way to reach the separation requirements. It is decided that speed changes are only allowed at the IAF and entry point of the PMS, to keep communication between the ATC and the pilots to a minimum. Additionally, the CDA profile is calculated for each different aircraft type. As a result the CDA duration varies for each aircraft type. Based on the points where a speed change occurs, the PMS is split into three segments shown in figure 4.10. Each segment requires different performance calculations. In the PMS three segments are identified:

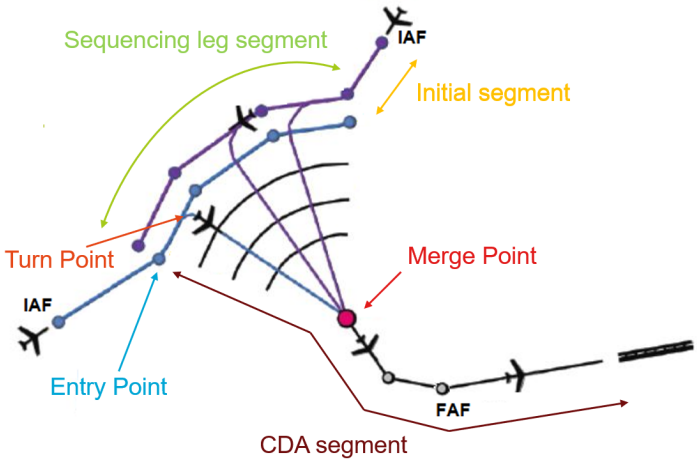

Figure 4.10: Segments inside the PMS.

1. **Initial segment**: This is the segment between the IAF and the entry point of the PMS. The initial segment is a fixed length and assumed to be level.

2. **Sequencing leg segment**: This is the segment between the entry point of the PMS and the point the aircraft receives the direct-to merge point instruction. This point is called the ”turn point”. The length of the segment is variable, because the aircraft can turn at any time on the sequencing leg. The height of the sequencing leg segment is level.

3. **CDA segment**: This is the final segment, between the turn point and the FAF. This segment is where the aircraft performs a CDA towards the FAF. The length of this segment is fixed, because of the iso-distance to the merge point from the sequencing leg.

In the next subsections, the TEM is derived to get the performance required for each segment. In subsection 4.3.1, the calculation required for the initial segment is explained. Next, in subsection 4.3.2,

the sequencing segment performance calculations are discussed. Last, in subsection 4.3.3, the calculations for the CDA are explained. Note that BADA can model the performance of turbofan, turboprop and piston engines. However, the amount of turboprop and piston aircraft is negligible at AAS, as a result the performance calculations are modelled for turbofan aircraft only. Furthermore, it is assumed that the mass of aircraft is constant from the beginning of the initial segment to the end of the CDA segment. The masses selected in this research, are the medium masses of each aircraft type found in the aircraft datasets of BADA.

4.3.1. Initial segment

In the initial segment, the aircraft is allowed to change the separation by speed control. The effect of changing the speed of the aircraft results in a change in fuel flow, which is different for each aircraft type. For this segment, a feasible velocity range and its effect on the fuel flow is required to be calculated. Both the feasible velocity range and fuel flow calculations are discussed in this subsection.

The initial segment is different for each of the three IAFs, because of the different distances from the IAFs to their respective entry points. As seen in the design, the sequencing legs for flights arriving from SUGOL and ARTIP is at a height of 10,000 ft and the sequencing leg of RIVER is at height of 9,000ft. It is assumed that the initial segment is level and at the same altitude as the sequencing leg. Additionally, it is assumed that the selected speed remains constant, if allowed within the velocity range. Level flight with constant speed is calculated in BADA as a cruise flight. A cruise flight is modelled by setting the thrust equal to the drag, reducing equation 4.1 to equation 4.2.

$$Thr = D \tag{4.2}$$

Thrust is equal to the drag as the change in height and speed over time is zero. Using BADA, the drag of each aircraft can be calculated and therefore the thrust can be obtained. Equation 4.3 is used to calculate the drag acting on the aircraft.

$$D = \frac{1}{2} C_D \rho V_{TAS}^2 S \tag{4.3}$$

The drag coefficient is calculated using the coefficients provided in BADA and using the lift coefficient. The lift coefficient is calculated using equation 4.4. It is assumed that aircraft in the initial segment are still in cruise configuration, which is called ”clean” configuration. In cruise configuration no lift devices or landing gear is deployed. For the sake of simplicity, the correction for bank angle in the lift coefficient is assumed to be zero.

$$C_L = \frac{2mg_0}{\rho V_{TAS}^2 S cos\phi} \tag{4.4}$$

The air density in equation 4.3 is depending on the altitude of the aircraft. For the initial segment, the air density is constant, because of the level flight. Also, the wing surface of the aircraft is constant, because the configuration does not change over time. Consequently, true airspeed is the only variable in the equation. When a true airspeed is chosen, the required amount of thrust is obtained. The thrust is used to calculate the thrust coefficient. Combining the thrust coefficient and the coefficients found in BADA, allows the fuel flow per second to be calculated. The fuel flow per second for a Boeing 737-800 aircraft is illustrated in figure 4.11a for a range of true airspeeds. The parabolic shape of the graph is the result of the quadratic true airspeed term in equation 4.3.

The time inside the initial segment is variable, because a free true airspeed can be chosen. However, the distance is fixed by design. Therefore, it is desired to know the fuel flow per nautical mile to calculate the total fuel consumption of the initial segment. The fuel flow per nautical mile is obtained by dividing the fuel flow for each true airspeed by the true airspeed.

Again, the Boeing 737-800 is taken as example. The fuel flow per nautical mile for a range of true airspeeds is shown in figure 4.11b. Following the calculation of the fuel flow per nautical mile, the feasible true airspeed range the aircraft can operate in has to be found. First, the maximum true airspeed. The maximum airspeed is defined by regulations at 250 knots calibrated airspeed, below 10,000 ft, which is valid for this case [44]. Using equation 4.5, the calibrated airspeed is converted to true airspeed. It can be seen that the true airspeed depends on the height of the aircraft. As a result,

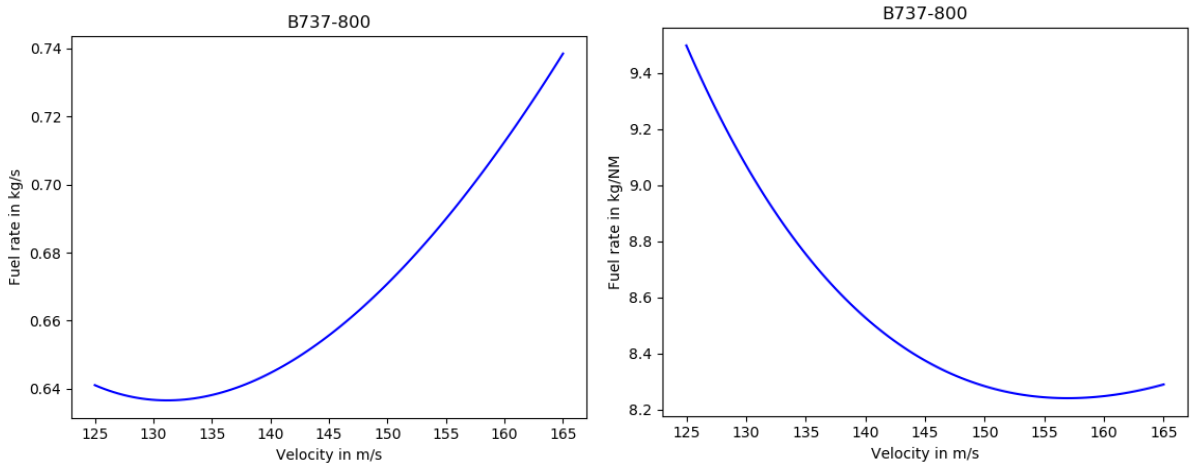

(a) Fuel flow per second (b) Fuel flow per nautical mile

Figure 4.11: BADA fuel flow calculation against airspeed at 10,000 ft for a Boeing 737-800 aircraft.

the maximum true airspeed at 10,000 ft is higher than the maximum true airspeed at 9,000 ft.

$$V_{TAS} = \left[\frac{2}{\mu}\frac{p}{\rho}\left(\left(1+\frac{p_0}{p}\left[\left(1+\frac{\mu}{2}\frac{\rho_0}{p_0}V_{CAS}^2\right)^{\frac{1}{\mu}}-1\right]\right)^{\mu}-1\right)\right]^{\frac{1}{2}} \tag{4.5}$$

Second, the minimum true airspeed. The minimum true airspeed in cruise is normally not lower than the maximum endurance speed. This is equal to the true airspeed where the fuel flow in kg/s is minimal (figure 4.11a). The feasible speed range is visualised in figure 4.12, with as minimum speed the maximum endurance speed and as maximum speed the 250 knots calibrated airspeed. It can be seen from figure 4.12, that the optimal true airspeed is outside the feasible airspeed range due to the maximum speed. As a consequence, the least amount of fuel is used when the aircraft fly at maximum allowed airspeed. This implies that decreasing the true airspeed will increase the amount of fuel used to cover a nautical mile.

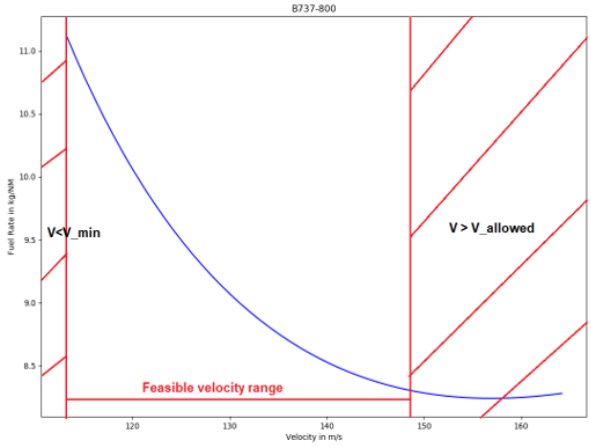

Figure 4.12: Illustration of the feasible speed range for a Boeing 737-000 aircraft.

The fuel consumption and speed range is calculated for each aircraft type. Both characteristics will be inputs for the scheduling model. Varying the true airspeed allows the arrival time at the entry point to be increased or decreased at the cost of additional fuel. Beside that, the amount of thrust required is an input for the noise model discussed in section 4.4.

4.3.2. Sequencing leg segment

After the initial segment, the sequencing leg segment begins. The length of the sequencing leg segment depends on the turn point the aircraft uses. When no path stretching is required, the length of this segment is zero. On the other hand, the maximum length is the total length of the sequencing leg. As input, the scheduling model requires the fuel flow and the feasible speed range of this segment. Similar to the initial segment, the aircraft performance of the sequencing leg segment is modelled as cruise flight. Therefore, the fuel flow calculations and the velocity speed range are obtained using the same calculations as for the initial segment.

4.3.3. Continuous descent approach segment

The CDA segment begins after the turn-point on the sequencing leg segment. Instead of level flight, the aircraft descents in this segment towards the runway. The scheduling model requires the fuel consumption and the flight time of the entire CDA profile for each aircraft type. This subsection explains how fuel consumption and the flight time are calculated for this segment.

Before the CDA performance calculations can be started, the definition of CDA needs to be defined. According to ICAO, CDA is defined as: *"the aircraft descends continuously, to the greatest possible extent, by employing minimum engine thrust, ideally in a low drag configuration, prior to the FAF"* [37].

In BADA, a descent can be reached by two independent control inputs: the throttle and the elevator. Three variables can be controlled using these control inputs namely: thrust, speed and rate of descent [25]. By controlling the speed and thrust, a rate of descent is obtained. By controlling the rate of descent and speed, a required thrust is obtained. By controlling the rate of descent and thrust, a speed is obtained.

Two control inputs are chosen. The CDA consists of two parts. During the first part, the aircraft is in clean configuration and during the second part, the approach/landing configuration is active. The second part is called the 'non-clean' configuration. Aircraft normally descend using a constant calibrated airspeed[43]. Therefore, BADA has defined standard airline procedures where the speed schedule of the descent is defined, making the airspeed the first control input for both parts. The second control input is different for each part:

- **Clean configuration part**: Based on the ICAO definition of CDA, the thrust for the clean configuration part is the minimum engine trust. In BADA, minimum engine thrust is defined as idle thrust. The idle thrust can be calculated using BADA. Therefore, for this part the trust is a controlled input.

- **Non-clean configuration part**: When the configuration switches to a non-clean configuration a constant rate of descent has to be flown, requiring the thrust to be increased to maintain the airspeed in the speed schedule[18]. Therefore, the rate of descent is a controlled input for this part .

In this subsection, first, the speed schedules are explained. Second, the calculations for the clean configuration part are shown. Finally, the calculations for the non-clean configuration part are explained.

Speed schedules

Standard airline procedures are defined by BADA. Included in the airline procedures are descent speed schedules, which are shown in table 4.2. For a range of heights, a descent CAS is defined. Between an altitude of 10,000 and 6,000 ft, either the standard descent CAS ($V_{des,1}$) is used, or the maximum velocity of 250 knots CAS is maintained, whichever CAS is lower. The standard descent CAS depends on each aircraft and is included in the BADA database. For altitudes between 3,000 and 6,000 ft, the CAS descent speed is the standard descent CAS ($V_{des,1}$) or 220 kts CAS, whichever is lower. Below an altitude of 3,000 ft, the descent CAS is a sum of the landing stall speed ($(V_{stall})_{LD}$) multiplied by the minimum speed coefficient (C_{Vmin}) and a descent speed increment (Vd_{DES}). The minimum speed coefficient is a constant of 1.23. The descent speed increment depends on the height and are shown in table 4.3.

Finally, the stall speed has to be calculated. Equation 4.4 can be rearranged to calculate the stall speed shown in equation 4.6. It can be seen that instead of the C_L, the maximum lift coefficient ($C_{L_{max}}$)

Table 4.2: Calibrated airspeed schedule in descent [25].

Height (ft)	CAS (knots)
from 0 to 999	$C_{Vmin} \cdot (V_{stall})_{LD} + Vd_{DES,1}$
from 1000 to 1499	$C_{Vmin} \cdot (V_{stall})_{LD} + Vd_{DES,2}$
from 1500 to 1999	$C_{Vmin} \cdot (V_{stall})_{LD} + Vd_{DES,3}$
form 2000 to 2999	$C_{Vmin} \cdot (V_{stall})_{LD} + Vd_{DES,4}$
from 3000 to 5999	$\min(V_{des,1}, 220)$
from 6000 to 10000	$\min(V_{des,1}, 250)$

Table 4.3: Descent speed increments [25].

Height (ft)	Variable Name	CAS increment (knots)
from 0 to 999	$Vd_{DES,1}$	5
from 1000 to 1499	$Vd_{DES,2}$	10
from 1500 to 1999	$Vd_{DES,3}$	20
form 2000 to 2999	$Vd_{DES,4}$	50

is used. This is dependent on the aircraft configuration and type of aircraft.

$$V_{TAS_{stall}} = \sqrt{\frac{2mg_0}{C_{L_{max}}\rho S}} \tag{4.6}$$

To get the landing stall speed, the landing configuration $C_{L_{max}}$ and air density of sea level is used. For the same reason as in equation 4.4, the bank angle is assumed to be zero for the entire descent.

Clean configuration

For the clean configuration part, idle thrust and speed are the controlled inputs. This leaves the rate of descent to be calculated. Equation 4.1 can be rearranged to have the rate of descent on the left hand side as shown in equation 4.7, where the idle thrust is calculated by BADA and the drag is calculated using equation 4.3.

$$\frac{dh}{dt} = \frac{(T_{idle} - D)V_{TAS}}{mg_0}\left[1 + \left(\frac{V_{TAS}}{g_0}\right)\left(\frac{dV_{TAS}}{dh}\right)\right]^{-1} \tag{4.7}$$

To get the flight time of the CDA segment, the height will be integrated over time. The initial height is the top of the descent phase, which is the height of the sequencing leg. The final height is the height where a configuration change is required. However, the speed change ($\frac{dV_{TAS}}{dh}$) is not a constant. When descending with constant CAS schedule, the TAS speed changes over time because of the varying density in equation 4.5. Additionally, because of the change in CAS speed schedule as seen in table 4.2, $\frac{dV_{TAS}}{dh}$ a variable. To overcome this issue, the integration is performed using numerical integration. At t_i, an initial height and speed are set and for that height, $\frac{dh}{dt}$ and $\frac{dV_{TAS}}{dt}$ are calculated. These are added to the initial speed and height to get the input for t_{i+1}. The time interval between t_i and t_{i+1} is one second. This is continued until the height a configuration change is required.

Non-clean configuration

The non-clean configuration part follows the clean configuration part at the height a configuration change is required, until sea level. A configuration change is required, when a certain altitude and speed limit is reached, shown in figure 4.13. The minimum cruise speed ($Vmin, CR$) is the stall CAS for cruise configuration times the safety factor of 1.23. The cruise stall speed is calculated using equation 4.6, using the maximum lift coefficient for cruise configuration. The minimum approach speed ($Vmin, CR$) is the stall CAS for the approach configuration of the aircraft times the 1.23 safety factor. This approach stall speed is calculated in the same way as the cruise stall speed except now the approach configuration maximum lift coefficient is used. In both cases an additional 10 knots is added.

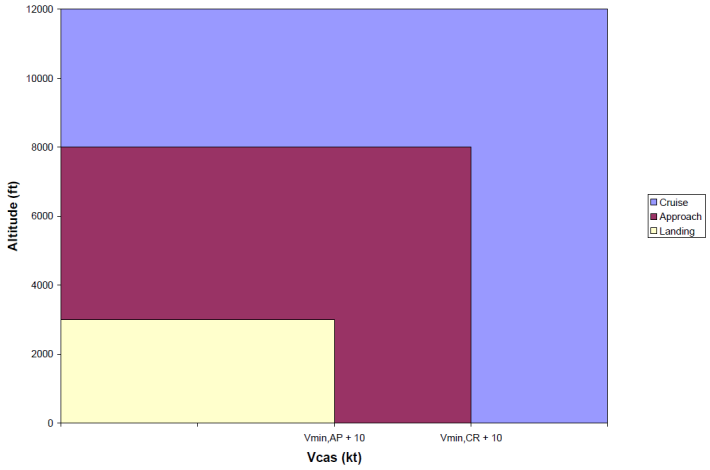

Figure 4.13: configuration change threshold on descent.

When the configuration change takes place, the aircraft follows a flight path angle of three degrees to intercept the glideslope of the ILS [2]. As a result of the required flight path, thrust has to be increased to maintain the speed defined in the speed schedule. The required amount of thrust is derived from equation 4.1. To implement the flightpath angle in equation 4.1, the $\frac{dh}{dt}$ in equation 4.1 is substituted by equation 4.8, obtaining equation 4.9.

$$\frac{dh}{dt} = V_{TAS} sin\gamma \tag{4.8}$$

$$(Thr - D) \cdot V_{TAS} = mg_0 V_{TAS} sin\gamma + mV_{TAS} \frac{dV_{TAS}}{dt} \tag{4.9}$$

By eliminating V_{TAS} on both sides and move D to the opposite of equation, equation 4.10 is obtained. Assuming level flight at constant speed is maintained equation 4.10 can be rearranged to equation 4.11[30].

$$Thr = D + mg_0 sin\gamma + m\frac{dV_{TAS}}{dt} \tag{4.10}$$

$$Thr = D + mg_0 sin\gamma + \frac{mg_0}{2\rho g_0} \frac{\partial \rho}{\partial h} V_{TAS}^2 sin\gamma \tag{4.11}$$

Based on the calculated thrust, the fuel flow can be extracted from BADA. The number of iterations determines the flight time and fuel consumption required to get from the sequencing leg to sea level. The fuel consumption is obtained by the summation of the fuel flow at each iteration. This completes the calculations of the entire CDA segment. An example CDA profile for three different aircraft types is shown in figure 4.14. Due to the different lift over drag ratios for each aircraft type, the distance required to perform the descent is different. However, the CDA segment is a fixed distance. To compensate for aircraft descending faster, a level segment at the initial height (the height of the sequencing leg) is added before the CDA until the total length of the CDA segment is reached.

Now that the calculation are complete, an example CDA profile for a Boeing 737-800 aircraft is shown in figure 4.15. The CDA is performed from a sequencing leg at a height of 10,000 ft to sea level. In figure 4.15a, the true airspeed and the calibrated airspeed versus time are shown. When the aircraft starts its descent, the true airspeed decreases while the calibrated airspeed is constant. Below a height of 6,000 ft, the calibrated airspeed changes according to the speed schedule shown in table 4.2. Note that the speed changes are instant.

In figure 4.15b, the fuel flow versus time is shown. Prior to the descent of the aircraft, a level segment is flown as shown in figure 4.15c. As a result, the fuel flow for the level part is high. The drop in fuel flow is due to the start of the CDA, limiting the thrust to idle. At about 300 seconds, the configuration of the aircraft changes to the approach configuration. Therefore, the thrust is increased to fly a three degrees flight path angle and maintain the speed provided in figure 4.15a. The sudden dip in fuel flow

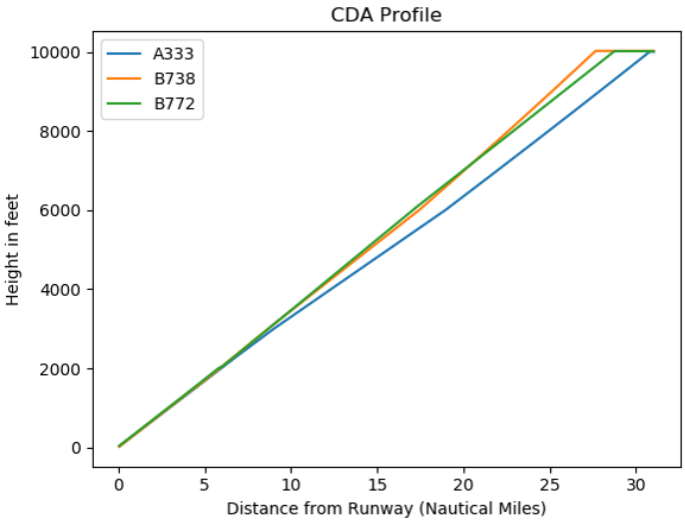

Figure 4.14: CDA profile for different aircraft from 10,000 ft.

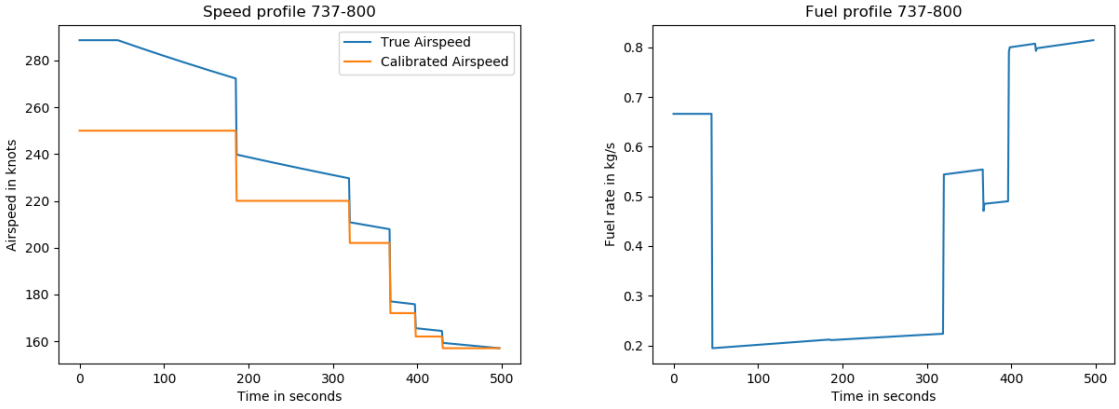

(a) Speed profile

(b) Fuel flow profile

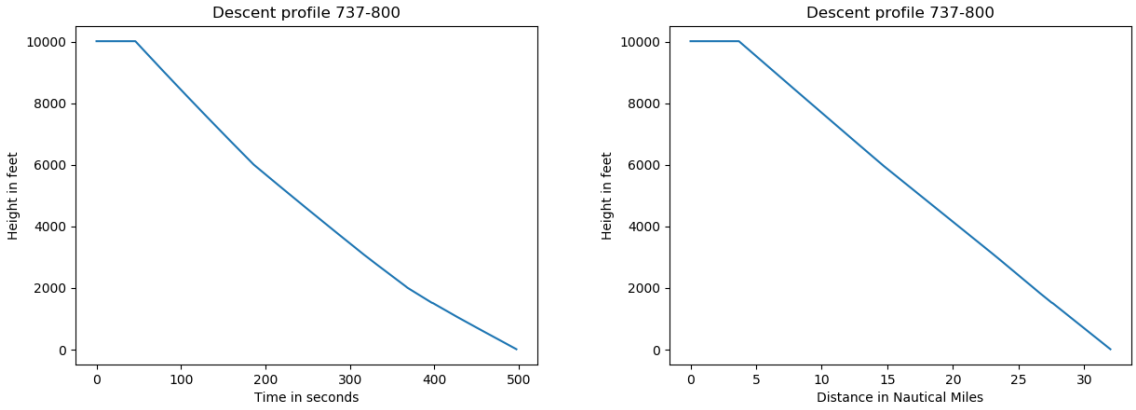

(c) Height profile.

(d) Height per distance travelled

Figure 4.15: BADA CDA calculation for a Boeing 737-800 aircraft from 10,000 ft.

is explained by the change of airspeed at that time. The fuel flow increases again when the approach configuration is changed to the landing configuration. In figure 4.15c and figure 4.15d the height versus

time and height versus distance travelled are shown.

The CDA segment calculations are performed for each aircraft type and for each sequencing leg. The total flight time, and fuel consumed obtained are stored and used as input for the scheduling model.

4.4. Noise Calculations

Following the performance calculations, the process of creating a noise contour map is explained in this section. Different to the performance calculations, the noise calculations are performed after the optimisation of the scheduling model. In figure 4.16, the process of generation a noise contour map according ICAO is shown. First, the flight path, geometry, speed and thrust are determined using the performance calculations. Second, the noise of each individual flight must be calculated. Third, the cumulative noise of each flight is added. The noise contour is calculated and lastly the data is processed into a graph. This same method is used in this thesis for calculating the noise contour map.

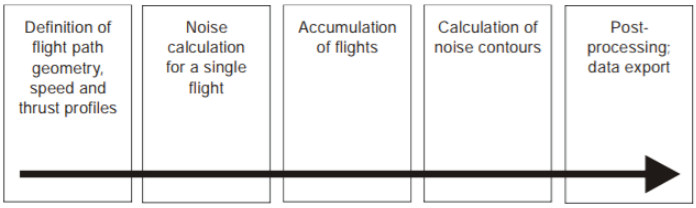

Figure 4.16: Process to generate a noise contour [39]

This section is divided into four subsections. In subsection 4.4.1, the method of defining the flight path, geometry, speed and thrust is elaborated. In subsection 4.4.2, the noise calculations of a single flight are discussed. In subsection 4.4.3, the method of calculating cumulative noise levels is explained. Finally, in subsection 4.4.4, the aircraft mix and engine selection used for calculating noise are shown.

4.4.1. Flight tracks and performance calculations

Before the noise of a single flight can be calculated, the flight path and flight performance of the flight has to be determined. The flight paths are noted by the x and y coordinates of the entire trajectory of the aircraft. The performance calculations required are: thrust, true airspeed and height at each coordinate of the flight path. Two different noise contour maps have to be made to compare the PMS with the current situation at AAS. The current situation is called the ”reference case”. For the PMS noise contour map, thrust, true airspeed and height for each aircraft are calculated using the performance calculations discussed in section 4.3. However, the x and y coordinates of this flights have to be calculated. On the other hand, for the reference case, the x and y coordinates and the height is already defined. Therefore, the thrust and true airspeed need to be obtained. In this subsection the way of obtaining the flight path of the PMS results is explained. After that, the calculation of thrust and true airspeed of the reference case is elaborated.

PMS results

For the PMS results, the x and y coordinates of aircraft are calculated. Each flight in the PMS has a common flight path in the initial and CDA segment. However, the sequencing leg segment is variable. The length of the sequencing leg segment depends on the turn-point of the flight. The output of the scheduling model includes the turn-point of each flight, defining the entire trajectory for all segments in the PMS. Coupled with the trust, true airspeed and height at each coordinate, the noise of each individual aircraft can be calculated.

Reference results

For the reference case, current flight data is used. This flight data contains the flight path coordinates of each aircraft in the dataset. However, the thrust and true airspeed need to be calculated. Both parameters are calculated using the performance calculations as seen in section 4.3. It is assumed that the speed profiles are equal to the speed schedules given in BADA, as shown table 4.2. As the speed, the vertical speed and coordinates are known, the thrust can be calculated. It is assumed that whenever the reference aircraft in cruise configuration is descending, thrust levels are idle. Comparable

to the performance calculations of the CDA segment in the PMS. However, if a part of the flight path in the flight data is level, thrust is calculated as cruise thrust. Setting the thrust equal to the drag as seen in equation 4.2. When the minimum clean configuration airspeed is reached a configuration change is performed using the limits shown in figure 4.13. In that case, the flight path angle is set to three degrees. In order to maintain the three degrees flight path angle and maintain the speed schedule, thrust is increased. Thrust in non-clean configuration is calculated using equation 4.11.

4.4.2. Single flight noise calculation

Following the trajectory and performance, noise of a single flight can be calculated. For both the PMS results and the reference results, the calculation of single flight noise is the same. For noise calculations of a single flight, the Integrated Noise Model (INM) is used, designed by the Federal Aviation Administration to compute standard noise assessments around the airport vicinity [12]. This research uses an adjusted version of the Integrated Noise Model (INM) without the user interface, to reduce computational time. Additionally, the adjusted version can be implemented into the post-processing of the scheduling model. This adjusted version is called the INMTM v3 model. The inputs of this model are: the entire flight path, trust and true airspeed at each coordinate of the flight path of a single flight. Additionally, a grid has to be defined where the aircraft noise is calculated. For this research, a 2D grid will be used. The dimensions of the grid are selected, such that the whole PMS fits inside the grid, as well as the arrival routes. The limiting factor of the grid is that the size cannot exceed $10,000\ km^2$ and the number of grid points cannot exceed $641,601$. The area where the noise for this research is calculated is shown in figure 4.17.

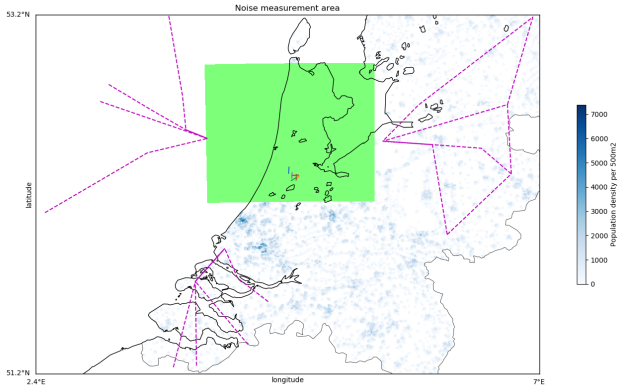

Figure 4.17: Noise measurement area.

The exact grid dimensions for measuring the noise are in rijksdriehoeks coordinates: a square which runs from 58,000m to 162,000m on the x axis and from 465,000m to 550,000m on the y axis, spanning an area of 88,400 km^2. Gridpoints are evenly spread 500 m apart, summing up to a total of 35,360 points. The area is chosen to fit all sequencing legs inside the grid. The rijksdiehoeks coordinate system is a coordinate system defined for the Netherlands with as centre the city of Amersfoort. The output of the model is the SEL, denoted as L_{AE} (dB), at each grid point for each individual flight. The INMTM v3 model calculates the SEL using equation 4.12.

$$L_{AE} = 10 \cdot \log\left(\frac{1}{t_0}\int_{t_1}^{t_2} 10^{\frac{L_A(t)}{10}}\,dt\right) \tag{4.12}$$

In equation 4.12, t_0 is the reference time of one second. The interval from t_1 to t_2 ensures that all significant noise is included when the event has passed.

4.4.3. Cumulative Noise Calculation

When the SEL is known for each individual aircraft the total noise exposure of all flights can be calculated using equation 4.13. This is the sum of all noise events during time interval T_0 at each grid point.

$$L_{DEN} = 10 \cdot \log\left(\frac{1}{T_0}\sum_{i=1}^{N} 10^{\frac{L_{AEi}+W_i}{10}}\right) \tag{4.13}$$

For computing the noise for an entire day, the noise interval T_0 is equal to 24 hours. However, in this research the noise contour is only calculated for the time span of the case study and not for the entire day. Depending on the time of day a weighting factor can be incorporated for flights during the day, evening and night. The weight during the day is 1 dB, for evening 3.162 dB and during the night 10 dB [26]. In this research, the weight penalty is less important because only the noise contours of the reference and the results PMS are compared. With the cumulative noise value determined for each grid point, a noise contour map can be made using python.

4.4.4. Aircraft Mix and Engines

Because BADA does not support all aircraft and the list of aircraft is limited, the following list of aircraft in table 4.4 are included in this research. The list is based on the most used aircraft at AAS, except for the Boeing 717 HGW, which represents the Embraer 190. Different types of aircraft in the case study are approximated by an aircraft in the list based on Maximum Take-off Weight (MTOW) and ICAO weight class. Two types of heavy aircraft are included. The INM requires an engine type to be selected for each aircraft, therefore for each aircraft an engine type is selected, shown in the last column of table 4.4.

Table 4.4: The aircraft where all aircraft are approximated by.

Aircrafttype	ICAO weight	MTOW (kg)	Engine Type
Airbus A330-300	Heavy	212000	CF680E
Airbus A319	Large	70000	CFM565
Airbus A320	Large	77000	CFM565
Boeing 737-800	Large	79016	CF567B
Boeing 737-700	Large	70080	CF567B
Boeing 717 HGW	Large	54884	BR715
Boeing 777-200	Heavy	286900	TRENT8

5

Mixed Integer Linear Programming Formulation

In the previous chapter the PMS route network design, flight calculations and noise calculations components of the methodology are discussed. This chapter continues with the final component of the methodology, namely the MILP formulation of the aircraft scheduling problem. The basis of this is the discrete routing and continuous time scheduling model used as in [14] by Capozzi. This model was adapted by Hong to be used for the PMS[35]. In this study, variable speeds are added to the model.

The chapter is divided into four sections to explain the MILP formulation used in the scheduling model. It begins by giving a brief overview of the MILP is in section 5.1. Section 5.2 identifies the different sets and parameters used for the MILP formulation. Section 5.3 shows the parameters which are decision variables. The objective functions are elaborated in section 5.4. Finally, in section 5.5, the constraints in the MILP form for this research are explained.

5.1. Mixed-Integer Linear Programming

The scheduling model for the PMS uses mixed integer linear programming in order to solve the problem. Linear programming is a mathematical model which describes the problem. It is called linear because all equations are required to be linear functions. Equation 5.1, shows the standard model.

$$\begin{aligned} &\text{minimize} && c^T x \\ &\text{subject to} && Ax \leq b \\ &\text{and} && x \geq 0 \end{aligned} \tag{5.1}$$

The goal is to minimise or maximise a linear function, which is called the objective function. This function has the form $c^T x$. The parameter c denotes the cost, which is coupled to a decision variable x. The parameter x is called the decision variable as it determines the cost increase or decrease. The decision variable is bound by a set of restrictions, called constraints. Two types of constraints are identified. First, the functional constraints which are in the form $Ax \leq b$. The functional constraints can be both equality and inequality constraints. Second, the non-negativity constraints, which assure the decision variable to be equal or greater than zero. The decision variable can be integer, binary or real-valued.

For the ASP, the MILP formulation is widely used to solve the static case[10]. The advantage of MILP is that it is an exact method, which yields an optimal solution. The downside is that for a larger set of aircraft and constraints the computational time grows exponentially. To overcome the increase in computational time, exact solutions, heuristics, meta-heuristics and different solving techniques can be used [3]. An elaboration of each technique can be found in the literature study [16]. It has to be noted that the solution found using (meta)-heuristics and other solution techniques are feasible, but not necessarily the optimal solution. The solutions can result in a near optimal (acceptable) solution in a shorter computational time. In this research a practical algorithm of Constraint Position Shift (CPS) is implemented and the rolling horizon technique is applied to help reduce the computational time. In this section, first, the method of CPS is explained. Second, the rolling horizon technique used is discussed.

5.1.1. Constraint Position Shift

To reduce the computational time needed to come up with an optimal solution, the number of possible order shifts in the sequencing are limited. Three possible CPS solutions exist: FCFS, Relative Position Shift (RPS) and Maximum Position Shift (MPS) [45]. The practical algorithm FCFS ensures that no position shifts are allowed, preventing the sequence to be changes after the IAF. The FCFS algorithm, reduces the number of possible order combinations, reducing the computational time. However, due to the separation requirements FCFS increases the makespan, which is undesirable. Therefore, MPS is introduced. This algorithm allows for aircraft to move up or down the sequence with a maximum number of positions. Normally, the maximum number of position shifts in the sequence is three[41]. In essence, the FCFS is a MPS of zero.

The closer the aircraft is to the runway, the less time there is available for switching positions and the more difficult it becomes. The technique of RPS defines a MPS depending on the position or place the aircraft has in the sequence. For example, closer to the runway the maximum position shift is lower than further away in the sequence.

This research uses the practical algorithms: FCFS and MPS. Limiting the aircraft to FCFS is used as a baseline to compare the PMS results to the current situation, where FCFS is used. A MPS of one and two position shifts will be used to examine the benefits obtained by allowing the sequence to be changed.

5.1.2. Rolling Horizon

When the number of flights increases, the landing time of the last aircraft does not influence the landing time of the aircraft as the landing times are far apart. If the timeline is long the interaction between these aircraft becomes negligible. Instead of solving the model for the entire aircraft set at once, a time-horizon or event-horizon can be introduced in order to decrease computational time [36][58]. For this research, an event horizon is introduced to break down the entire timeline into several smaller sub-problems. The event based rolling horizon used for this research is explained using the example illustrated in figure 5.1.

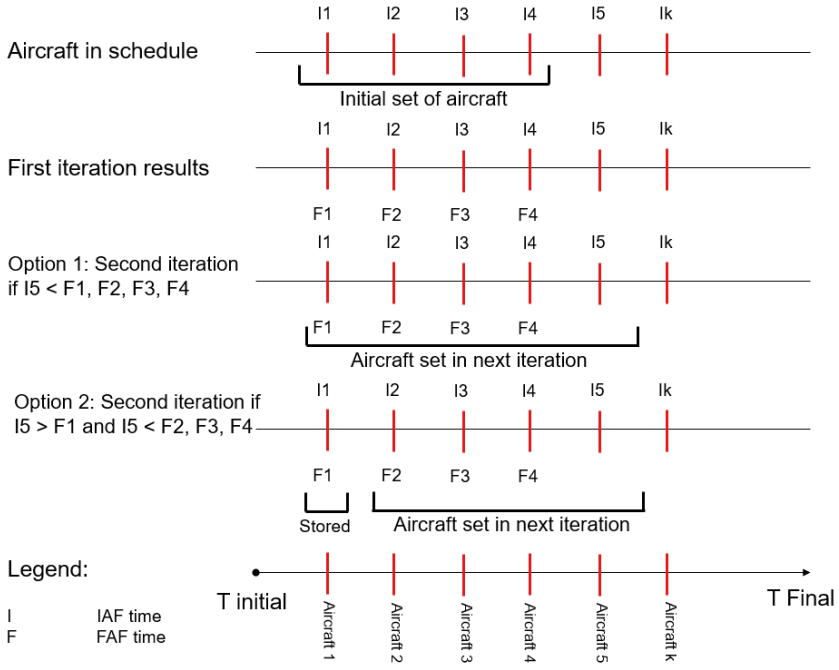

Figure 5.1: Event based rolling horizon example for FCFS.

A total set of k aircraft has to be scheduled (shown by the red lines). The IAF time (I) of each aircraft is known and the total set is sorted by in the order of arrival at the IAF. First, a limited set of aircraft, denoted as the initial set of aircraft, is solved and a solution is found. The amount of initial aircraft is a manual input. A minimum of one aircraft can be used as initial set, up to a maximum of all aircraft in the set. If all aircraft are in the initial set, the static case is performed. For the example in figure 5.1, a set

of 4 aircraft is chosen as initial set, shown in the first row. For the initial set, the schedule is optimised and the FAF times (F) are obtained for each aircraft in the set (shown in the ”first iteration result” row). The following aircraft, in the total set of k aircraft, is added for the next iteration. In the example aircraft 5 is added. Based on the IAF time of aircraft 5, two options can occur:

- **Option 1**: The IAF time of aircraft 5 is earlier than the FAF times of the aircraft in the initial set. This means that when aircraft 5 enters the system, all preceding aircraft are still in the PMS. As a result, aircraft 5 is added to the initial set. The new set of 5 aircraft is used as set for the next iteration.

- **Option 2**: The IAF time of aircraft 5 to the set is later than one or more FAF times of aircraft in the initial set. The data of the aircraft with a FAF earlier than the IAF of the added aircraft are stored and the aircraft is removed from the next iteration. In the example shown in figure 5.1, aircraft 5 has a IAF time later than the FAF time of aircraft 1. Therefore, aircraft 1 is removed from the next iteration and the output of the scheduling model of that aircraft is stored in a database.

After each iteration, the following aircraft in the total set of k aircraft is added, until the last aircraft, aircraft k, is added. The IAF time of the added aircraft is compared to the FAF times of the aircraft set performed in the prior iteration. When this IAF time is earlier than the FAF times of the aircraft in the set, a new iteration is performed (option 1). On the other hand, when the IAF time is later than one or more FAF time of the aircraft in the set, the aircraft are removed and stored for the next set of aircraft (option 2). The window of aircraft slides because of the aircraft which are stored and not included into the next the iteration, while a new aircraft is added each iteration. The rolling horizon method of figure 5.1 holds for the FCFS case. However, when position shift in the sequence is allowed, the case shown in figure 5.2 can occur.

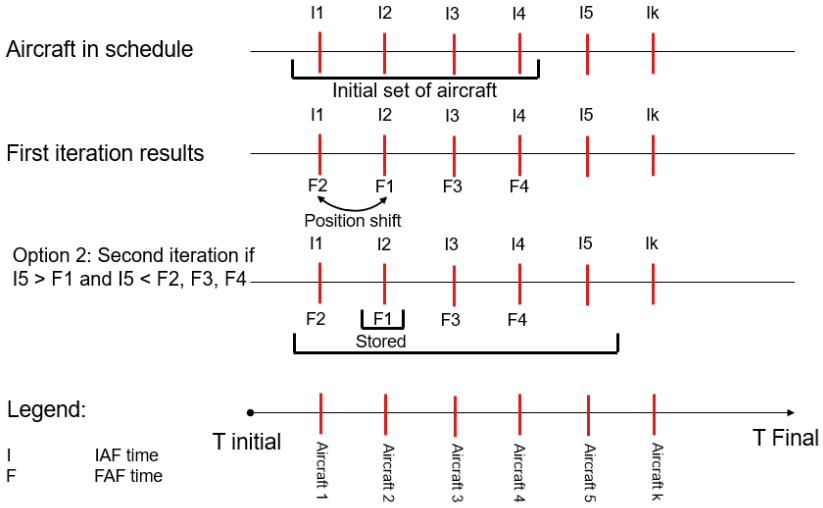

Figure 5.2: Event based rolling horizon example for MPS.

In this case, a position shift takes place, switching the FAF times of aircraft 1 and 2. Aircraft 5 is added to the initial set, but now the IAF time of aircraft 5, is later than the FAF time of aircraft 2. However, aircraft 2 is not removed from the next iteration, because the trajectory of aircraft 1 depends on the trajectory of aircraft 2. Both aircraft 1 and 2 are removed only after the FAFs are both before the IAF time of new aircraft added to the set of aircraft.

5.2. Sets and parameters

In the previous sections the principle of MILP is explained and the exact algorithms CPS and event-based rolling horizon are introduced. Now the formulation for the scheduling model in MILP form can be shown. First, the sets and parameters, as used in the MILP formulation, need to be identified. The

MILP formulation uses the following sets:

$f \in \mathcal{F} \equiv \{f_1, f_2, \dots, f_{N_f}\}$ = set of all flights, where N_f is the total number of flights.
$r \in \mathcal{R} \equiv \{r_1, r_2, \dots, f_{N_r}\}$ = set of all routes, where N_r is the total number of routes.
$p \in \mathcal{P} \equiv \{p_1, p_2, \dots, f_{N_p}\}$ = set of all points, where N_p is the total number of points.

The MILP formulation of the scheduling problem comprises the following parameters:

P_F : final point which in this research is the FAF.
P_I : is the initial point of the PMS which is equivalent to the entry point of the sequencing leg.
P_T : The actual point on the sequencing leg where the aircraft turns towards the merge point.
T_f^{IAF} : IAF arrival time in seconds of aircraft f.
$T_{f,r}^{CDA}$: Total duration in seconds of the CDA procedure for aircraft f on route r.
$V_{f,r,p}^{max}$: Maximum true airspeed in knots allowed for aircraft f on route r at point p.
$V_{f,r,p}^{min}$: Minimum true airspeed in knots allowed for aircraft f on route r at point p.
d^{leg} : the discrete distance in nautical miles between turn-points on the sequencing leg.
$d_{r,p_I}^{initial}$: Distance in nautical miles from the IAF to the initial point of the PMS on route r.
$d_{f,r}^{turn}$: Total distance from the entry point to the turnpoint for aircraft f on route r.
d_r^{seq} : Maximum length of the sequencing leg for route r in miles.
$SEP_{f,f'}$: Minimum wake vortex separation (in NM) between leading aircraft f and trailing aircraft f'.
$V_{initial_f}$: The initial true airspeed of aircraf f in the initial segment of the PMS.
V_{leg_f} : The sequencing leg true airspeed of aircraf f over the sequencing leg segment of the PMS.
V_{final_f} : The final approach true airspeed of aircraf f.

5.3. Decision variables

Using the sets and parameters the following decision variables are defined:

$A_{f,r}$ – A binary value which is 1 if aircraft f is assigned to route r and zero otherwise.
$T_{f,r,p}$ – A real variable which represents at which time, flight f on route r arrives at point p.
$S_{f,f',r,r',p}$ – A binary variable which is 1 when flight f on route r is before flight f' on route r' checked at point p.
$Z_{f,r,p}$ – A real variable which represents the fuel used by flight f on route r at point p.

5.4. Objective Function

Two objective functions are defined in this section. The first objective concerns the makespan. This is the total time span between the landing time of the first aircraft in the sequence and the landing time of the last aircraft in the sequence. By minimising the makespan the runway throughput is maximised. The second objective is to minimise the sum of the total fuel each aircraft uses. This relates to the environmental impact as more fuel-used causes more emissions. In the following two subsections both objective functions are discussed.

5.4.1. Minimize total time

In equation 5.2 the performance index of this optimisation problem is shown. The total sum of final time is minimised. For all aircraft in the set and all routes in the set, the time at the final point p_F is summed, but only if the aircraft flies over that particular route $A_{f,r}$.

$$J = \min \sum_{f \in \mathcal{F}} \sum_{r \in \mathcal{R}^f} A_{f,r} T_{f,r,p_F} \tag{5.2}$$

The equation is not linear as it is a product of two variables. The variable $A_{f,r}$ is a logical value which is binary while T_{f,r,p_F} is a real-continuous value. By introducing an auxiliary variable, the objective function can be converted into a linear function [9]. The following variable is introduced:

$$\delta^T_{f,r,p_F} \triangleq A_{f,r} T_{f,r,p_F} \tag{5.3}$$

Upon, substituting equation 5.3 into equation 5.2, the following objective function is obtained:

$$J = \min \sum_{f \in \mathcal{F}} \sum_{r \in \mathcal{R}^f} \delta^T_{f,r,p_F} \tag{5.4}$$

Along with the set of equations in equation 5.5, the objective function is converted to a linear function using the so-called big M approach [32]. In equation 5.5, the parameter M is an arbitrarily large number.

$$\begin{aligned} \delta^T_{f,r,p_F} &\geq T_{f,r,p_F} - M(1 - A_{f,r}) \\ \delta^T_{f,r,p_F} &\leq T_{f,r,p_F} + M(1 - A_{f,r}) \end{aligned} \tag{5.5}$$

5.4.2. Minimise total fuel-used

Instead of maximising the capacity, fuel-used can be minimised. In this case, the objective function is expressed as in equation 5.6, where Z_{f,r,p_F} denotes the total-fuel used at the final point. In this study, the fuel-used can vary as a result of the variable speed and the variable time in the sequencing leg. The total fuel-used comprises the fuel-used in the initial, sequencing leg and CDA segment.

$$J = \min \sum_{f \in \mathcal{F}} \sum_{r \in \mathcal{R}^f} Z_{f,r,p_F} \tag{5.6}$$

Both equation 5.6 and equation 5.3 can be combined to optimise for both fuel burn and the makespan. A weight factor $w \in [0, 1]$ is added to combine the two equations and to see the effect when making one criterion more important than the other. The combined objective function is shown in equation 5.7, where $w^z = w$ and $w^T = (1 - w)$.

$$J = \min \sum_{f \in \mathcal{F}} \sum_{r \in \mathcal{R}^f} w^z \cdot Z_{f,r,p_F} + w^T \cdot \delta^T_{f,r,p_F} \tag{5.7}$$

5.5. Constraints

In this section, the constraints of the scheduling model in MILP form are explained. In total, eight sets of constraints are included into the model.

5.5.1. Single Route

The first set of constrains assures that at least one route is assigned to each aircraft and that only one route is assigned to each aircraft. Because the aircraft are in the air, a route has to be assigned.

$$\sum_{r \in \mathcal{R}^f} A_{f,r} = 1, \quad \forall f \in \mathcal{F} \tag{5.8}$$

5.5.2. Initial Time and Speed

Before the aircraft enters the PMS, the initial segment is flown from the IAF to the entry point of the PMS. The airspeed on this segment can vary, which affects the entry time of the aircraft in the system. This constraint is shown in equation 5.9.

$$A_{f,r} \left(T_{f,r,p_I} - T^E_{f,r,p_I} \right) \geq 0, \quad \forall f \in \mathcal{F}, \quad \text{and} \quad \forall r \in \mathcal{R}^f \tag{5.9}$$

If a flight is assigned to route A, the initial time at the first point in the PMS is greater or equal to a specified minimum initial time. This equation is also non-linear, but by introducing an axillary variable δ^T_{f,r,p_I}, as in equation 5.5, equation 5.9 is converted to a linear form shown in equation 5.10.

$$\delta^T_{f,r,p_I} - A_{f,r} T^E_{f,r,p_I} \geq 0, \quad \forall f \in \mathcal{F}, \quad \text{and} \quad \forall r \in \mathcal{R}^f \tag{5.10}$$

The parameter T^E_{f,r,p_I} is the earliest time the aircraft can arrive at the entry point and is calculated using equation 5.11. The earliest time the aircraft can be in the PMS is when it flies its maximum allowed speed, which is calculated as in section 4.3. Thus, T^E_{f,r,p_I} is the IAF time of the aircraft, plus the distance in nautical miles to the initial point of the PMS divided by the maximum true airspeed in knots.

$$T^E_{f,r,p_I} = T^{IAF}_f + \frac{d^{initial}_{r,p_I} \cdot 60 \cdot 60}{V^{max}_{f,r,p}} \tag{5.11}$$

This is the earliest time the aircraft can be in the PMS, but there is also a minimum speed the aircraft can fly. Therefore, a constraint is added for the latest time an aircraft can arrive at the entry point (T^L_{f,r,p_I}). This can be seen in equation 5.12:

$$\delta^T_{f,r,p_I} - A_{f,r} T^L_{f,r,p_I} \leq 0, \quad \forall f \in \mathcal{F}, \quad \text{and} \quad \forall r \in \mathcal{R}^f \tag{5.12}$$

Instead of the maximum speed now the minimum speed depends on the latest time the aircraft can be at the PMS. This can be seen in equation 5.13.

$$T^L_{f,r,p_I} = T^{IAF}_f + \frac{d^{initial}_{r,p_I} \cdot 60 \cdot 60}{V^{min}_{f,r,p}} \tag{5.13}$$

The earliest and latest time differ per aircraft type, as the maximum speed and minimum speeds are different for each aircraft type. But it also changes per sequencing leg, as the height of the sequencing leg also influences the minimum and maximum speeds. As the initial speed can variate between the minimum and maximum speed, the actual speed flown by the aircraft has to be determined to calculate the fuel-used. Based on the segment length from the IAF to the PMS the actual speed flown can be calculated as in equation 5.14.

$$\delta^T_{f,r,p_I} - A_{f,r} T^{IAF}_f - \frac{d^{initial}_{r,p_I} \cdot 60 \cdot 60}{V_{initial_f}} = 0, \quad \forall f \in \mathcal{F}, \quad \text{and} \quad \forall r \in \mathcal{R}^f \tag{5.14}$$

5.5.3. Sequencing leg time and speed

The airspeed in the sequencing leg can vary as well. This means that the aircraft can be earlier or later at the turn-point of the flown route. As both the speed and distance to the turn-point are variable, the sequencing leg is discretised into segments of 1 nautical mile in length, to have at least one parameter fixed.

An example PMS discretised into three segments of 1 NM is shown in figure 5.3. It is shown that aircraft fly a common initial segment, but after the entry point (P_I), the aircraft can choose four different routes, depending on the required separation. For route 1, the turn-point is P_I, for route 2 the turn-point is P_1, etc. The speed along the sequencing leg can vary however, due to the constant speed in the sequencing leg the minimum and maximum travel time to each turn-point for each route can be calculated. The constraint for minimum time to travel from the entry point P_I to the turn-point p of route r is shown in equation 5.15.

$$A_{f,r}\left(T_{f,r,p_T} - T^E_{f,r,p}\right) \geq 0, \quad \forall f \in \mathcal{F}, \quad \text{and} \quad \forall r \in \mathcal{R}^f \quad \text{and} \quad \forall p \in \mathcal{P}^r \tag{5.15}$$

To transform equation 5.15 into a linear form, an axillary variable δ^T_{f,r,p_T} is introduced for each (turn)-point on the sequencing leg. This establishes the travel time from p_I to the turn-point for each route. By substituting axillary variable δ^T_{f,r,p_T} in equation 5.15, equation 5.16 is obtained.

$$\delta^T_{f,r,p_T} - A_{f,r} T^E_{f,r,p} \geq 0, \quad \forall f \in \mathcal{F}, \quad \text{and} \quad \forall r \in \mathcal{R}^f \quad \text{and} \quad \forall p \in \mathcal{P}^r \tag{5.16}$$

The minimum travel time on the sequencing leg depends on the distance from the entry point to the turn-point and the maximum true airspeed of the aircraft type, shown in equation 5.17. The distance between the entry-point and the turn-point is the sum of each segment before the turn-point, where the distance of each segment (d_{leg}) is equal to 1 NM. In the example shown in figure 5.3, the distance of on the sequencing leg of route 3 is the summation of the distance between P_I and P_1, and the distance between P_1 and P_2. The maximum true airspeed differs for each aircraft type and the altitude of the sequencing leg.

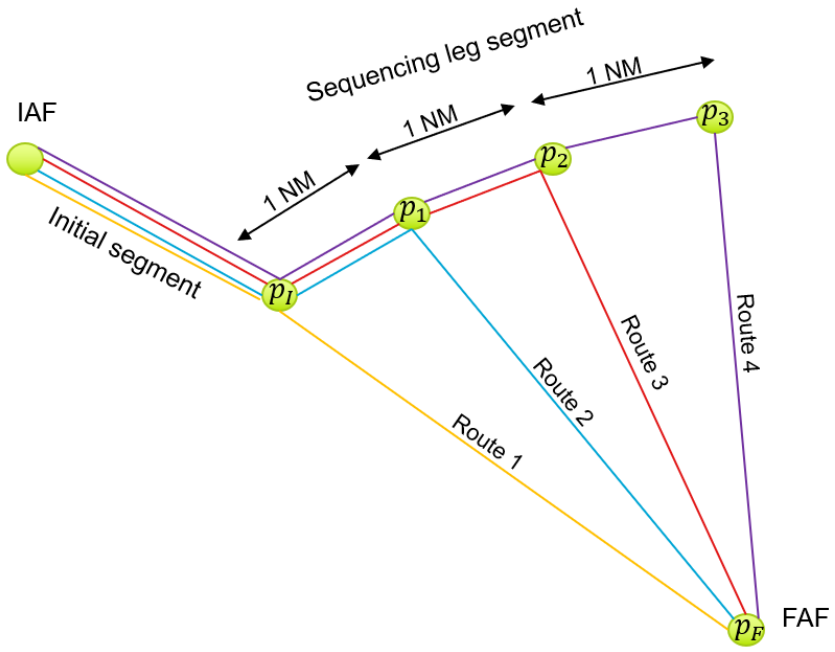

Figure 5.3: Example PMS discretised in segments of 1 NM.

$$T^E_{f,r,p} = \sum_{p_I}^{p_T} \frac{d_{leg} \cdot 60 \cdot 60}{V^{max}_{f,r,p}} \quad \forall p \in \mathcal{P}^r, \quad p \leq p_L \tag{5.17}$$

The same method used for calculating the minimum travel time is used for calculating the the maximum travel time. Instead of the maximum speed, the minimum true airspeed is taken. By replacing the earliest travel for the latest travel time equation 5.18 and 5.19 are obtained.

$$\delta^T_{f,r,p_T} - A_{f,r} T^L_{f,r,p} \leq 0, \quad \forall f \in \mathcal{F}, \quad \text{and} \quad \forall r \in \mathcal{R}^f \quad \text{and} \quad \forall p \in \mathcal{P}^r \tag{5.18}$$

$$T^L_{f,r,p} = \sum_{p_I}^{p_T} \frac{d_{leg} \cdot 60 \cdot 60}{V^{min}_{f,r,p}} \quad \forall p \in \mathcal{P}^r, \quad p \leq p_L \tag{5.19}$$

Finally, the actual true airspeed flown by the aircraft on the sequencing leg has to be calculated for the fuel consumption. The true airspeed on the sequencing leg is equal to the travel time at the turn-point divided by the distance between the entry point and the turn-point, shown in equation 5.20. The speed is obtained in knots.

$$\frac{\delta^T_{f,r,p_T}}{\sum_{p_I}^{p_T} d_{leg}} - \frac{60 \cdot 60}{V_{leg_f}} = 0, \quad \forall f \in \mathcal{F}, \quad \forall r \in \mathcal{R}^f, \quad \forall p \in \mathcal{P}^r, \quad p \leq p_L \tag{5.20}$$

5.5.4. Continuous Descent Approach time and speed

After the sequencing leg segment is completed, the CDA segment begins. Also, for this segment the time and speed has to be calculated. There is only one CDA profile for each route the aircraft can fly, which is the ideal CDA profile. The CDA profile differs for each aircraft type and sequencing leg. The constraint for travel time in the CDA segment is shown equation 5.21.

$$T^{CDA}_{f,r} = A_{f,r} T_{CDA_{f,r}}, \quad \forall f \in \mathcal{F}, \quad \text{and} \quad \forall r \in \mathcal{R}^f \tag{5.21}$$

The CDA travel time of from the turn-point to the FAF is denoted as $T_{CDA_{f,r}}$ in equation 5.21. The total CDA travel time have been determined in the performance calculations.

5.5.5. Ordering Constraint

To calculate the separation between aircraft, first the order in which the aircraft are sequenced has to be determined. For each pair of flights travelling on the same route or a different route with a shared common scheduling points, the order has to be determined. The general equation to determine the order at shared points is shown in equation 5.22.

$$\begin{gathered} S_{f,f',r,r',p} + S_{f',f,r',r,p} = A_{f,r}A_{f',r'} \\ \forall f, f' \in \mathcal{F}, \quad f \neq f', \quad \forall r \in \mathcal{R}^f, \quad \forall r' \in \mathcal{R}^{f'}, \quad \forall p \in \left[\mathcal{P}^r \cap \mathcal{P}^{r'}\right] \neq \emptyset \end{gathered} \tag{5.22}$$

The variable $S_{f,f',r,r',p}$ is a binary number which is 1 when flight f, travelling on route r is in front of flight f', travelling on route r', analysed at all shared points p. Equation 5.22 is non-linear and therefore, following the same method as for equation 5.5, an axillary variable $\delta^A_{f,f',r,r'}$ is introduced to obtain a linear form, where:

$$\delta^A_{f,f',r,r'} \triangleq A_{f,r}A_{f',r'} \tag{5.23}$$

By substituting equation 5.23 into equation 5.22, equation 5.24 is obtained. This is a linear equation, where $\delta^A_{f,f',r,r'}$ is a product of two logical variables subjected to the set of constraints of equation 5.25[9].

$$S_{f,f',r,r',p} + S_{f',f,r',r,p} = \delta^A_{f,f',r,r'} \tag{5.24}$$

$$\begin{gathered} -A_{f,r} + \delta^A_{f,f',r,r'} \leq 0 \\ -A_{f',r'} + \delta^A_{f,f',r,r'} \leq 0 \\ A_{f',r'} + A_{f,r} - \delta^A_{f,f',r,r'} \leq 1 \\ \forall f, f' \in \mathcal{F}, \quad f \neq f', \quad \forall r \in \mathcal{R}^f, \quad \forall r' \in \mathcal{R}^{f'}, \quad \forall p \in \left[\mathcal{P}^r \cap \mathcal{P}^{r'}\right] \neq \emptyset \end{gathered} \tag{5.25}$$

As the order can only be changed once in the PMS, only the order at the entry point (P_I) and the final point (P_F) has to be checked. The order is changed if the trailing aircraft turns towards the merge point earlier that the leading aircraft. The order at the entry point and final point can be calculated using equation 5.26 and 5.27, respectively.

$$S_{f,f',r,r',p_I} + S_{f',f,r',r,p_I} = \delta^A_{f,f',r,r'} \quad \forall f, f' \in \mathcal{F}, \quad \forall f \neq f' \quad \forall r \in \mathcal{R}^f, \quad \forall r' \in \mathcal{R}^{f'} \text{ and } \forall r = r' \tag{5.26}$$

$$S_{f,f',r,r',p_F} + S_{f',f,r',r,p_F} = \delta^A_{f,f',r,r'} \quad \forall f, f' \in \mathcal{F}, \quad \forall f \neq f' \quad \forall r \in \mathcal{R}^f, \quad \forall r' \in \mathcal{R}^{f'} \tag{5.27}$$

Because the sequencing legs are at different altitude, the entry point order of the PMS is only relevant for aircraft in the same system and sequencing leg. However, all aircraft have a common final point, the FAF of the runway used for landing.

To incorporate the FCFS order constraint, an extra constraint is introduced at the final point to force S_{f,f',r,r',p_F} to 1 preventing aircraft from switching position in the sequence. Note that, the parameter S_{f,f',r,r',p_F} only denotes the sequence between a pair of aircraft, but does not imply that a given aircraft is positioned directly prior to or after its pair. It only shows that an aircraft is sequenced some time prior to or after its pair. For implementing MPS, the T^{IAF}_f of the trailing aircraft f' behind leading aircraft f are sorted to know the immediate order behind aircraft f. The aircraft f' within the allowed maximum position shift uses the normal ordering constraint as in equation 5.27. However, for the aircraft positioned outside the allowed maximum positions shift, the parameter S_{f,f',r,r',p_F} is forced to 1 meaning that the trailing aircraft f' can not overtake aircraft f in the sequence. Note that the maximum number of allowed position shifts is a manual input.

5.5.6. Separation

Now the constraints determining the sequence of aircraft are known, the constraints to maintain the separation requirements are discussed in this subsection. In the PMS, the vertical and lateral separation requirements are maintained by design. Therefore, only on kind of longitudinal separation violations can occur in the PMS, trailing conflicts as illustrated in figure 5.4. Trailing conflicts occur when the trialling aircraft catches up the leading aircraft due to a speed difference.

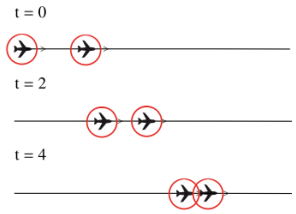

Figure 5.4: Two potential loss of separation conflicts: (a) cross conflict, (b) trailing conflict [11].

It is assumed that aircraft are sufficiently separated when entering the TMA. They fly at constant speed in each segment of the PMS, however the speed between aircraft in the same segment can be different. Therefore, the separation requirements have to be checked at each point a speed change occurs. Looking at figure 5.3, the following potential conflicting points can be identified:

- At the entry point of the PMS (P_I). As the initial segment is a common path and aircraft can fly at different airspeeds, trailing conflicts can occur.
- At the FAF point of the PMS (P_F). As in the CDA segment the aircraft merge to one point, there is a risk of trailing conflicts at the merge point.
- Over the common path on the sequencing leg. As aircraft can have different speeds on the sequencing leg, there is a risk of a trailing conflict. The common path is important, because depending on the route the aircraft take, the common path differs for each aircraft type.

The minimum longitudinal separation distance required is based on the ICAO vortex separation distances mentioned in table 3.4 of 3. This subsection, first explains the separation constraints at the entry and FAF of the PMS. Then, the separation constraints on the sequencing leg are identified.

Separation entry point and FAF
The longitudinal separation is checked at the entry point for both arriving and departing flights [17] as illustrated in figure 5.5. The aircraft are required to be at least the vortex longitudinal separation distance in miles separated measured at the entry point (p_I). Because the aircraft fly at different speeds, the distance based separation standards are converted to a time based separation standards by dividing it by the airspeed. Two conditions have to be checked:

- First, if aircraft f arrives at the entry point (p_I), the trailing aircraft f' should arrive at least the minimum vortex separation time later at the entry point. The minimum vortex separation time dependents on the minimum vortex separation distance between aircraft f and f'($SEP_{f,f'}$) and the initial segment airspeed of trailing aircraft f'($V_{initial_{f'}}$). This is called the separation between aircraft f and f' for arriving at point p.
- Second, if aircraft f' arrives at entry point (p_I), the leading aircraft should be at least the minimum separation time later at the entry point. However, now the minimum vortex separation time dependents on $SEP_{f,f'}$ and the sequencing leg segment airspeed of trailing aircraft f'($V_{leg_{f'}}$). This is called the separation between aircraft f and f' for departing point p.

In MILP form, the first condition is ensured by equation 5.28, the second condition is ensured by equation 5.29. It can be seen that the critical condition is the situation where the largest minimum vortex separation time is required.

$$A_{f',r'}T_{f',r',P_I} \geq A_{f,r}T_{f,r,P_I} + \frac{SEP_{f,f'}}{V_{initial_{f'}}} - M\left(1 - S_{f,f',r,r',p_I}\right) \tag{5.28}$$

$$A_{f',r'}T_{f',r',P_I} \geq A_{f,r}T_{f,r,P_I} + \frac{SEP_{f,f'}}{V_{leg_f}} - M\left(1 - S_{f,f',r,r',p_I}\right) \tag{5.29}$$

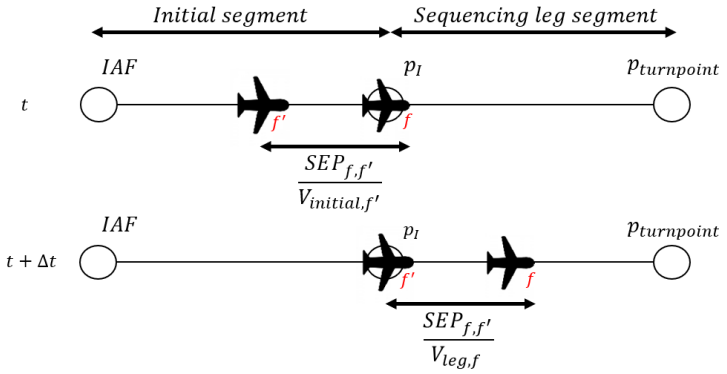

Figure 5.5: Separation checked between aircraft f and f', arriving and departing a point p.

For the FAF separation the same method is used to ensure the longitudinal vortex separation requirements, except now the final approach speed of aircraft is taken (V_{final_f}). The set of constraints in for this situation is shown in equation 5.31 and 5.30.

$$A_{f',r'}T_{f',r',P_F} \geq A_{f,r}T_{f,r,P_F} + \frac{SEP_{f,f'}}{V_{final_{f'}}} - M\left(1 - S_{f,f',r,r',p_F}\right) \tag{5.30}$$

$$A_{f',r'}T_{f',r',P_F} \geq A_{f,r}T_{f,r,P_F} + \frac{SEP_{f,f'}}{V_{final_f}} - M\left(1 - S_{f,f',r,r',p_F}\right) \tag{5.31}$$

Separation over sequencing leg

The constraint for maintaining the minimum vortex separation required over the sequencing leg follows the same principle as at the entry point and FAF, however the separation needs to be checked only at the common path of the aircraft pair on the same sequencing leg. This is a result of the different turn-points the aircraft can use to increase the separation distance. A pair of leading aircraft f and trailing aircraft f', when both flying over the same sequencing leg three situations can occur as shown in figure 5.6:

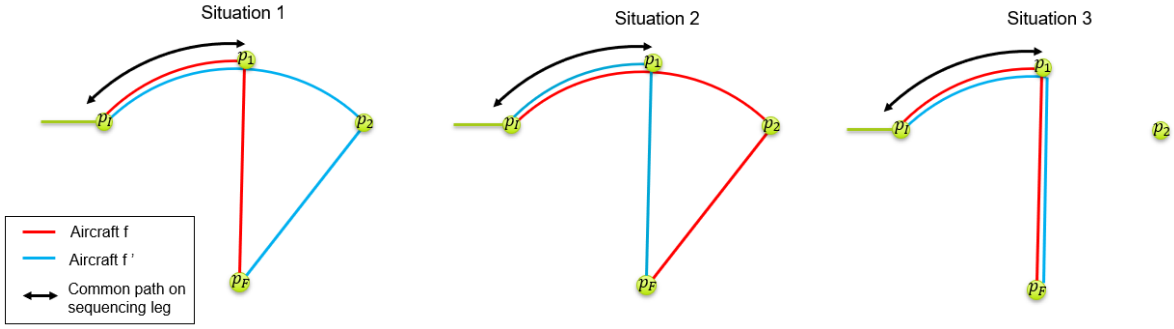

Figure 5.6: Three situation which can occur between a pair of aircraft on the sequencing leg.

1. Aircraft f has a turn-point on the sequencing leg before the turn-point of aircraft f'.
2. Aircraft f' has a turn-point on the sequencing leg before the turn-point of aircraft f.
3. Aircraft f and aircraft f' turn at exactly the same point on the sequencing leg.

For each of these situations, the separation has to be checked at the end of the common path, thus at the turn-point of the aircraft turning first. First, three slack variables are introduced to determine which of the three situations occurs. For situation 1, binary slack variable $S_{turn_{f,r}}$ is introduced. The parameter is 1 when the turn-point of aircraft f is before the turn-point of aircraft f'. For situation 2,

slack variable $S_{turn_{f',r'}}$ is introduced, which is 1 when the turn the turn-point of aircraft f' is before the turn-point of aircraft f.

$$\frac{d_{f,r}^{turn} A_{f,r}}{d_r^{seq}} - \frac{d_{f',r}^{turn} A_{f',r}}{d_r^{seq}} + S_{turn_{f,r}} \geq 0 \tag{5.32}$$

$$\frac{d_{f',r}^{turn} A_{f',r}}{d_r^{seq}} - \frac{d_{f,r}^{turn} A_{f,r}}{d_r^{seq}} + S_{turn_{f',r'}} \geq 0 \tag{5.33}$$

For situation 3, both $S_{turn_{f',r'}}$ and $S_{turn_{f,r}}$ are 0. An additional parameter $S_{equal_{f,r}}$ is added, which is 1 when the aircraft turn at the same turn-point on the sequencing leg. The equality constraint shown in equation 5.34 is added to make sure that in this case the $S_{equal_{f,r}}$ becomes 1 when $S_{turn_{f',r'}}$ and $S_{turn_{f,r}}$ are both 0.

$$S_{turn_{f',r'}} + S_{turn_{f,r}} + S_{equal_{f,r}} = 1 \tag{5.34}$$

As the order on the sequencing leg is the order at which the aircraft arrive into the system, for each three situations the initial order (S_{f,f',r,r',p_I}) is multiplied with the variables introduced in equation 5.32, 5.33 and 5.34. As this is not a linear form, but a product of two logical variables, an equivalent set of equations as in equation 5.25 is added. Situation 1 is true, if δ^S_{f,f',r,r',P_T} of equation 5.35 is 1, in this case the leading aircraft turns prior to the trailing aircraft on the sequencing leg. Situation 2 is true, if δ^S_{f',f,r',r,P_T} of equation 5.36 is 1. In this case the trailing aircraft turns at a point prior to the turn-point of the leading aircraft. Situation 3 is true, if δ^S_{f,f',r,r',P_E} is 1, when the turn-point of the leading and trailing aircraft are at the same point.

$$S_{turn_{f,r}} \cdot S_{f,f',r,r',p_I} = \delta^S_{f,f',r,r',P_T} \tag{5.35}$$

$$S_{turn_{f',r'}} \cdot S_{f,f',r,r',p_I} = \delta^S_{f',f,r',r,P_T} \tag{5.36}$$

$$S_{equal_{f,r}} \cdot S_{f,f',r,r',p_I} = \delta^S_{f,f',r,r',P_E} \tag{5.37}$$

For each of the three situations, the point where the common path on the sequencing leg ends, is where the separation requirement is checked. For situation 1, the common path ends at the turn-point of aircraft f (p_1). There is one general assumption for all situations: once an aircraft turns, it is off the sequencing leg and no separation has to be checked after the aircraft turns. The separation constraint for situation 1 is shown in 5.38.

$$A_{f',r'} T_{f',r',P_I} + \frac{A_{f,r} d_{f,r}^{turn}}{V_{LEG_{f'}}} \geq A_{f,r} T_{f,r,P_T} + \frac{SEP_{f,f'}}{V_{LEG_{f'}}} - M\left(1 - \delta^S_{f,f',r,r',P_T}\right) \tag{5.38}$$

The left-hand-side of equation 5.38, can be identified as the time aircraft f' arrives at the turn-point of aircraft f. This is equal to the entry time of aircraft f' plus the distance on the sequencing leg to the turn-point of aircraft f divided by the speed of aircraft f'. The left hand side must be equal or bigger than the turn-time of aircraft f plus the minimum required separation time between aircraft f and f'. Only the separation requirement for aircraft f arriving at the turn-point of aircraft f has to be checked, due to the constraint that once an aircraft turns, it is off the sequencing leg.

For situation 2, aircraft f continues over the sequencing leg after the point aircraft f' turns. Therefore, this situation both the separation requirement of aircraft f departing and arriving the turn-point of aircraft f' has to be checked. Equation 5.39 and 5.40 show the separation constraints for situation 2.

$$A_{f',r'} T_{f',r',P_T} \geq A_{f,r} T_{f,r,P_I} + \frac{A_{f',r'} d_{f',r}^{turn}}{V_{LEG_f}} + \frac{SEP_{f,f'}}{V_{LEG_{f'}}} - M\left(1 - \delta^S_{f',f,r',r,P_T}\right) \tag{5.39}$$

$$A_{f',r'} T_{f',r',P_T} \geq A_{f,r} T_{f,r,P_I} + \frac{A_{f',r'} d_{f',r}^{turn}}{V_{LEG_f}} + \frac{SEP_{f,f'}}{V_{LEG_f}} - M\left(1 - \delta^S_{f',f,r',r,P_T}\right) \tag{5.40}$$

For situation 3, when both aircraft turn at the same point the separation requirement is checked using the same method as for the entry point and the FAF and is shown in equation 5.41. The turn-time of aircraft f' must be larger than the turn-time of aircraft f plus the required vortex separation time.

$$A_{f',r'} T_{f',r',P_T} \geq A_{f,r} T_{f,r,P_T} + \frac{SEP_{f,f'}}{V_{LEG_{f'}}} - M\left(1 - \delta^S_{f,f',r,r',P_E}\right) \tag{5.41}$$

5.5.7. Total Transit Time

One of the decision variables included into the objective function is the total transit time (T_{f,r,p_F}). The total transit time is calculated using equation 5.42. The total transit time is equal to the sum of the duration of the initial segment (T_{f,r,p_I}), sequencing leg segment (T_{f,r,p_T}) and the CDA segment ($T_{f,r}^{CDA}$).

$$A_{f,r}\left(T_{f,r,p_F} - T_{f,r,p_I} - T_{f,r,p_T} - T_{f,r}^{CDA}\right) = 0 \tag{5.42}$$

5.5.8. Fuel Consumption Constraint

Fuel consumption is calculated using the equations in section 4.3. The fuel rate is non-linear function and therefore, it needs to be approximated by a piecewise linear function in the MILP formulation. An illustration is shown in figure 5.7 for a Boeing 737-800 aircraft flying at 10,000 ft. The fuel rate is approximated by two linear functions called a special ordered set. Where the slope changes halfway the feasible velocity range. Let the approximation of the fuel rate be as in equation 5.43[53].

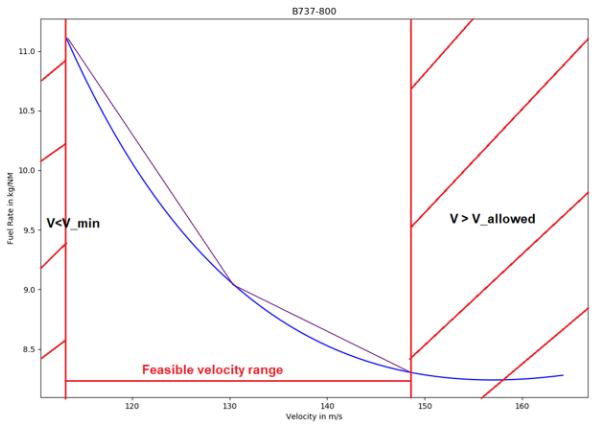

Figure 5.7: Stepwise linear approximation of the fuel rate per nautical mile.

$$FR_{f,r} = \begin{cases} \alpha_{f,r}^1 V_{LEG_{f,r}} + \beta_{f,r}^1 & \text{for} \quad V_{f,r,p}^{min} \leq V_{LEG_{f,r}} \leq \frac{V_{f,r,p}^{max} - V_{f,r,p}^{min}}{2} \\ \alpha_{f,r}^2 V_{LEG_{f,r}} + \beta_{f,r}^2 & \text{for} \quad \frac{V_{f,r,p}^{max} - V_{f,r,p}^{min}}{2} \leq V_{LEG_{f,r}} \leq V_{f,r,p}^{max} \end{cases} \tag{5.43}$$

The fuel rate which is in kilograms per nautical mile has to be converted to the fuel used in kilograms as can be seen in equation 5.44.

$$Z_{LEG_{f,r}} = FR_{f,r} d_{f,r}^{turn} \tag{5.44}$$

Substituting equation 5.43 in 5.44:

$$Z_{LEG_{f,r}} = \begin{cases} \left(\alpha_{f,r}^1 V_{LEG_{f,r}} + \beta_{f,r}^1\right) d_{f,r}^{turn} & \text{for} \quad V_{f,r,p}^{min} \leq V_{LEG_{f,r}} \leq \frac{V_{f,r,p}^{max} - V_{f,r,p}^{min}}{2} \\ \left(\alpha_{f,r}^2 V_{LEG_{f,r}} + \beta_{f,r}^2\right) d_{f,r}^{turn} & \text{for} \quad \frac{V_{f,r,p}^{max} - V_{f,r,p}^{min}}{2} \leq V_{LEG_{f,r}} \leq V_{f,r,p}^{max} \end{cases} \tag{5.45}$$

The resulting two linear functions are modelled using a special ordered set of type 2[6]. For implementing a special ordered set, the non-negative real variables of equation 5.46 are introduced for each aircraft and route.

$$V_{LEG} = V_{f,r,p}^{min} V_{LEG_1} + \frac{V_{f,r,p}^{max} - V_{f,r,p}^{min}}{2} V_{LEG_2} + V_{f,r,p}^{max} V_{LEG_3} \tag{5.46}$$

where:

$$V_{LEG_1} + V_{LEG_2} + V_{LEG_3} = 1 \tag{5.47}$$

Then the fuel in the leg as seen in equation 5.43 can be rewritten as:

$$Z_{LEG_{f,r}} = \left(\alpha_{f,r}^{1} V_{f,r,p}^{min} + \beta_{f,r}^{1}\right) d_{f,r}^{turn} V_{LEG_1} + \left(\alpha_{f,r}^{1} \frac{V_{f,r,p}^{max} - V_{f,r,p}^{min}}{2} + \beta_{f,r}^{1}\right) d_{f,r}^{turn} V_{LEG_2} + \left(\alpha_{f,r}^{2} V_{f,r,p}^{max} + \beta_{f,r}^{2}\right) d_{f,r}^{turn} V_{LEG_3} \quad (5.48)$$

The set of equation 5.47 is the special ordered set of type 2. This means that at most two consecutive variables are greater than zero. For simplicity $V_{LEG_{f,r}} = \frac{A_{f,r} T_{f,r,P_T}}{d_{f,r}^{turn}}$ is substituted into equation 5.45 which results in equation 5.49.

$$Z_{LEG_{f,r}} = \alpha_{f,r}^{1} A_{f,r} T_{f,r,P_T} + \beta_{f,r}^{1} d_{f,r}^{turn} \quad (5.49)$$

This approach is duplicated also for the fuel in the initial segment. The fuel used during the continuous descent approach segment comes directly from the performance calculations of section 4.3. The total fuel used for each aircraft is calculated using equation 5.50.

$$Z_{f,r,P_F} - Z_{f,r,P_I} - Z_{LEG_{f,r}} - Z_{CDA_{f,r}} = 0 \quad (5.50)$$

6

Scheduling Model

In the previous two chapters, the methodology for the scheduling model is explained. This chapter explains how the methodology components are combined and implemented into the scheduling model. The chapter is structured as follows: The first part consists of the concept description. In the second part, the structure of the scheduling model is explained. This chapter ends with a brief conclusion and its assumptions.

6.1. Concept Description

After the conceptual design of the PMS is complete, an analysis has to be performed to quantitatively measure the performance of the PMS compared to the current situation. Furthermore, it is used to check if the system is able to handle the required flow of aircraft. The scheduling model is able to optimise different flight schedules for both the single and dual runway configuration PMSs. Based on a set of constraints identified in chapter 5, the model optimises the makespan or fuel-burn of the flights. The scheduling and sequencing in the PMS can be seen as a special case of the ASP as seen in chapter 2. The main task is to sequence, schedule and assign a runway to each inbound aircraft. Different sizes of aircraft come from different directions into the TMA and all need to land. The aircraft have to merge at the runway. However, they have to be spaced in such a way that the aircraft do not arrive at the same time. That is why the aircraft must be scheduled at an unique time and maintain separation requirements. Currently, the FCFS order is widely used for scheduling aircraft in the TMA[5]. However, as aircraft arriving at major airports often feature different weight classes, it can be beneficial to position a lighter aircraft before an heavier aircraft. The scheduling of the PMS needs to determine the aircraft routing and optimise the sequence in order to optimise the schedule.

6.2. Requirements

The following set of requirements are identified which the scheduling model should implement, to be able to answer the research question of this thesis. The scheduling model:

- shall be able to include medium and heavy aircraft classes and different weights in the system
- shall include variable speed in the initial leg and the sequencing leg.
- shall include the path travelled.
- shall include an optimal solution with minimal total fuel used.
- shall include the sequencing of aircraft and the restricted constraint position shift and FCFS.
- shall include an optimal solution with minimum makespan.
- shall include the IFR separation constraints of ICAO.
- shall be applicable to both the single runway and dual runway configuration at AAS.
- shall have a computational time within acceptable bounds.

6.3. Structure of the model

The model structure is shown in figure 6.1. First, the input is pre-processed and the constraints are prepared in ”lp-file”, then the constraints are optimised using an commercial solver. The results, which are obtained during the optimisation phase, are post-processed and an output is generated. This output is used to obtain an noise contour map. This section discusses each of the blocks seen in figure 6.1. First, the input is discussed. Second, the pre-processing is explained. Third, the optimiser and post-processing are elaborated. Last, the output of the scheduling model is discussed.

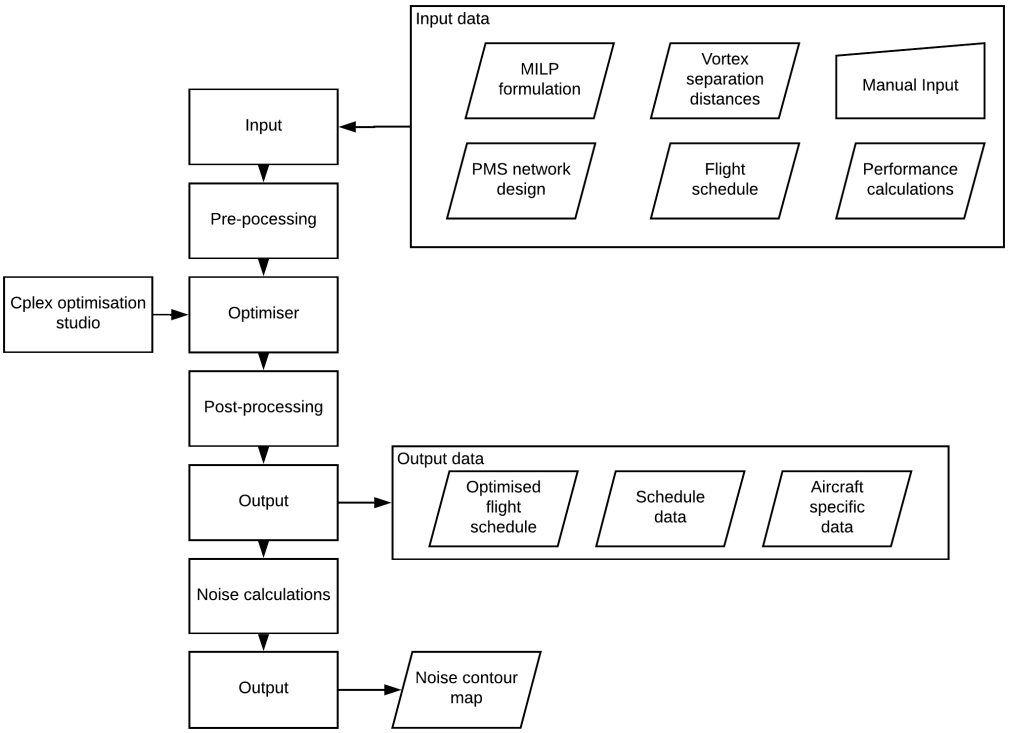

Figure 6.1: The structure of the scheduling model.

6.3.1. Model inputs

As shown in figure 6.1, six different model inputs are required for this model. The first two are the MILP formulation, as shown in chapter 5. The vortex separation distances are the distances in table 3.4 shown in chapter 3. The manual inputs, PMS design, performance calculation and scheduling is discussed below.

Manual input

Three manual inputs are required to run the model. First, the MPS allowed has to be chosen. Three different settings can be selected: FCFS, MPS-1 and MPS-2. The first setting allows no positions to be changed. The second setting allows the aircraft to change its order in the sequence by a maximum of one position. The last, MPS-2, allows the aircraft to change its order in the sequence by a maximum of two positions.

The second manual control input is the objective function selected for the scheduling model. One can choose to optimise for minimum fuel used or for minimising the makespan. Using the weighting factor discussed in chapter 5, both objectives can be combined.

The final manual control input is the initial set of aircraft for the event based rolling horizon, discussed in chapter 5. Depending on the amount of aircraft an initial set of aircraft can be chosen, which is a set between 1 and all aircraft. Normally, a set of 15 aircraft is chosen, because the model is able to solve this amount of aircraft relatively quick (less than 3 minutes).

PMS network route design
The route design used in the scheduling model is the PMS route network designed is section 4.2. Depending on the amount of traffic, a one runway configuration or dual runway configuration is used. If the dual runway configuration is used, the east and west system are independent.

For each IAF, a different sequencing leg is used. All sequencing legs are discretised into 20 segments of 1 NM, resulting in a total sequencing leg of 20 NM, illustrated in figure 6.2. Each discretised point is a turn-point. Therefore, for each aircraft, 21 different routes exist. Route 0 is the most-direct route towards the merge point, without using the sequencing leg. Route 20 is the route with maximum distance, using the full sequencing leg. A separate route exists for each turn-point.

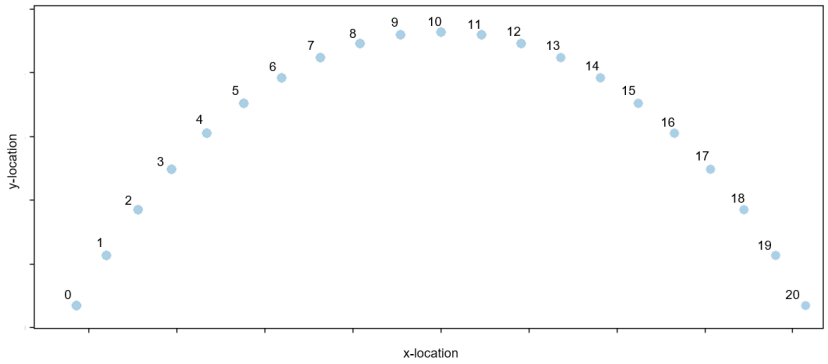

Figure 6.2: One sequencing leg discretised in 20 segments of 1 NM.

Flight schedule
A flight schedule is required as input and is optimised by the scheduling model. An example flight schedule can be seen in table 6.1 for four aircraft. The required information is the flight number, which

Table 6.1: Example flight schedule input.

Flight	IAF time	Weight	Aircraft	Routes
KLM92Z	0	Large	B738	SUGOL
KLM1502	72	Large	B717	RIVER
DAL244	139	Heavy	A330	SUGOL
KLM1034	207	Large	B717	ARTIP

identifies the aircraft scheduled. The IAF time is the difference between the IAF of the first aircraft and its own IAF time in seconds. The ICAO weight class determines the separation requirements. The aircraft type required for the flight performance calculations. Finally, the routes, determining what IAF is used and therefore, what sequencing leg the aircraft uses.

Performance calculations
The performance calculations for each segment in the PMS have been explained in section 4.3. For the initial segment from the IAF to the entry point, the minimum true airspeed, maximum true airspeed and fuel flow is required for each aircraft type at an altitude of 10,000 ft and 9,000 ft. The altitude depends on IAF the aircraft come from. The same performance calculations are required for the sequencing leg segment.

For de CDA segment, the CDA profile for each aircraft type from each sequencing leg is required. The time duration, total fuel used and final approach speed are used as input. The distance and sequencing leg height differs for each sequencing leg. The CDA profile used are shown in appendix C.

6.3.2. pre-processing
The inputs, as seen in figure 6.1, first have to be processed before the actual optimisation is started. The basis of this model will be the MILP formulation as shown in chapter 5. The model is written using the programming language python 2.7. The constraints, bounds and objective function for this formulation are added to the model as an lp-file which is required as input for the solver.

6.3.3. Optimiser

The optimiser used is the IBM ILOG CPLEX optimisation studio 12.7.1 optimiser[15]. CPLEX is a high performance solver for linear programming. It is seen as a black box where the lp file is the input. The solver CPLEX, selects its predefined optimisation algorithm to optimise the objective function. An optimal solution is the output. The outputs are the values of the objective functions and the value of each decision variable. These are then the inputs for the post-processing module.

6.3.4. Post-Processing

The goal of the post-processor is to transform the values of each decision variable in a readable format. Also, for this module python 2.7 is used as programming language. To get a readable output a table is generated, an example of one is shown in 6.2

Table 6.2: Example flight schedule output.

Flight	IAF time	Route	Entry time	V initial	Leg time	CDA time	Final time	V leg	Fuel initial	Fuel leg	Fuel CDA	Aircraft	turn-point
BAW440	0.00	SUGOL	41.58	290.92	0.00	571.20	612.78	0.00	27.39	0.00	221.83	A320	0
TRA6332	124.01	RIVER	166.24	286.40	0.00	582.90	749.14	0.00	26.52	0.00	254.78	B737	0
BMI77Z	163.01	SUGOL	213.44	239.86	40.84	568.50	822.78	264.46	28.80	23.86	230.36	B737	3
IBE32YY	211.01	RIVER	262.93	232.97	50.37	586.00	899.30	285.88	31.36	33.40	247.41	A320	4

The following outputs are obtained:

- Flight is the identification number of the aircraft.
- IAF time is the time the aircraft arrives at the IAF in seconds from the IAF time of the first aircraft.
- Route is the IAF the aircraft used and shows which sequencing leg is used.
- Entry time is the time at the end of the initial segment, the time the aircraft enters the PMS.
- V inital means the true airspeed in knots in the initial segment.
- Leg time is the flight time in seconds over the sequencing leg.
- CDA time is the flight time in the CDA segment.
- Final time is the time in seconds the aircraft arrives at the runway.
- V leg is the speed in the sequencing leg.
- Fuel initial, fuel leg and fuel CDA, are the fuel used in the initial segment, sequencing segment and CDA segment, respectively.
- Aircraft denotes the aircraft type.
- Turn-point identifies which route the aircraft has taken on the sequencing leg.

6.3.5. Output

In figure 6.1, the outputs of the model are shown. The output data are the optimised flight schedule and aircraft specific data. The aircraft specific data contains for each flight the route, the x-y-z coordinates, the thrust, the speed in each segment. The aircraft specific information is used in the noise calculations to create a noise contour map.

6.4. Conclusion

In this chapter a scheduling model has been conceived using MILP formulation. The model uses a commercial solver to optimise the objective function. The model includes preprocessing to create a lp-file, the solution of formulated linear programming problem and finally the post-possessing. To speed up the model, a maximum position shift is implemented. Three levels of position shifts are identified, namely FCFS, a MPS of 1 and a MPS of 2. Also an event-based rolling horizon is implemented, as the dependencies of flight entering the system and flights exiting the system before the entry point are limited. Two objective functions are defined to optimise the fuel or optimise the makespan. The different route options, implemented in the MILP model, are a route for each turn-point on the discretised

sequencing leg. The output is an optimised schedule containing the information which can be used for calculating the noise contour map. The following assumptions are made:

- Speed in initial leg is constant.
- Speed in sequencing leg is constant.
- Speed changes are instantaneous and have no fuel cost.
- Turning towards merge point is instantaneous.
- Minimum speed is the maximum endurance speed for the considered aircraft type.
- Maximum speed is 250 CAS set as maximum speed at and below 10000 ft.
- Continuous descent is performed by having idle thrust as long as possible.
- Sequencing leg is discretised into segments of equal length.
- Bank angle is assumed to be zero, even in the sequencing leg.
- Runway occupancy time of aircraft is not taken into account.

7

Case Study Amsterdam Airport Schiphol

To test the performance of the scheduling model discussed in chapter 6 and to evaluate the advantages or disadvantages of implementing point merge arrival management at AAS, a case study is performed. Based on actual AAS flight data, a comparison is made between the current situation and the new proposed situation. Three cases are demonstrated. The aircraft in each case are scheduled, sequenced and allocated to come up with an optimal capacity or minimal fuel-usage. Based on key performance indicators, the advantages or drawbacks are quantified and conclusions are drawn. This chapter is structured the following way. In section 7.1 the experimental set-up is explained and the cases are defined. In section 7.2, 7.3 and 7.4 the results of each of the three cases are presented and discussed; each of them compared to the actual flight data. In section 7.5 a sensitivity analysis is done for one of the cases. Finally, this chapter ends with conclusions.

7.1. Experimental set-up

To test the performance of the PMS compared to the current situation, a case study is performed. Multiple performance indicators are compared. This section first describes the scenario description, second the model input and finally the actual analysis and visualisations done.

7.1.1. Scenario description

At AAS during the day multiple runway configuration switches occur depending on the wind directions, the preference table and traffic. Ideally, for all runway configuration a PMS design exist, however this is not possible in the context of this thesis. Therefore, only two runway configurations are implemented in this research. The first configuration uses 18R as landing runway and the second configuration uses both 18C and 18R for landing. Both configurations are part of preference two shown in table 3.1 as seen in chapter 3. Although preference two is not the most preferred runway configuration it is expected to be the most used as at approximately 40% of the time. Now it is desired to test the most constraining cases, to find potential bottlenecks of the PMS. The cases considered, only include arrivals at runway 18R or 18C. The cases all begin at the IAF. In the reference cases the aircraft are guided to the runway by radar vectoring, where the tracks are widespread depending on the amount of traffic. For the cases, the flights are scheduled and sequenced using the introduced PMS route structure. Using the scheduling model an optimal solution is found. Starting at the same point as the reference flights and landing at AAS makes it possible to compare the reference flights and the case flights to find advantages and disadvantages for the PMS compared to the current situation.

7.1.2. Assumptioms

This case study uses the following assumptions.

- Based on flight data of one day.
- No wind is taken into account.
- Visibility conditions are assumed to be such that they provide good visibility during uniform daylight periods.

- The actual flight may not start at the IAF because, on ATC discretion a short-cut is given. It is still assumed that these flights start at the closest IAF.
- The weight of the aircraft are assumed to be known and constant during the whole procedure.
- All assumptions mentioned in chapter 6 are in place.
- Only turbofan aircraft are incorporated.
- Only aircraft with ICAO weight class Heavy and Medium are included.

7.1.3. Model input

The input during this case study is a flight schedule of 22 October 2010. The data contains all arriving flights from each of the three IAFs for the entire day from the top of descent to the runway. Every flight is made up of a set of position coordinates and a time stamp at each position. Because of the runway configuration changes during the day, first all flights not arriving at either runway 18R or 18C are removed. A 2D visualisation of the flight arriving at runway 18C or 18R can be seen in figure 7.1. The three arrival directions from SUGOL, RIVER and ARTIP are clearly visible.

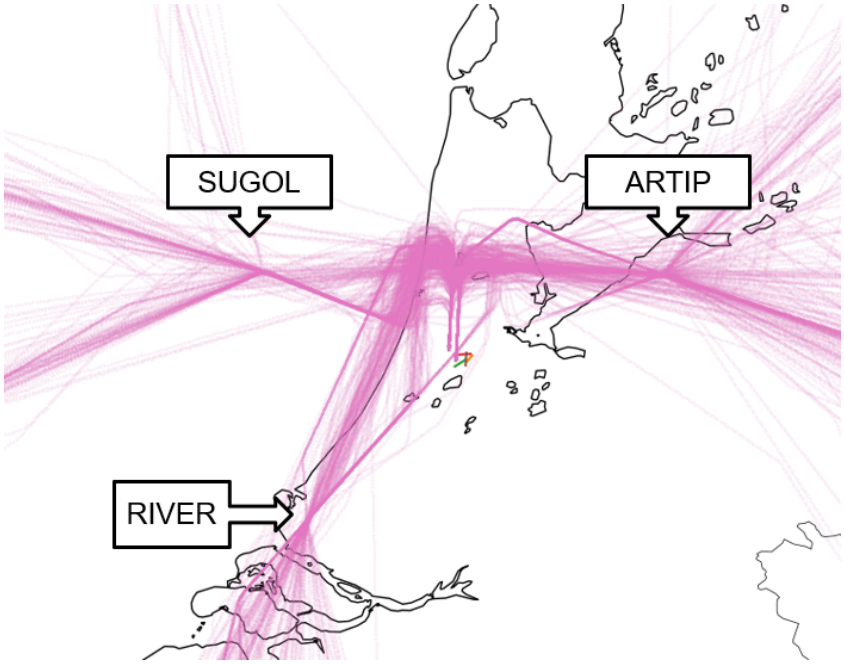

Figure 7.1: All flights arriving at runway 18C and 18R at 22 October 2010.

In all, 36 different aircraft types are found in the data set. As seen in section 4.4, not all aircraft types are available in BADA, and therefore, the aircraft performance are approximated by the aircraft listed in table 4.1. Figure 7.2 shows the resulting aircraft mix, when the actual aircraft have been substituted by the six aircraft of table 4.1. Note that two of the 36 different aircraft types in the actual flight data are turbo propeller aircraft, which take up a share of 0.68% arrivals during the whole day. As seen in section 4.3, these aircraft types are substituted by a turbofan aircraft.

When looking at figure 7.2, the Boeing 717-200 is the most common aircraft type of ICAO code 'Large' and the Boeing 777-200 is the most common aircraft type of ICAO code 'Heavy' in the data set. Note that no small aircraft are included into the data, because general aviation mainly use the Schiphol-Oost runway. The majority of the aircraft are large in size, with 82%, while 18% is of the heavy in size.

The flight data set consists of 584 arriving aircraft. It is decided to split the data into three cases and analyse them individually for two reasons. First, the runway configuration changes from single runway to a dual runway configuration multiple times during the day, depending on the amount of arriving aircraft. Second, the computational time of the scheduling model increases with an increase in the

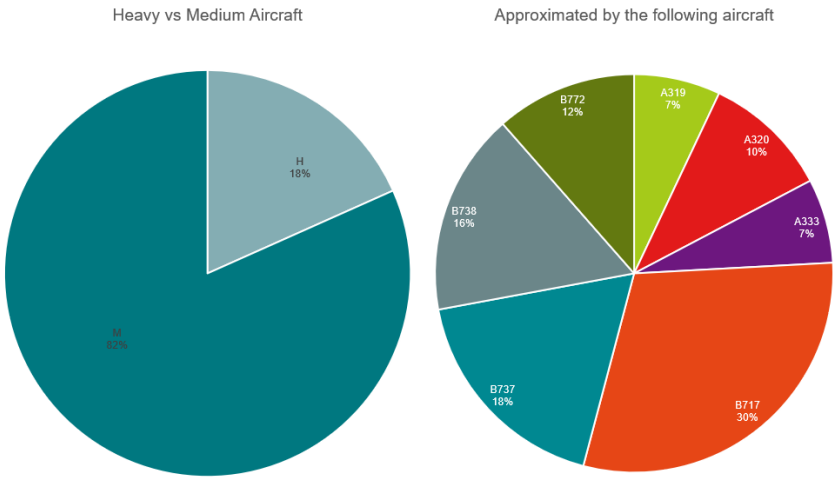

Figure 7.2: Aircraft mix and size of all flights arriving at runway 18C and 18R at 22 October 2010.

amount of aircraft to be scheduled. To find the cases, first the arrival peaks are identified. The number of arrivals per hour are shown in figure 7.3. Upon close inspection of the arrivals, four peaks can be

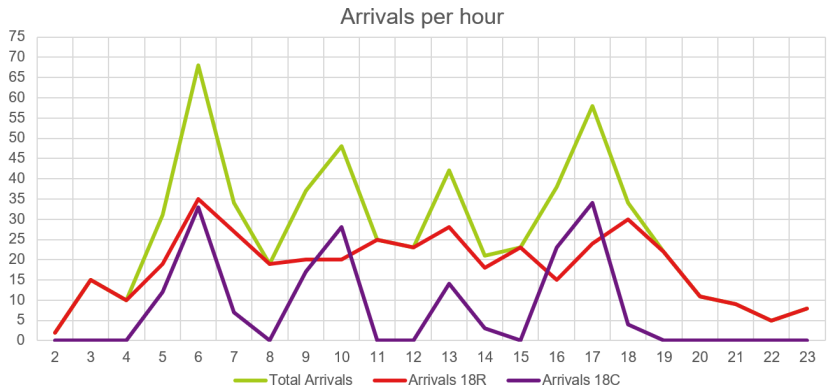

Figure 7.3: Hourly demand of arrival aircraft at runway 18C and 18R on 22 October 2010.

identified in figure 7.3. The first morning peak is the highest with most arrivals. Then, two smaller peaks can be seen and the day ends with a higher peak. At all four peaks, the configuration changes from 18R only, to both 18R and 18C. To further analyse the data, the exact times of the runway changes are analysed and teh results are summarised in table 7.1 for each peak. The duration of the peak can be seen along with the amount of total arrivals and the arrivals for each IAF. Finally, the amount of heavy aircraft are included. To see the maximum capacity of the proposed PMS, peak 1 and peak 2 are chosen as case 1 and 2, respectively.

Table 7.1: Peak times and number of arrivals where both 18C and 18R are used.

Peak	Start time	End time	Arrivals	ARTIP	RIVER	SUGOL	Amount Heavy
Peak 1	05:38:00	07:19:00	98	39	25	34	12%
Peak 2	09:20:00	10:55:00	74	30	23	22	12%
Peak 3	13:27:00	14:03:00	29	14	11	3	10%
Peak 4	16:19:00	18:09:00	96	46	28	24	10%

Considering the dual runway configuration also one off-peak single runway case is analysed. The off-peak times and arrivals are shown in table 7.2. Between the peaks, five off-peak moments are found. Off-peak 2 is selected as the third case as the amount of heavy aircraft is relatively large compared to the other off-peaks and the timespan is small.

Table 7.2: Off peak times and number of arrivals where 18R is used.

Peak	Start time	End time	Arrivals	ARTIP	RIVER	SUGOL	Amount Heavy
off peak 1	00:01:00	05:38:00	42	23	5	14	83%
off peak 2	07:19:00	09:20:00	50	20	9	21	32%
off peak 3	10:55:00	13:27:00	65	30	15	20	14%
off peak 4	14:03:00	16:19:00	48	18	13	17	10%
off peak 5	18:09:00	23:59:00	83	34	29	20	6%

The flight data includes the full descent of the aircraft, which takes place outside the TMA. Before the data can be used as input, the time the aircraft enters the IAF is required. Due to short cuts, some flight do not cross the IAF; for these cases the IAF time is the time the aircraft is closest to their respective IAF. This time will be the initial time for both the reference scenario as well as the PMS analysis of the case. Beside the model input, the inputs described in chapter 6 are included.

7.1.4. Performance analysis and visualisation

Based on the main research question a comparison between the reference case and the PMS results is performed. For each of the PMS cases the results are shown, compared to the reference case and discussed in this section. For each case, first a data analysis is performed of the reference case to analyse how the aircraft are sequenced currently and what volume of noise is produced. Second, the flight schedule results, which are the output of the scheduling model, are shown. Both the fuel-used and makespan are discussed. The FCFS cases are compared. Also the results of allowing a shift of 1 and 2 positions in the sequence are included. These are compared to the FCFS. Third, the trajectory results are shown to asses the effect of actual routes flown and to compare these to the reference case of that case. Also, the height profiles of the cases are analysed. Finally, the noise contour map of the FCFS of the PMS is shown and discussed. To compare the reference case to the PMS case, the noise contour of noise equal and higher to 48 dB is compared. This is a requirement discussed in the Alders table.

7.2. Case 1

In this section the numerical results of case 1 with the PMS are compared to the reference case 1 without the PMS. First, the reference scenario is analysed. The section continues discussing the PMS case based on the flight schedule, trajectory and the noise contour.

7.2.1. Data analysis of reference scenario

The first case consists of 98 arriving aircraft between 05:38 and 07:19 hours in the morning. The ground trajectories of these flights are shown in figure 7.4. The routes from ARTIP, mostly arrive at runway 18C and from SUGOL and RIVER on runway 18R. The results show that in order to separate the aircraft, the aircraft coming from SUGOL fly towards the Schiphol VOR and when instructed head toward north, which is called the downwind leg, and make a 180 degree turn, which is called the base leg towards the runway. Extending the downwind leg is used at AAS to increase the spacing between aircraft which is called tromboning.

The noise contour map for all routes for this case is shown in figure 7.5. The current procedure makes the aircraft descent until 2,000 ft or 3,000 ft is reached depending on the amount of traffic and runway. The aircraft then follow a level flight path until the FAF is crossed, where a three degrees flight path is followed until landing. Because the relatively long downwind leg, the aircraft have a long level segment at an relatively low altitude. The noise contour confirms this by the relatively wide 45 dB contour area.

7.2.2. PMS Flight Schedule Results

The results of the simulation for this first case are split up into the results for flights coming from SUGOL and RIVER and the results from flights coming from ARTIP. Both systems are independent as flights from ARTIP are assigned to runway 18C only and flights from SUGOL and RIVER are assigned to runway 18R. The full flight schedule for both cases for the optimal FCFS case can be seen in the Appendix D in figure D.1 and figure D.2 for flights from SUGOL and RIVER, and ARTIP, respectively.

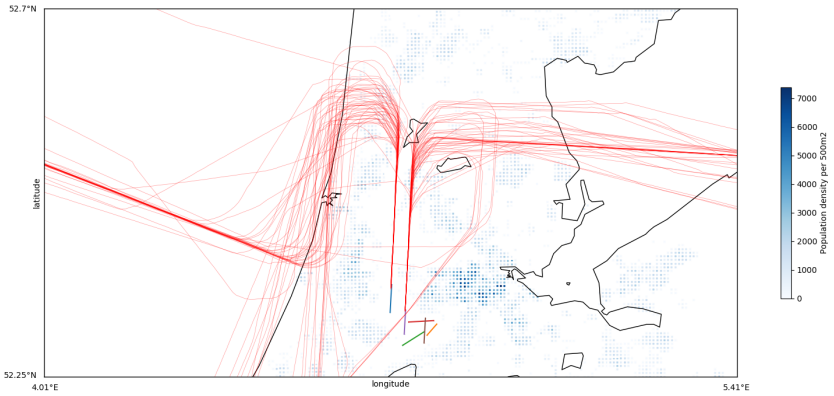

Figure 7.4: Ground track of arriving flights case 1.

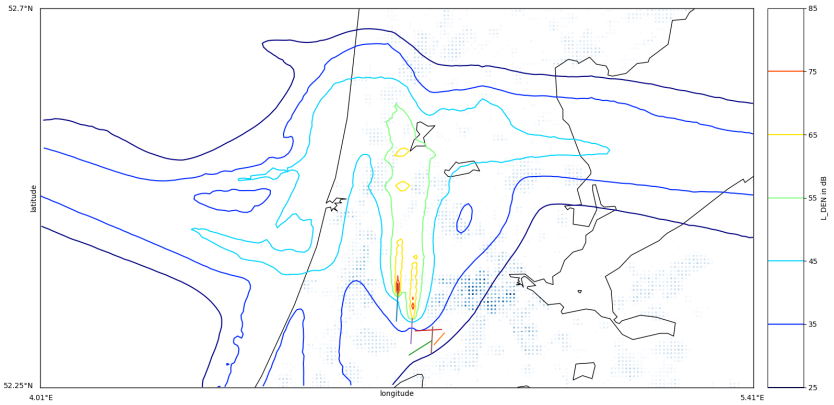

Figure 7.5: Noise contour arriving flights case 1.

SUGOL and RIVER

Case 1 comprises of 24 aircraft arriving through RIVER and 34 through SUGOL into the TMA. By implementing the PMS, the total makespan can be reduced from 215,339 seconds to 208,796 in the FCFS case. This is an improvement of 3.04%, which can be explained by the sequencing at a higher altitude in the sequencing legs of the PMS, where speeds are faster than at lower altitude. Beside the makespan improvement, the PMS improves the amount of fuel-used from 27,831.7 kg to 18,627.2 kg for the fuel optimised FCFS case, a reduction of 33.07%. This reduction is the result of the continuous descent from the sequencing leg to the FAF. Due to the higher speeds at a higher level and no level of segments after the turn towards the merge point, the average travel time per aircraft is reduced from 774.22 seconds to 663.32 seconds, which is a saving of 14.3% on average per aircraft and therefore an increase in capacity. As seen in section 2, the FCFS order is not always the most optimal order. By allowing the aircraft to change its order in the sequence by one or two positions, the total makespan and fuel-used can improved compared to the FCFS results. The results are shown in figure 7.6a and 7.6b for the makespan and fuel-used, respectively. Makespan-optimised results are depicted in the left (blue) bar and fuel-optimised results are depicted in the bar on the right (orange).

Optimising makespan and increasing the maximum order, the makespan can be reduced by 0.042% and 0.062% for a position shift of 1 or 2 respectively. This can be explained by switching a smaller aircraft in front of a large aircraft, but also by switching aircraft with a lower final approach speed. However, as there is no constraint on the fuel-used, the amount of fuel-used fluctuates as with a MPS of 1 the fuel-used increases while the for a MPS of 2 the fuel-used decreases. Optimising for makespan and a MPS of 1 in total 12 shifts take place. This is increased to 20 shifts by allowing a a MPS of 2. The downside is that the aircraft switching position in the sequence is delayed, enabling other aircraft to overtake the aircraft. This results in delay to only one aircraft while profits in makespan are small. For example, one aircraft is delayed 141 seconds as a result of this. The full schedule and time in the sequencing leg shown in a Gantt chart is shown in appendix E. In this appendix the effect of allowing

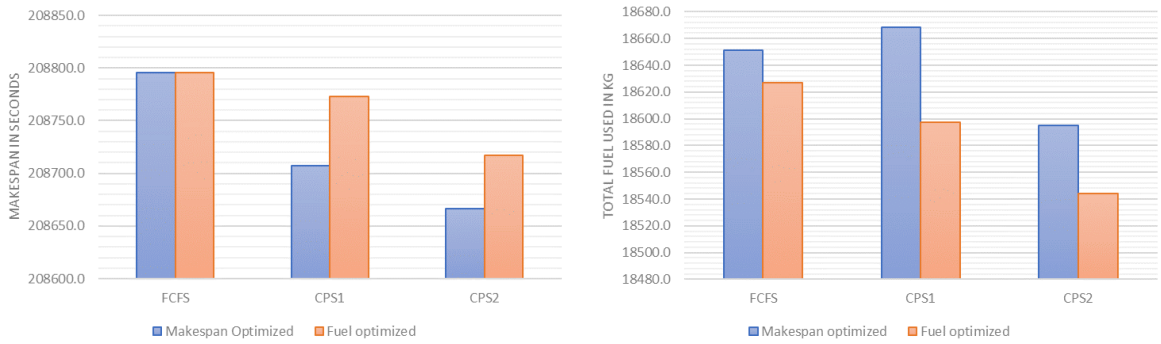

(a) Makespan

(b) Total fuel used

Figure 7.6: Effect on makespan and fuel by allowing a maximum position shift of 1 or 2 positions in the sequence. (a) Optimised for makespan, (b) optimised for fuel.

a position shift can be seen for case 1, showing which aircraft are delayed in order to switch position.

If the schedule is optimised for minimal fuel-usage, the same makespan is found for the FCFS case as when optimised for makespan. This can be explained by the fact that flying faster decreases the fuel used; thus less fuel accounts for reduced makespan. However, the result changes when MPS is allowed. It can be seen that the fuel-used decreases when the maximum number of positions shifts increases. Optimising for a MPS of 1 and 2 positions reduces the fuel-used, compared to the optimal fuel during FCFS, with 0.16% and 0.44%, respectively. However, the improvements in makespan if at all are less dramatic than the makespan optimised case. In this case the maximum position shift is 12 for MPS 1 and 18 for MPS 2.

ARTIP

Case 1 comprises of 39 aircraft arriving in the TMA through ARTIP. These aircraft are all scheduled to land at runway 18C. By optimising the aircraft arriving from ARTIP and minimising the span for the FCFS case, the total makespan can be reduced from 150,926 seconds to 148,314 seconds, which is a reduction of 1.73%. With the help of the CDA, the fuel-used is reduced from 13,389.7 kg to 11,474.7 kg, a reduction of 14.30%. No improved result is found by allowing position shifts, as path stretching is not required due to the larger spacing between aircraft.

7.2.3. Trajectory Results

The ground tracks of all routes for the FCFS-makespan optimised case is shown in figure 7.7. Due to the dense traffic density from SUGOL and RIVER, path stretching is required. This can be seen in figure 7.4 by the long downwind leg. However, in the PMS, path stretching is obtained by increasing the length travelled on the sequencing leg, as seen by the large part of the sequencing legs are used. For flights arriving from ARTIP, no path stretching is required and, therefore, only a small part of the sequencing leg is used. Implementing the PMS and restricting the aircraft to FCFS, results in a reduction in total distance travelled for flight arriving from SUGOL and RIVER of 7.28%. However, an increase of 7.03% in distance travelled is encountered for flights arriving from ARTIP. This is the result of the fixed route structure, as the same PMS design is used for the one or two runway configuration. Therefore, the aircraft arriving from ARTIP make a slight detour towards runway 18C. Also, the flexibility of radar vectoring makes it possible for aircraft to take a shortcut reducing the flight path. Combining both systems results in an decrease of distance travelled from 8,151 km to 7,990 km, which is an 1.98% decrease.

In figure 7.8a, and 7.8b the height profiles can be compared, between the reference results and the optimised results. In figure 7.8a, it can be seen that aircraft perform in the current situation a stepped descent, because when path stretching is required the aircraft fly a level downwind leg. The PMS governed flights level off at 10,000 or 9,000 ft depending on the sequencing leg, to create the required spacing. That is why two different level segments can be seen in figure 7.8b. When the required separation is reached a CDA is performed without level segments.

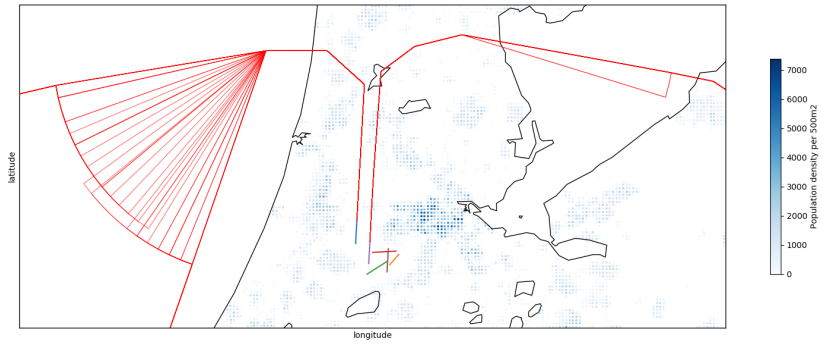

Figure 7.7: Ground tracks for arriving flights, case 1 using the PMS.

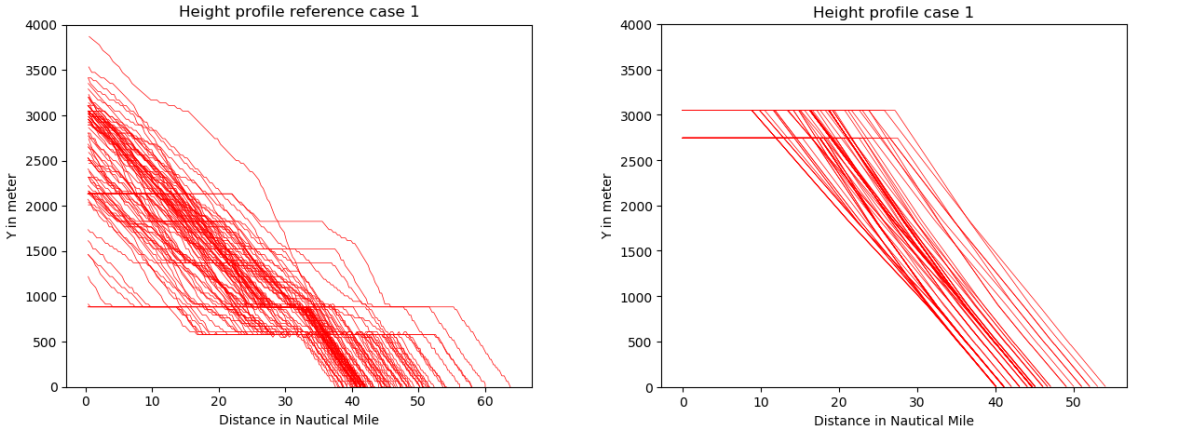

(a) Height profile of the reference case 1.

(b) Height profile of the FCFS optimised schedule for case 1.

Figure 7.8: Comparison of the height and distance travelled inside the terminal area.

7.2.4. Noise Contour Map

Due to the sequencing of flights at higher altitude and the CDA, the noise contours are reduced in size. The L_{DEN} values are calculated for the entire duration of the case. The contour map is shown in figure 7.9. The route structure of the PMS is a predefined path, that makes the noise contour contained around this path. It can be seen in the the noise contour of the reference case in figure 7.5, that the contours are scattered as each aircraft flies a different route. Also due to the CDA, the noise levels are high in the proximity of the airport, but have a relatively small footprint. The aircraft in the reference case level at lower altitudes, increasing the footprint of the higher noise levels. In the PMS, the flights from ARTIP, do not have to use the sequencing leg. Therefore, noise is centred around the direct route and not underneath the west PMS sequencing leg. As seen in chapter 3, rules and regulation are in place for the maximum number of households exposed to L_{DEN} values equal or higher than 58 dB and number of persons highly annoyed by L_{DEN} values equal or higher than 48 dB. To see the advantage of the PMS, the noise contour levels of 48 dB and 58 dB are shown for the reference case in figure 7.10b and for the FCFS case in figure 7.10a. It can be seen that the footprint resulting from the PMS is smaller than the footprint of the reference case.

7.3. Case 2

In this section the results of case 2 are shown, discussed and compared between the novel PMS and the current situation. First the reference data is analysed, second, the flight schedule, which is the output of the scheduling model is discussed. Then, the trajectory differences are assessed and, finally, the noise impact is discussed.

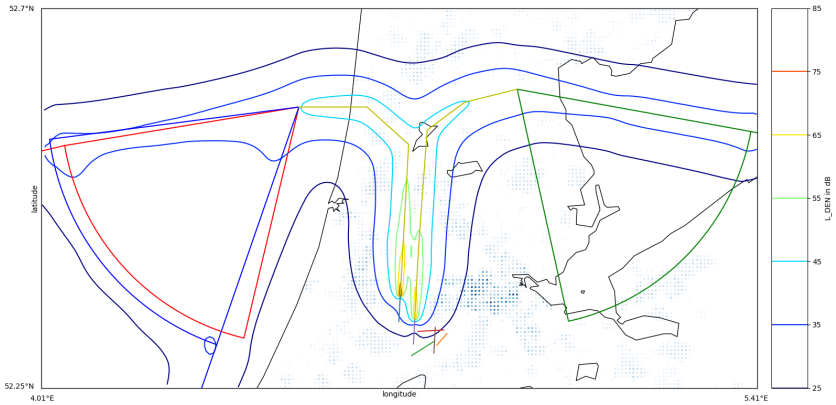

Figure 7.9: Noise contour map for arriving flights, case 1 using the PMS.

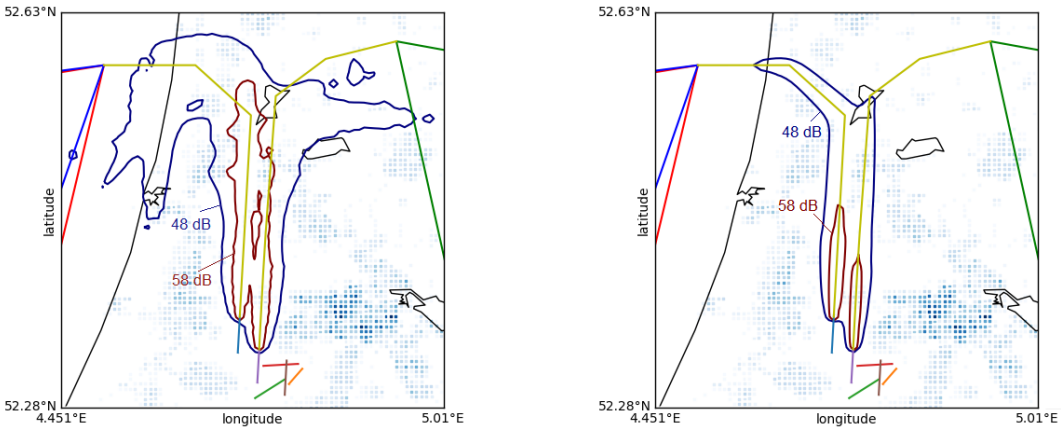

(a) Noise contour map reference case 1.

(b) Noise contour map case 1 using PMS.

Figure 7.10: Noise contour for L_{DEN} levels of 48 dBA and 58 dBA for both the reference case and the PMS case.

7.3.1. Data analysis

The second case consists of 96 aircraft arriving between 16:19 and 18:09 in the afternoon. This is the last wave of the day and consistent with case 1, where also two runways are in use. The amount of heavy aircraft types is 10%. The ground tracks of the routes are shown in figure 7.11. Compared to case 1, it can be seen that the downwind leg for aircraft coming from SUGOL and RIVER is less obvious than in case 1. This indicates that the time separation between aircraft at the IAF is larger compared to case 1 and therefore, less path stretching is required. On the other hand, it can be seen that for flights coming from ARTIP the paths are more scattered. Therefore, it is expected that the time separation between aircraft coming from ARTIP is less than in case 1. The noise contour map for case 2 is shown in figure 7.12. As expected the 45 dB noise contour of the flight coming from SUGOL and RIVER is smaller than case 1. Due to the larger separation between aircraft at the beginning of the procedure, the level segments at lower altitude are shorter. However, there is an increase in the noise contour area from flights arriving from ARTIP as more separation is required.

7.3.2. PMS Flight Schedule Results

As for case 1, the flight schedule is split up for flights coming from ARTIP and for flights from SUGOL and RIVER. Also, in this case two runways are in use, making the west and east PMSs independent. The full flight schedule is shown in Appendix D in figure D.3 and figure D.4 for flights from SUGOL and RIVER, and ARTIP, respectively.

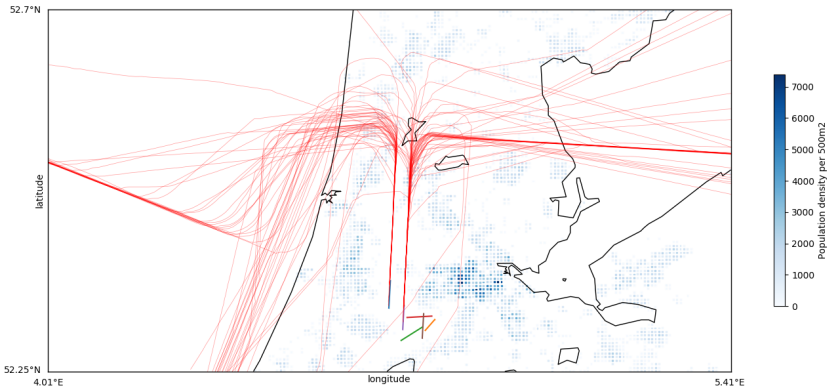

Figure 7.11: Ground track of arriving flights case 2.

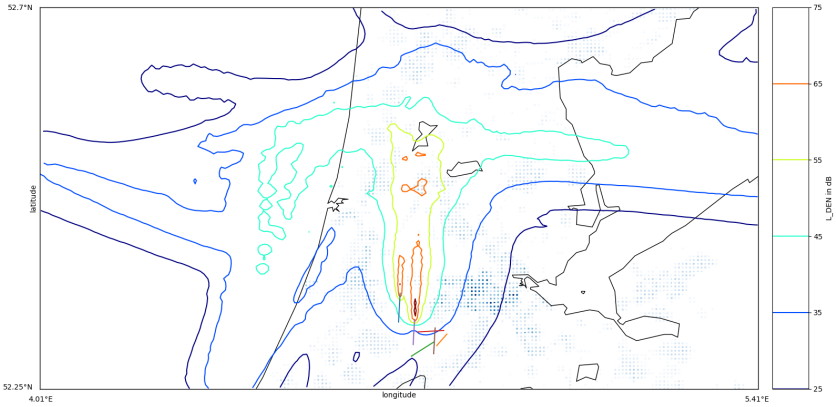

Figure 7.12: Noise contour map of arriving flights for case 2.

SUGOL and RIVER

Case 2 comprises of 28 aircraft coming from RIVER and 24 aircraft arriving from SUGOL. Optimising the reference schedule to minimise makespan for the FCFS case reduces the makespan from 177,682 seconds to 175,218 seconds. An improvement of 1.39%, which is smaller than the improvement of case 1. This is the result of the initial separation between aircraft that is larger and thus the effect of using the PMS is limited. The total fuel-used is decreased from 18,006 kg to 13,549 kg. This is an improvement of 24.75%. For the same reason as for the makespan this is lower than the savings obtained in case 1. The difference between the reference case and the PMS solution can be explained by the CDA. The average travel time per aircraft is decreased from 681.27 to 633.49 seconds, an improvement in throughput capacity of 6.95%. The decrease in travel time, is due to the path stretching at higher altitude where aircraft fly faster. Allowing aircraft to change the order in the sequence with 1 or 2 positions, can improve the solution. The makespan results are shown in figure 7.13a and the fuel optimised results are shown in 7.13b.

The makespan can be improved with 21.67 seconds as a result of a MPS of 1, an improvement of 0.012%. The optimal solution with a MPS of two aircraft in the sequence is exactly the same. Notice that the results of the fuel-optimal makespan are equal to that of the makespan-optimal makespan, due to the fact that increasing speed in the sequencing leg reduces both makespan and fuel-usage. The fuel used can be reduced by 10 kg, a saving of 0.08%.

ARTIP

Case 2 comprises of 44 aircraft arriving through ARTIP in the TMA. Through optimisation of the makespan for the FCFS case, the total makespan is reduced from 186,343 to 182,705 seconds. This implies a reduction of 1.95%. The CDA segment allows for an fuel-used reduction of 18.3% from 20,590.5 kg to 16,823.7 kg. Consistent with case 1, the FCFS case is the optimal case, and allowing MPS does not improve the solution. Therefore, the results based on a MPS are not further discussed

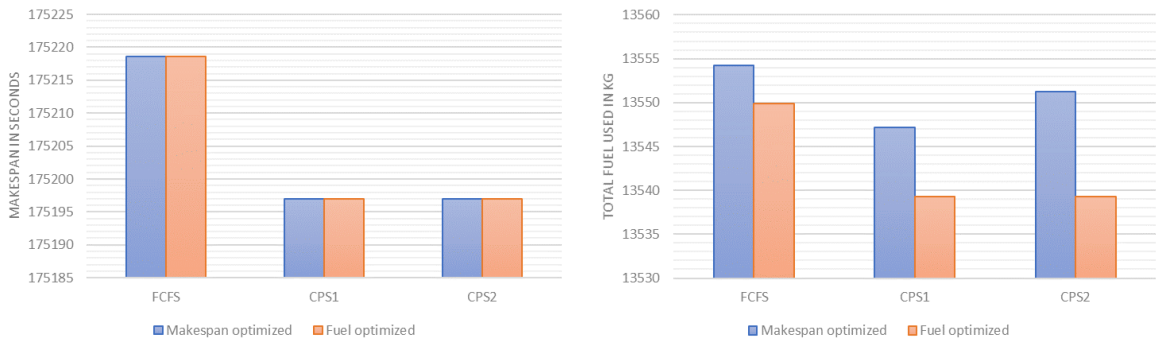

(a) Makespan.

(b) Total fuel used.

Figure 7.13: Effect on makespan and fuel by allowing MPS of 1 or 2. (a) Optimised for makespan; (b) optimised for fuel.

here.

7.3.3. Trajectory Results

The ground trajectory of all flights arriving for case 2 with FCFS are shown in figure 7.14. In comparison to case 1, the sequencing legs for flights arriving from SUGOL and RIVER are used less extensively due to the lower traffic density. However, flights coming from ARTIP require extra path stretching on the sequencing leg. The maximum number of turn-points for the RIVER sequencing leg is 6, for the SUGOL sequencing leg 4 and for the ARTIP sequencing leg 5. Implementing the PMS increases the total distance travelled for flight from SUGOL and RIVER by 1.89%. As shown in figure 7.11, a significant amount of flights take a short cut from SUGOL towards the runway, while in the PMS fixed routes are flown. For flights coming from ARTIP, also an increase in total distance travelled is noticed. The total distance travelled increases from 3,401 km to 3,682 km which is an increase of 8.24%. Combining the east and west PMSs results, shows an increase in distance travelled of 353 km, which is an increase of 4.80% .

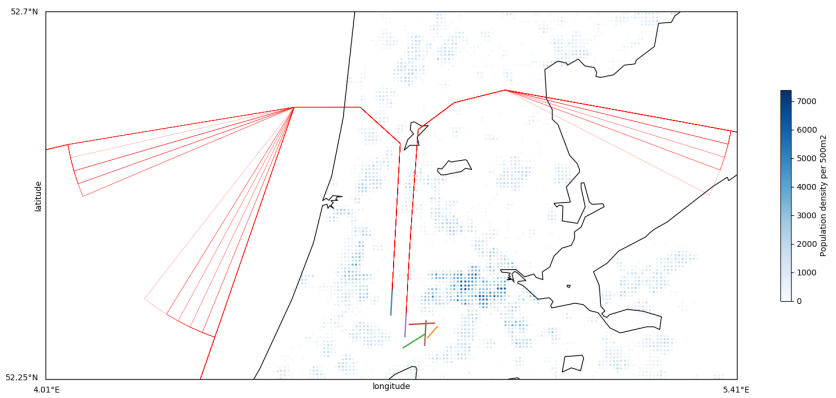

Figure 7.14: Ground track for arriving flights for case 2 using the PMS.

In figure 7.15a and 7.15b, height profiles of the reference case and the PMS results of case 2 are shown. Comparing the reference height profile to the profile of case 1, it can be seen that there are less level segments due to the initial separation. However, still level segments occur. In the PMS case, aircraft level off at the IAF, then, continue level over the initial segment and the sequencing leg until the turn-point is reached. From that point a CDA is performed. Also in these figures it can be seen that the distance travelled is smaller for the reference case than the distance travelled in the PMS due to the possibility of short cuts.

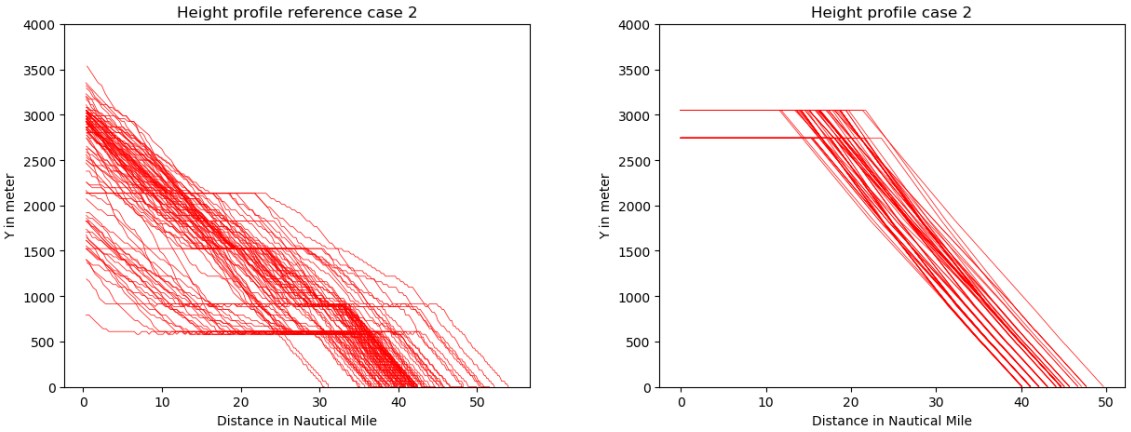

(a) Height profile of the reference case 2.

(b) Height profile of the FCFS optimised schedule for case 2.

Figure 7.15: Comparison of the height and distance travelled inside the terminal area.

7.3.4. Noise Contour Map

Finally, the noise contour of case 2 is shown in figure 7.16. As not the full sequencing legs are used, the noise is concentrated around the flight path. This explains the v-shape in the west PMS. The noise is concentrated around the flight path and the higher levels of noise are seen close to the runway due to the CDA. Comparing this noise contour map to the noise contour map of case 1, it can be seen that comparable noise levels occur. This is a result of the same route structure and the case comprises approximately the same number of flights. Comparing the noise contour map to the map of reference case 2, the noise of the reference case is more spread-out due to the short-cuts and path stretching at lower altitude.

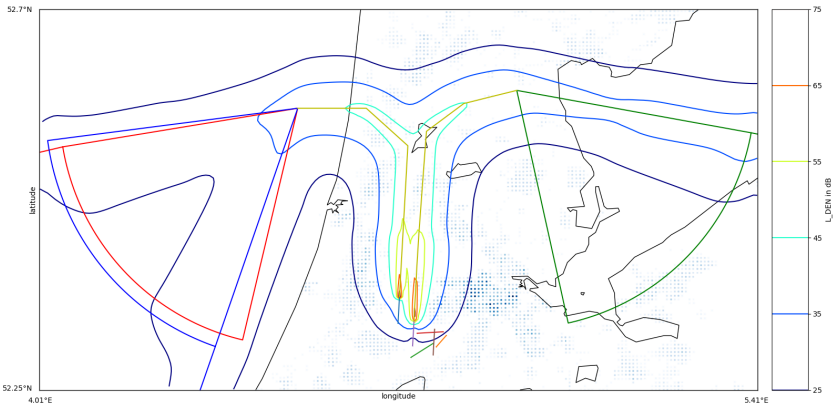

Figure 7.16: Noise contour map for arriving flights, case 2 using PMS.

In figure 7.17a and 7.17b, the L_{DEN} noise areas of 48 dB and 58 dB are shown for the reference case and the PMS results. The footprint of the reference case is smaller compared to the reference case of case 1 due to the limited number of aircraft requiring path stretching. However, it is still larger than the noise footprint of the PMS results due to the CDA approach without level segments and fixed route structure. The noise contour map of case 2 compared to case 1 differ because the flights from east and west are more balanced. In case 1, about 60% of the flights come from ARTIP and RIVER and in case 2 about 46%. This results in a larger noise contours centred around the approach route towards runway 18C and a reduction of the noise contours around approach route for runway 18R.

7.4. Case 3

In this section the results of case 3 are discussed and compared to the reference case 3. First, the reference scenario is analysed. The section continues by discussing the PMS case based on the flight

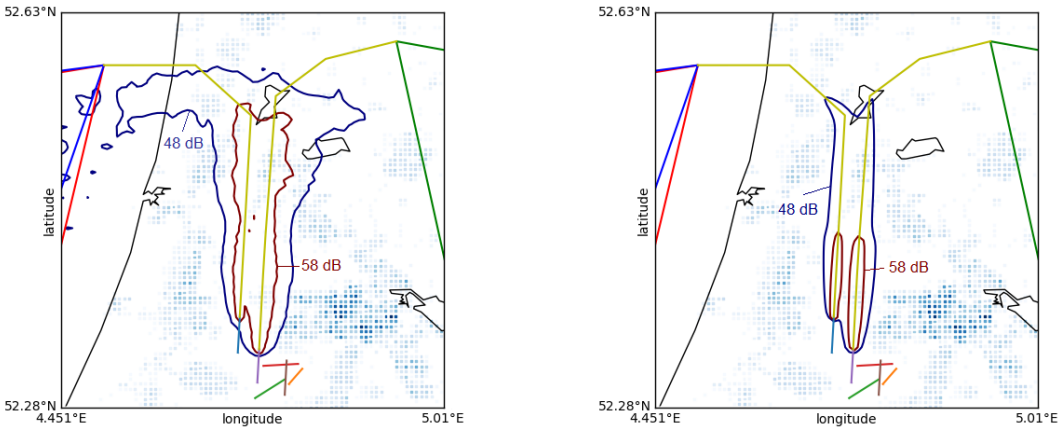

(a) Noise contour map reference case 2.

(b) Noise contour map case 2 using PMS.

Figure 7.17: Noise contour for L_{DEN} levels of 48 dBA and 58 dBA for both the reference case 2 and the PMS case 2.

schedule, trajectory and the noise contour.

7.4.1. Data analysis

Fifty flights arriving between 7:19 and 9:20, are considered in case 3. Compared to the other two cases this is an off-peak case which means that one runway is in use, namely runway 18R. The ground tracks are shown in figure 7.18. As the span of this case is longer than the other two cases it can be seen that some aircraft arriving from SUGOL take a shortcut but also the downwind leg is visible to increase the separation distance. This indicates that the spacing at SUGOL differs over time. Also, it is clear to see a downwind leg for flights coming from ARTIP.

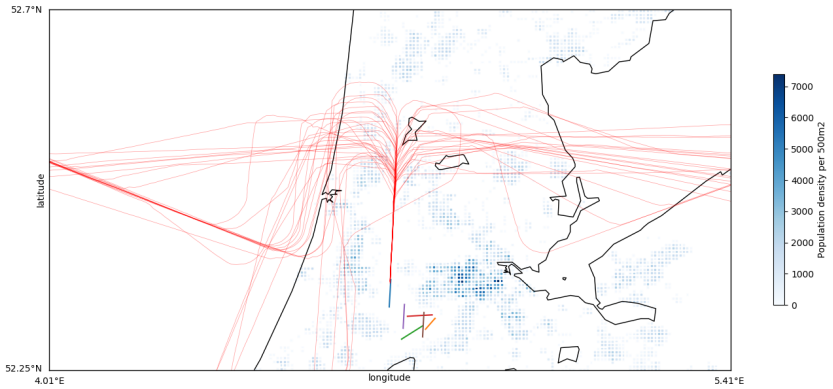

Figure 7.18: Ground track of arriving flights case 3.

The noise contour map for reference case 3 is shown in figure 7.19. Compared to the other two cases the noise contours are centred around runway 18R. Obviously, because it is the only runway used. The effect of subtracting the timespan to calculate L_{DEN} values as shown in equation 4.13 can be seen. Due to the larger timespan and lower amount of flights, L_{DEN} values are reduced. However, the same patterns are visible as in case 1 and 2. The downwind leg causes aircraft to level at low altitude close to the runway, making the footprint larger. Due to the downwind legs for flights coming from ARTIP, the noise footprint on the east of the runway is larger than the other cases.

7.4.2. PMS Flight Schedule Results

The flight schedule, which is the output of the scheduling model, is shown in Appendix D in figure D.5. The optimised schedule for the FCFS case reduces the total makespan from 235,469 seconds to 213,605 seconds, which is an improvement of 9.29%. The same holds for case 3 as for case 1 and 2.

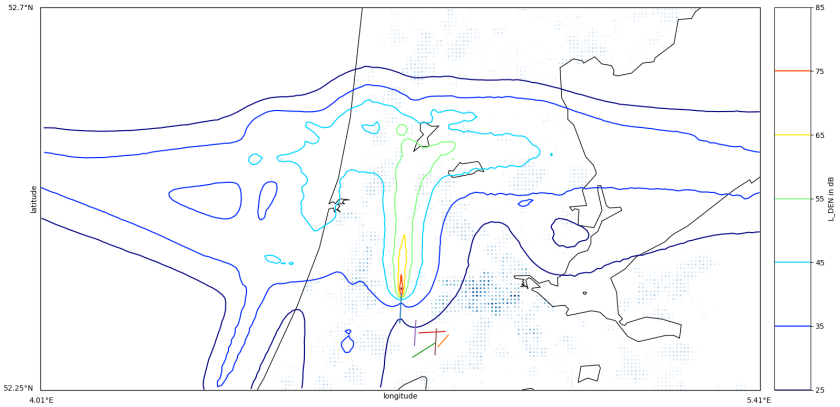

Figure 7.19: Noise contour of arriving flights case 3.

The sequencing of aircraft takes place at a higher altitude where aircraft fly faster, which reduces the makespan. The total amount of fuel used for the FCFS case optimised by minimising the total amount of fuel used is reduced from 22,671 kg to 18,799 kg, this is an improvement of 17% due to the CDA. The average travel time is reduced from 699.48 seconds to 659.15 seconds, an improvement of 5.77%. As in this case 33% of the aircraft is heavy, changing the allowed position shift improves the results. The results can be seen in figure 7.20a and figure 7.20b for an optimised makespan and optimised fuel, respectively.

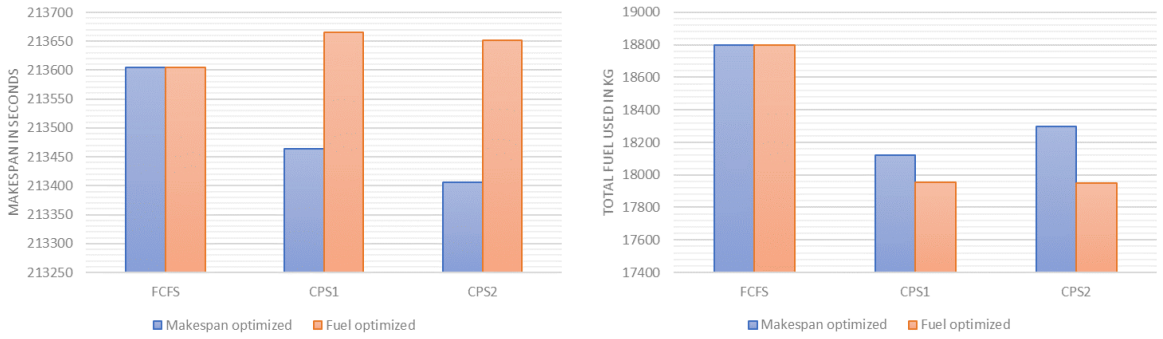

(a) Makespan.

(b) Total fuel used.

Figure 7.20: Effect on makespan and fuel by allowing constraint position shifts of 1 and 2. (a) Optimised for makespan. (b) optimised for fuel.

Increasing the MPS to 1 results in a reduction for makespan to 213,464 seconds, a reduction of 0.07% and a decrease in average flight time from 659 seconds to 656 seconds increasing the capacity. Allowing a MPS of 2 the makespan reduces to 213,406 seconds a reduction of 0.09%. The decreased makespan is caused by 14 position switches for an MPS of 1 and 18 position switches for an MPS of 2. To switch a position in the sequence, the leading aircraft is delayed by continuing over the sequencing leg. This allows the trailing aircraft to overtake the leading aircraft by turning earlier to the merge point. For an MPS of two, this means that the whole sequencing leg is used to absorb the delay of the leading aircraft. Reducing the flexibility for additional delay. Optimising the makespan results in an reduction of fuel for the MPS of case 1 of 3.74%. However, allowing 2 position shifts comes at the cost of an increase in the fuel used. On the other hand, when fuel-used is optimised the fuel reduces compared to the FCFS case with 4.71% and for the MPS of 2, with 4.74%. However, since no cost is added to the makespan for the optimised fuel, the makespan increases with 0.03%, adding 1 minute to the total makespan. The average flight time per aircraft is increased with 0.43%, decreasing the capacity.

7.4.3. Trajectory Results

All ground trajectories of case 3 are shown in figure 7.21. It can be seen that although there are less flights than in case 1 and case 2 as well as a larger span, all three sequencing legs are used. This can be explained by the higher ratio of heavy aircraft and the fact that all aircraft have to land at the same runway. If the FCFS results are compared to the reference case the total distance travelled is increased from 3,745 km to 4,004 km, an increase of 6.92%. Two reasons cause this increase. First, in order to make both PMSs symmetrical, the distance flown over the fixed routes of the PMSs is larger than the direct track used in the reference case. Second, at more quiet times deviation from the normal route is used to reduce the travel time in current operations, which is not allowed in the PMS. Increasing the MPS can improve the distance travelled to 3,985 km, an improvement of 0.46%. However, still a larger distance than the reference case 3.

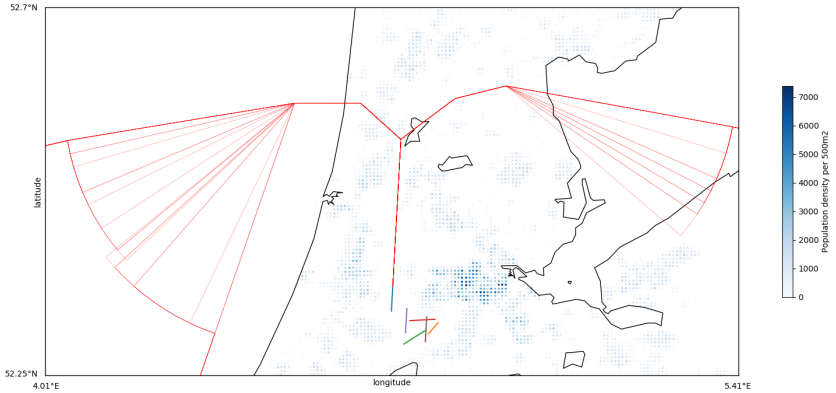

Figure 7.21: Ground track for arriving flights case 3 using the PMS.

In figure 7.22a and 7.22b height profile of the reference case and the PMS results of case 3 are shown. The results show again that the reference case descents using level segments where the separation is created. Upon inspection of figure 7.22a, four level segments are visible. For the PMS results, CDA is performed and only level segments occur at the entry of the IAF.

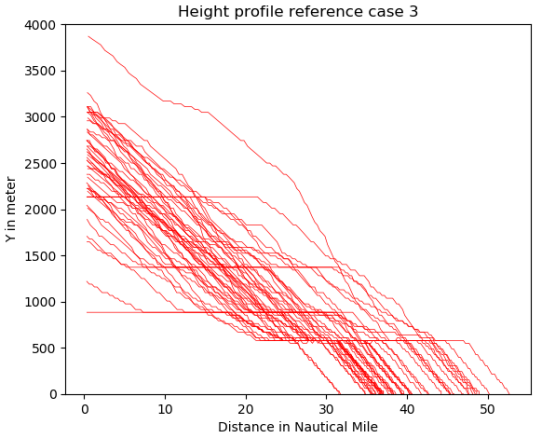

(a) Height profile of the reference case 3.

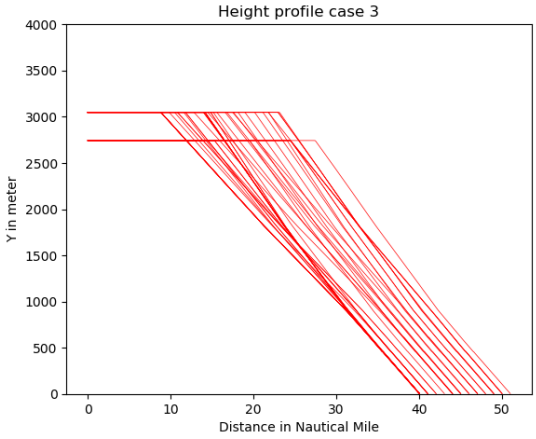

(b) Height profile of the FCFS optimised schedule for case 3.

Figure 7.22: Comparison of the height and distance travelled inside the terminal area.

7.4.4. Noise Contour Map

The noise contour map for the FCFS is shown in figure 7.23. Comparing this to case 1 and 2 the effect of using a single runway can be seen. The footprint of the higher noise levels near the runway is smaller and therefore, the impact on the population is lower. Comparable to case 1, both the sequencing leg for flight from SUGOL and the leg for flights from RIVER are used about have midway. Making the

noise contour comparable to case 1. Now that path stretching is required for flights from ARTIP, the sequencing leg is used up to the tenth turnpoint. The noise contours are therefore larger for flights from this direction compared to case 1 and 2. As the route structure is fixed and flights cannot deviate from the path, the noise contours are centred around the PMS flight path.

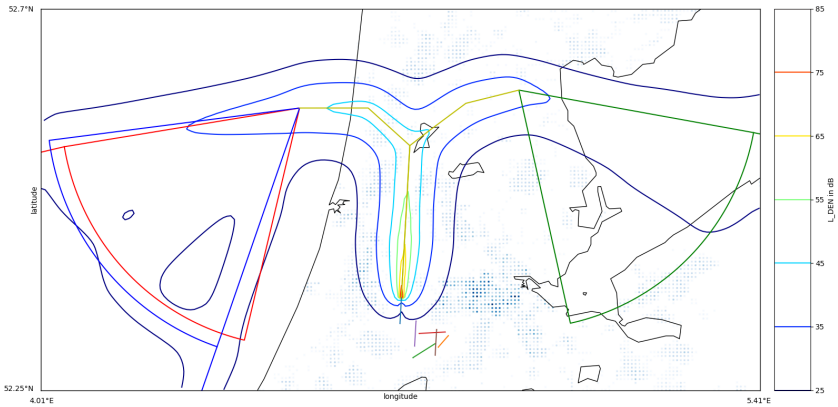

Figure 7.23: Noise contour for arriving flights case 3 using PMS.

In figure 7.24a and 7.24b, the L_{DEN} noise areas of 48 dB and 58 dB are shown for the reference case and the PMS results. For the reference case, path stretching is required for both east and west flights, resulting in level segments at low altitude. This explains the wider noise contours compared to the PMS results. Compared to the noise contours of case 1 and case 2, noise contours pertaining the reference case are smaller, because a single runway is used. Additionally,the average number of flights per hour are lower due to off-peak time. This means that a larger timespan is considered in the L_{DEN} calculation. The PMS case 3 shows a smaller footprint as well for the same reasons. The peak towards the west PMS is caused by more flights coming from SUGOL and RIVER than from ARTIP.

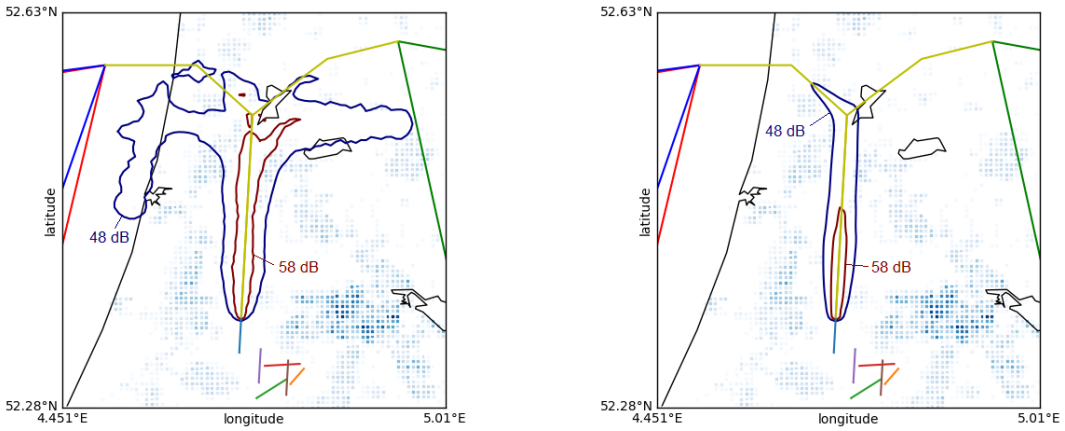

(a) Noise contours for reference case 3

(b) Noise contours case 3 using PMS.

Figure 7.24: Noise contour for L_{DEN} levels of 48 dBA and 58 dBA for both the reference case and the PMS case.

7.5. Sensitivity analysis

To check the influence of important parameters of the PMS scheduling model, a sensitivity analysis is performed. Two major parameters are checked. First, this section discusses the sensitivity of the makespan due to a change in wake vortex separation standards. Second, the dependence between makespan and fuel is analysed by combining both objective functions in a composite performance criterion and varying the weighting factors.

7.5.1. Change in wake vortex separation standards

The wake vortex separation standards are important parameters, as they determines the time separation the aircraft require before landing. This has direct impact on the total makespan, fuel-used and the throughput capacity of the system. Furthermore, it is important to know the sensitivity, as the criteria is not the same in each country. For this analysis the separation standards are reduced and increased by 0.5 nautical miles. The separation standards for the relaxed case are shown in table 7.3. The separation standards of the tightened case are shown in table 7.4.

Table 7.3: Separation standards in nautical miles for the relaxed case.

	Heavy	Large	Small
Heavy	3.50	4.50	5.50
Large	2.50	2.50	3.50
Small	2.50	2.50	2.50

Table 7.4: Separation standards in nautical miles for the tightened case.

	Heavy	Large	Small
Heavy	4.50	5.50	6.50
Large	3.50	3.50	4.50
Small	3.50	3.50	3.50

The sensitivity results are explored for case 3, being the case with the highest mix of heavy aircraft. The baseline case has been discussed in the section above. The makespan is shown in figure 7.25 for three cases, namely, the baseline separation, reduced separation and increased separation. Also the effect on makespan by allowing a maximum position shift is implemented to see if the same trend is followed. As expected, an increase in separation standards results in an increase in total makespan; A decrease in separation standards results in a decrease of total makespan. It can be seen that the increase in makespan between the baseline and tightened separation standards is greater than the increase in makespan between the relaxed and the baseline separation standards. This can be explained by the fact that the smaller the separation distance becomes, the larger the influence of the initial separation is. By allowing a MPS of 1 and 2, the same trend of the baseline is followed, as expected. For the FCFS case, by relaxing the separation standards, the makespan can be reduced by 0.32% compared to the baseline. However, an tightening the separations standards by 0.5 NM results in an increase in makespan of 0.47%. As expected, the capacity increases when relaxing the separation standards, as the average travel time decreases from 656 to 645 seconds per aircraft, which is an improvement of 1.63%.

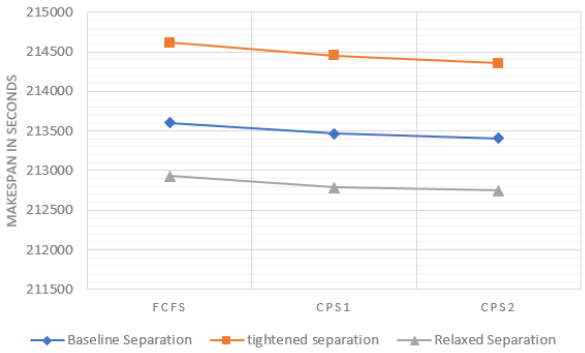

Figure 7.25: Effect on makespan by changing the wake vortex separation standards, for FCFS and a MPS of 1 and 2.

7.5.2. Composite cost function

In the case studies performed, the objective functions related to makespan and fuel-usage have been considered independently. As shown in chapter 6, a composite objective function is also possible. To

test the sensitivity and dependence between makespan and fuel-usage, both objective functions are combined using a weight factor. To compare the dependency between the makespan and fuel-usage, ten optimisation runs have been performed using case study 3, where weighting factor w is increased from 0 to 1 in steps of 0.1. The results for makespan are shown in figure 7.26a and fuel-usage in 7.26b.

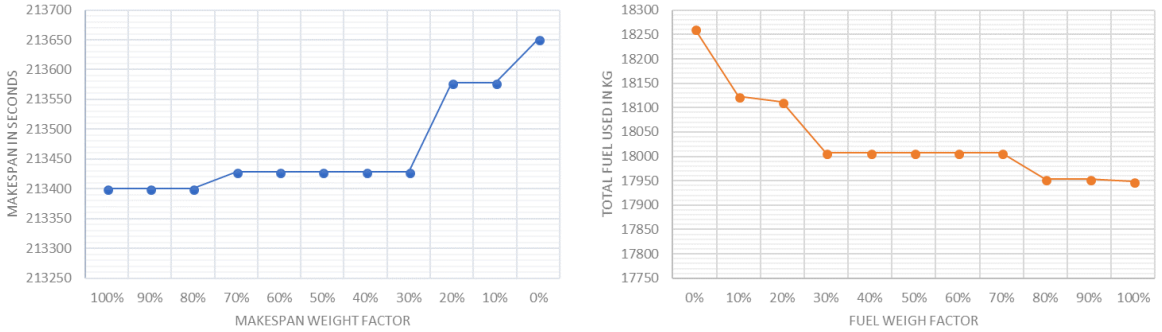

(a) Makespan.

(b) Total fuel used.

Figure 7.26: Effect on the makespan and fuel-used by combining the importance of fuel and makespan. (a) for the makespan results. (b) the results for total fuel-used.

The makespan is lowest when 100% of the makespan is accounted for in the objective function, this means that 0% of the fuel weight is included. However, it can be seen that the fuel used in this situation is highest as no cost of fuel is included. The largest decrease in fuel-used is reached when the weight factor of fuel is set to 10%, as now fuel is implemented in the objective function. By decreasing the importance of the makespan, the makespan increases. By increasing the importance of the fuel-used, the fuel-used decreases. The difference between the highest and lowest makespan is 251 seconds or 0.12%. The difference in fuel is 313 kg which is 1.72%. Again a logical trend is followed.

7.6. Conclusion

Three cases have been explored based on actual flights in this chapter. Two cases take place during peak hours where two runways are in operation, namely 18C and 18R. The first case is the morning peak and the second case is the afternoon peak, both about 1.5 hours in duration and comprising 98 and 96 aircraft in total, with approximately 10% of heavy aircraft. The third case takes place during non-peak hours where one runway is in operation, namely, runway 18R. Case 3 is two hours long and consists of 50 aircraft, where 32% is made up of heavy aircraft types.

The actual flights of the cases are analysed and used as reference scenario to explore the improvements of the PMS. When analysing the reference scenarios, it was found that when there is a high amount of approaching aircraft, the trajectories of the flights change from a direct path to the runway towards a trombone shape by increasing the downwind leg. By entering one of the three IAFs, the aircraft descend on ATC discretion however, when separation is required, a level downwind leg is performed.. Most aircraft feature the downwind leg in close proximity of the runway at an altitude of approximately 2,000 ft or 3,000 ft. As the aircraft are vectored by ATC, the trajectories during dense arrival traffic aircraft are widely dispersed. This results in a larger footprint of the noise contour map noise levels.

Using the scheduling model for each of the three cases, an optimal schedule is found without the need of increasing the length of the sequencing leg. Comparing the FCFS PMS results to all reference case scenarios, it was found that the required capacity is met for all three cases. The total makespan was reduced by sequencing aircraft at higher altitude, where aircraft fly faster and there are no level segments after the turn-point. For the same reason the average travel time is reduced by a maximum of 14%. In terms of fuel usage, the PMS performs better than the reference scenarios for all cases. The CDA allows aircraft to save up to 33% of fuel. By adjusting the maximum position shifts allowed, the makespan and fuel-used can be improved. In this thesis a MPS of 1 and 2 have been investigated and compared to the FCFS PMS results. The main reasons for a position shift in the sequence are; the difference in final approach speed and the ICAO weight classes. If a heavy aircraft type closely succeeds a large aircraft type, the large aircraft type switches position in the sequences, because the

lower separation standards. During FCFS, the time in the sequencing leg is higher than when position shifts are allowed. However, the aircraft switching position in the sequence is delayed and therefore introduced to a time and fuel penalty. Depending on whether the objective is to minimise fuel-usage or to minimise makespan the fuel-usage or makespan can be reduced by introducing a MPS. By optimising the fuel during MPS of 2, a maximum of 4.74% of fuel used can be saved. However, introducing a MPS, let to small profits in makespan for the makespan optimised case, as the aircraft switching position in the sequence is delayed. However, there is an improvement in average travel time per aircraft. The average travel time decreases with up to 4 seconds per flight increasing the throughput capacity.

The trajectories for the FCFS case are investigated and compared to the reference scenarios. For all cases, the trajectories are more constrained than the reference scenarios. The only variability is the turn point the aircraft uses, with the aim to delay the aircraft. This makes the dispersion of flight paths limited and clear. In terms of distance flown, the improvements of the PMS depends on the configuration used and the amount of traffic. It was found that when no sequencing is required, the total distance flown increases in the worst-case by more than 8%. However, during heavy traffic a maximum reduction of 7% can be obtained. Due to the flexibility of flight paths in the current situation, the aircraft can fly in a more direct line towards the runway. The increase in distance is compensated by the decrease in fuel-used.

For each case a noise contour map is made for the FCFS strategy. In all cases the noise footprint decreases, because CDA performed and the fixed flight tracks. The level segment of the reference scenario caused an increase in the noise footprint area and therefore, an increase in footprint occurs during peak times.

8

Verification and Validation

Part of this thesis is the design of a model to schedule the incoming flights into the PMS. To check whether the model performs correctly and the output is accurate, model verification and validation is performed. This chapter describes first, the verification process of the model and second, the validation process of the model.

8.1. Verification

Verification is the process where the model is checked if it follows the mathematical model correctly and that the output is logical and consistent. The verification process is split up into two elements; first, code verification and, second, calculation verification [48]. As seen in figure 6.1, the model consists of different blocks of code which serve as input of the scheduling model. Code verification checks if each of the code blocks does not produce errors.

In view of the fact that no errors were found in the individual blocks, a simplified case is performed for the verification calculation. The block calculating the aircraft performance is compared to the performance table data included in the BADA software package[25]. For each aircraft, for different height, speed, configuration, thrust mode and lift devices, the thrust, drag, fuel consumption and rate of descent can be calculated. It was found that the model produces the same results as in the performance tables and is therefore assumed to be correct. This data is also used to verify the distance covered in the CDA for the different aircraft. In BADA three different aircraft weights are included in the performance table data and for each weight the full CDA was calculated and checked whether the difference was as expected.

The INM block is assumed to work correctly as it works as a verified black box. However, the output is analysed for a single flight case. This to check whether the inputs are in the right format and the noise contour map was centred around the actual flight path. Also, the maximum noise levels found are compared with other research papers to find if unrealistic high noise levels are obtained [30]. It was found that the levels are comparable and therefore the INM code block is assumed verified. To verify the noise contour map of multiple flights, two equal aircraft are used as input flying different routes, while the same height and speed profiles are used. The result proved to be as expected.

Lastly, the scheduling model itself is verified. A simplified case is performed based on the case study presented in the paper by Hong [35]. In this paper a small case is performed using 4 aircraft of equal size, two sequencing legs discretised into 12 segments and constant speed in the sequencing legs and during CDA. The scheduling model in this study produced, using the same input, the exact output as found by Hong. Next, in a follow up paper of Hong [34], the level of difficulty was increased by introducing different aircraft classes and 7 aircraft. This case was also run by the model and produced the same results. Compared to the other study, the present study includes variable speed before the entry point of the PMS, variable speeds over the sequencing leg and an additional sequencing leg. This resulted in extra separation constraints over the legs. To verify these calculations, a case of 2 or 3 aircraft are made, run by the scheduling model. At the critical points the separation conditions were checked and found to be operative and correct. As the comparable models only use a maximum of 7 aircraft, the performance of more than 7 aircraft was checked. This led to the implementation of

the event-based rolling horizon. To check the solution of the rolling horizon, a case of 25 aircraft was solved integrally over the complete horizon and solved using rolling horizon approach. The solutions where within 0.5% of each other, verifying the rolling horizon approach. Also, the improvement in computational time is checked. The case of 25 aircraft with a MPS of 2 is performed on a quad core 2.8 GHz processor with 8 GB of RAM. By introducing the event-based rolling horizon approach the computational time improved from 98 minutes to 7 minutes.

8.2. Validation

Validation is used to check if the models output is representing the real-world situation and determine the accuracy of the model. As the PMS is not implemented at AAS, it is difficult to validate the model with real-data of AAS. Besides, the model is based on numerous assumptions which makes it difficult to validate. One important parameter of the scheduling model is the duration of the CDA segment of the PMS. A CDA is performed at AAS during night hours. However it was chosen to compare the descent time of aircraft arriving at Dublin international airport. Because, this airport uses the PMS approach [40]. To compare the CDA segment durations at AAS and Dublin international airport, following assumptions are made:

- the initial time is the time the aircraft passes through an altitude of 10,000ft.
- the final time is the landing time.
- only direct flights are taken into account, without considering time in the sequencing leg.
- five flights are taken for each aircraft type to get the average flight time.

Direct flights are used to assess the duration of the continuous descent only and ignoring the time added in the sequencing leg. Three aircraft types are tested, namely the Boeing 737-800, Airbus A320-200 and the Airbus A330-300. The A330-300 is a heavy aircraft type and the remaining two types are large aircraft. Other aircraft types are not selected, as their amount of landings at Dublin international airport is negligible. The flight times are taken directly from FlightAware live flight tracking [29] during one day for the same runway configuration. The results can be seen in table 8.1.

Table 8.1: CDA flight times at Dublin international airport for 3 different aircraft types compared to the CDA flight times calculated in the scheduling model.

Aircraft type	Flight time aircraft 1	Flight time aircraft 2	Flight time aircraft 3	Flight time aircraft 4	Flight time aircraft 5	Average in seconds	Numerical in seconds	Difference in seconds	Difference in %
A320	547	593	682	575	699	619.2	612.79	6.41	1.05%
B738	560	562	599	594	671	597.2	597.39	0.19	0.03%
A330	673	647	613	641	653	645.4	624.39	21.01	3.36%

For each aircraft types the average duration is taken and compared to the numerical flight time which is the output of the PMS scheduling model. The difference between the actual and numerical flight time is shown. It can be seen that the B738 is closest to the actual situation while the A330 shows the highest offset. However, with a difference of 3.36%, it is assumed acceptable and therefore the CDA times are assumed validated. In chapter 7 a case study is presented, where actual flight data is compared to the output of the PMS scheduling model. Although routes and approaches were different, the order of magnitude can be compared. No outliers or unexplainable results were found.

As the procedure is not currently implemented at AAS a validation of the new PMS in the TMA of AAS is required. This is not in the scope of this thesis. The validation of the PMS at AAS can be done by fast- or real-time simulations or validation using flight trails [21].

No relevant papers about noise contours are available where the PMS is applied. Therefore, no comparison to actual cases can be made. Instead, the noise validation is done by consulting experts in the field of noise at the Air Transport and Operations department of the faculty of aerospace engineering at the university of Delft, to validate this model.

9

Conclusions and Recommendations

In the previous chapters the results of the PMS have been shown and discussed and the scheduling model has been validated. In this chapter the conclusions and recommendations are drawn. The conclusions for this study are shown in section 9.1. The limitations of the scheduling model are identified in section 9.2. The recommendations for future work are discussed in section 9.3.

9.1. Conclusions

The objective of the research is to explore the potential benefits and drawbacks of implementing PMS based arrival management for one single and one dual runway configuration at AAS. The benefits and drawbacks have to be drawn in terms of environmental impact, capacity, delay, fuel efficiency and safety. The performance of the PMS is evaluated and demonstrated by the design of a scheduling model based on a MILP formulation. Based on a case study, the performance of the PMS applied at AAS is analysed.

First of all, it is concluded that the PMS arrival management can be implemented in the current TMA of AAS, without the need of enlarging the TMA. Also, significant advantage of the PMS compared to the current situation have been found. In the following three subsections, the advantages and drawbacks of the PMS are explained in detail. First, the conclusions in terms of environmental impact and fuel efficiency are discussed. Then, the conclusions in terms of capacity and delay are elaborated. Finally the conclusions in terms of safety are examined.

9.1.1. Environmental impact and fuel efficiency

Implementing the PMS at AAS was shown to have a positive impact on the environment. By design, the aircraft sequenced at a higher altitude and follow a CDA towards the FAF. The CDA causes the aircraft to decent without level segments after the sequencing leg unlike the stepped approach employed in the current situation. Therefore, the aircraft are higher in altitude compared to the aircraft during the current situation and fly more efficient. As a result, the noise contour levels higher than 48dB are relatively close to runway, but also the noise impact further away from the runway is improved. The aircraft routes are more constrain and therefore the noise contours are situated around the PMS, reducing the noise footprint.

The fuel efficiency is also improved by implementing the PMS. Due to the CDA, the PMS saves fuel in every case compared to the reference scenario. The minimum fuel saving is 14.30% and the maximum fuel saving is 33.07%. Also, the sequencing at higher altitude where aircraft performance is more efficient contributes to the fuel savings. However, when less aircraft are in the sequence the fuel savings decrease. By allowing the aircraft to switch up to two positions in the sequence, a total of 4.74% of fuel can be reduced compared to the FCFS case. However, at the cost of a slight increase in makespan. Depending on the amount of traffic, the distance flown increases or decreases compared to the reference case. The maximum improvement found is 7.28% while the maximum increase in total travel time was found to be 8.24%. This increase is caused by the fixed route structure of the PMS instead of the radar vectoring which is more flexible.

9.1.2. Capacity and delay

Implementing the PMS has advantages in terms of throughput capacity. However, the improvements are small. The improvements ranges from 1.73% to a maximum of 9.29%. Improvements are a result of the sequencing at a higher levels where speeds are faster, but also by the CDA, which is faster than a stepped descent. A larger improvement is reached when the aircraft stream consists of more heavy aircraft. The total makespan can be reduced by allowing the positions in the sequence to be changed. However, the profits are limited compared to the FCFS case as the maximum improvement of the makespan is 0.062%. The improvement in makespan is due to the delay of aircraft switching positions in the sequence, causing additional flight time for these aircraft. The average travel time per aircraft is reduced in the PMS, improving the throughput capacity of the system and reducing the delay. The average travel time improvement from the IAF to the FAF is ranges from 5.77% to 14.3%. This is caused by the sequencing at higher altitude.

9.1.3. Safety

By design, the PMS route structure is clearer and more intuitive, increasing safety. Currently, using radar vectoring the area of flight tracks covers a large area. The PMS has a predefined horizontal and vertical envelop, due to the wedge to the merge point. This results in easier deconfliction of objects compared to vectoring aircraft. Due to the different levels in the system, more attention has to be given to the altitude of aircraft in order to assure safety. The PMS is a closed loop intervention. Compared to the current situation at AAS, closed loop intervention provides that the aircraft are kept on lateral navigation, even during periods of dense traffic. This means that the PMS reduces the number of tactical interventions. However, there is less flexibility for ATC as the aircraft have to follow the fixed route structure of the PMS.

9.2. Limitations

Due to the simplifications and the limited amount of time available to complete this thesis, the following limitations are identified:

- The sequencing leg is discretised in segments of 1 NM in length. This means that aircraft can only turn at the end of such a segment. To compensate the time error, the speed of the aircraft is adjusted, but that results in increasing the fuel-used. Additionally, in the model the turn-time is instant at the moment the direct to instruction is given. In a real-world simulation, the aircraft gets the direct to instruction from ATC and there is some delay before the aircraft turns. This decreases capacity.

- The aircraft types examined in the cases are limited to just six types. The flight performance of these six aircraft types represent all aircraft currently flying at AAS. Therefore, a difference in the optimal solution might exist when all aircraft types are included in the scheduling model. For example, propeller aircraft are not included. Also the noise contour map is calculated based on the six aircraft types, affecting the fidelity of the noise contour map.

- The speed changes in the system and during the CDA are assumed to take place instantaneously. This means that there is no additional cost and time penalty for aircraft changing speed. This can result in speed changes that would not take place in real-world conditions.

- The CDA is based on an idle descent, as long as possible which makes the descent angle for every aircraft different. Due to the fixed route structure of the PMS, the distance for the CDA segment is fixed. As the aircraft have different descent angles, the top of descent is different for each aircraft. Therefore, each aircraft is required to add a level cruise segment from the sequencing leg to the top of descent. The consequence is an optimal height profile, due to the steep descent. However, not necessary minimal fuel-used for the entire CDA segment.

- The design of the PMS is only valid for the two runway configurations used in this thesis. Before it can be used in practice, more research has to be performed concerning the validity and applicability in the current airspace and for the combination with departing traffic. Also missed approaches, should be explored.

- The results and conclusions are drawn from the case studies of October 22 in 2010, during three different peaks. This might not represent the noise of a full day or a full year of operations. Ideally a whole day or year is analysed to check the impact of weather, runway configuration and variable PMS geometry parameters.
- In this study the noise contour map is calculated, but not the amount of households exposed to the noise. As there is a limit to the number of households exposed, a 24 hour analysis has to be performed. Also noise, is not included in the optimisation model. The noise contour maps are calculated after the optimisation.

9.3. Recommendations

Based on the conclusions and limitations the following recommendations are drawn.

- Currently, the optimisation is performed with respect to makespan, fuel-used or a combination of the two. Due to the high population density in the vicinity of AAS, it is a noise sensitive airport. Therefore, the multi-objective can be extended to include noise, based on the noise the houses are exposed to. The design of the PMS can also be implemented in the optimisation to come up with an optimal design which minimizes noise impact.
- The departure traffic is not included into the current optimization and design. The departure routes should be implemented in both the design of the PMS and the design of the scheduling model.
- Further research has to be performed to explore other runway configurations, to check if the PMS can be used for every configuration and to explore how the airspace is affected.
- In this thesis potential advantages to safety have been explored. However, due to the radical change in procedure a thorough safety and risk analysis is required to find the major hazards and risks of the PMS at AAS. Also, a validation of the system has to be done to check the change in workload for the ATC as well as the pilots.
- The sequencing legs in the proposed PMS are level. However, a CDA can also be conducted along a sequencing leg. A non-level sequencing leg can be included into the model for additional fuel savings.
- Instead of an event-based rolling horizon approach, an approach can be taken based on dynamic optimisation using heuristics, which can be updated every second for live updates.
- Perform a full day of simulations to establish the actual noise contour map representing a full day.
- Scenarios, such as closed runways and missed approaches, have to be explored to see if the system is able to withstand runway closure, and to see whether aircraft can be readily resequenced.
- Alternative optimisation algorithms can be explored with the aim to decrease the computational time.
- Further research should be performed for variable aircraft weight and wind conditions.

A

Point Merge System Coordinates

Table A.1: Coordinates of the point merge system proposed at AAS.

NAME	Latitude	Longitude
ARTIP	52.511214	5.569081
EH604	52.589444	4.837222
EH607	52.583889	4.646944
EH608	52.539444	4.728056
EH621	52.462703	4.721097
EH626	52.398056	4.745833
EH630	52.433814	4.749456
NIRSI	52.583878	4.513372
PMS170E	52.605034	4.940405
PMS172E	52.554801	5.397544
PMS172W	52.308693	4.410417
PMS173E	52.543506	5.488806
PMS174E	52.556489	4.764314
PMS181	52.300819	4.35175
RIVER	51.912778	4.1325
RWY18C	52.331397	4.740031
RWY18R	52.360258	4.711725
SUGOL	52.525556	3.967222

B

Standard appoach routes and night approach

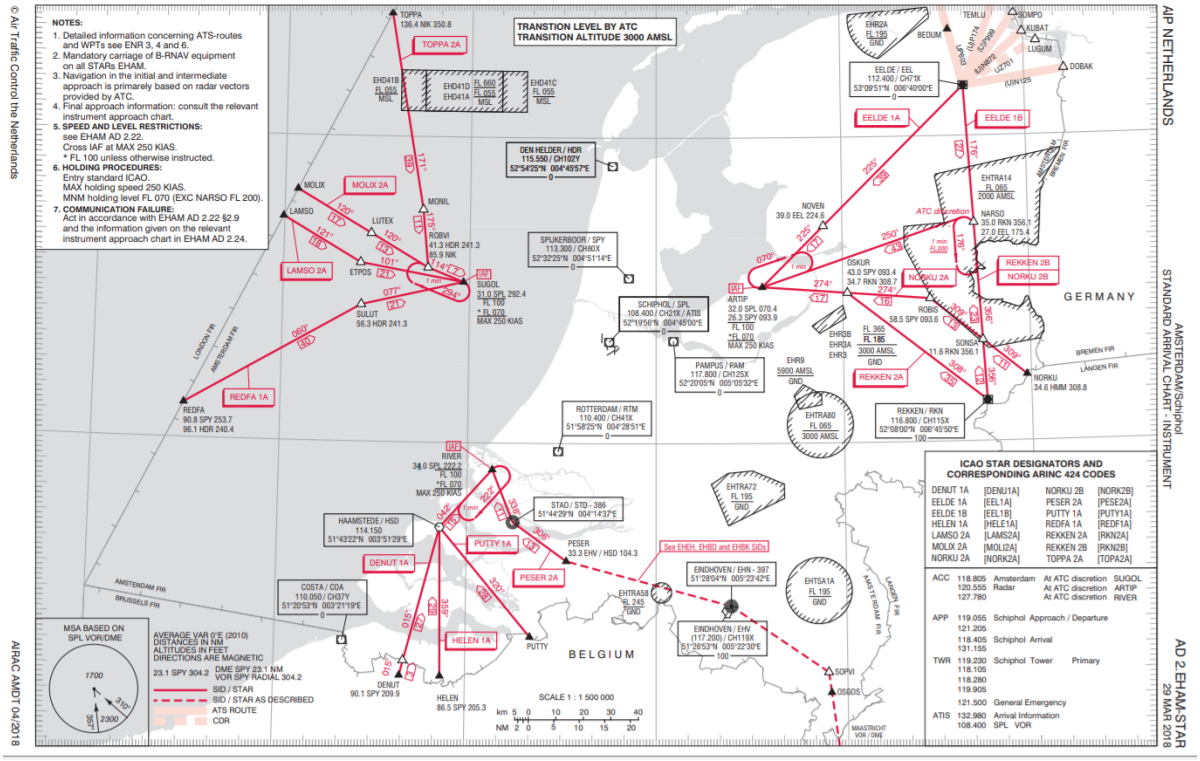

Figure B.1: Standard approach chart at AAS [1].

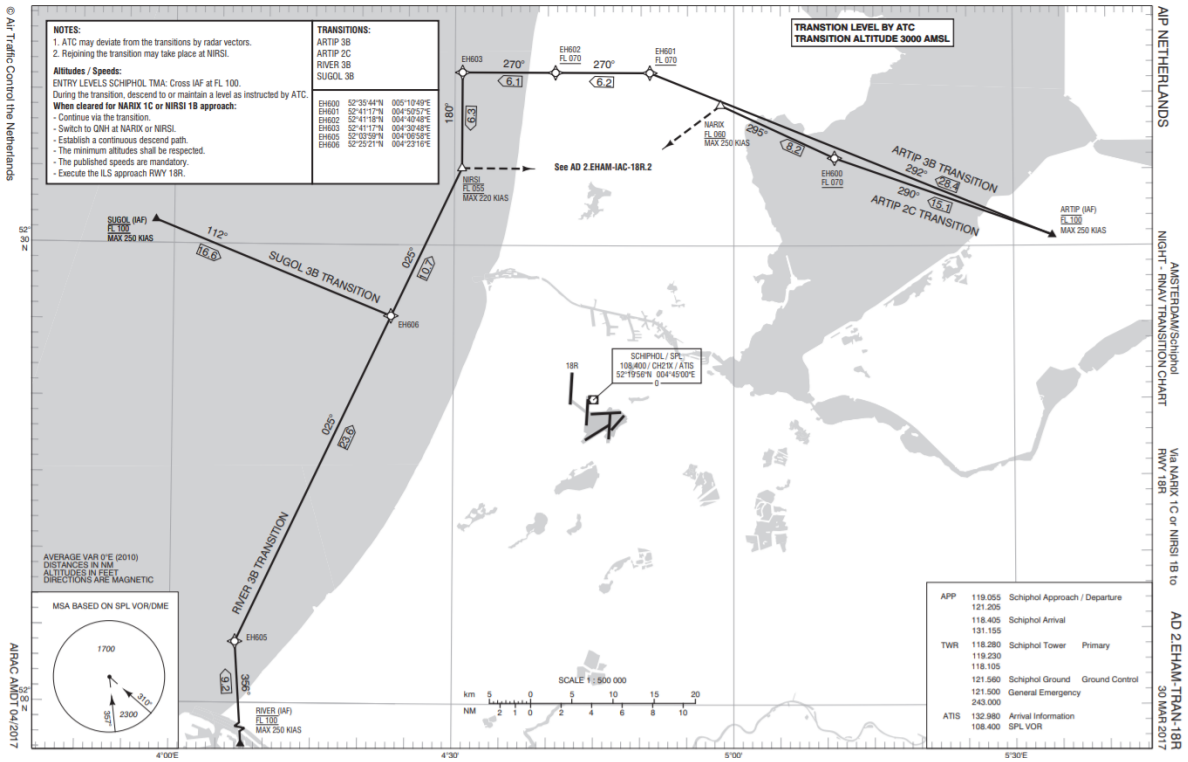

(a) Transition chart to runway 18R

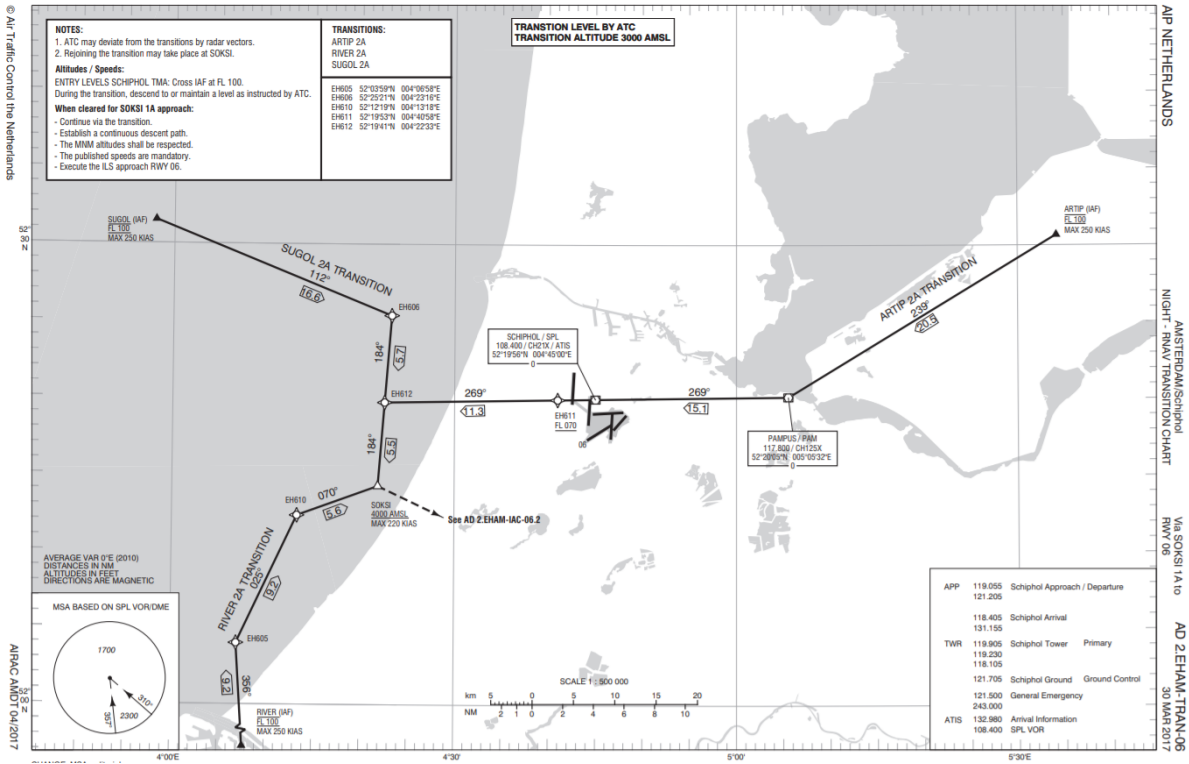

(b) Transition chart to runway 06

Figure B.2: Night hours RNAV transition charts [1]

C

Continuous descent approach calculations

Table C.1: The CDA profile for RIVER from the sequencing leg at 9,000 ft to runway 18R.

Aircraft type	Total distance in (nm)	Duration in (s)	Fuel in (kg)	approach TAS (kts)
B738	37.7	570.2	274.6	157.0
B772	37.7	573.8	625.9	154.8
A320	37.7	586.0	247.4	141.1
B737	37.7	582.9	254.8	146.7
A330	37.7	596.7	469.1	139.3
B717	37.7	575.6	202.0	149.7
A319	37.7	605.3	235.5	127.8

Table C.2: The CDA profile for ARTIP and SUGOL from the sequencing leg at 10,000 ft to runway 18R.

Aircraft type	Total distance in (nm)	Duration in (s)	Fuel in (kg)	approach TAS (kts)
B738	36.7	555.8	248.1	157.0
B772	36.7	559.5	543.6	154.8
A320	36.7	571.2	221.8	141.1
B737	36.7	568.5	230.4	146.7
A330	36.7	582.8	404.4	139.3
B717	36.7	560.7	182.1	149.7
A319	36.7	590.3	212.2	127.8

Table C.3: The CDA profile for ARTIP from the sequencing leg at 10,000 ft to runway 18C.

Aircraft type	Total distance in (nm)	Duration in (s)	Fuel in (kg)	approach TAS (kts)
B738	37.8	569.5	257.3	157.0
B772	37.8	573.2	569.2	154.8
A320	37.8	584.9	230.8	141.1
B737	37.8	582.2	238.8	146.7
A330	37.8	596.5	424.2	139.3
B717	37.8	574.4	189.4	149.7
A319	37.8	604.1	220.7	127.8

D

Flight Schedule Results

Table D.1: Flight results of the SUGOL and RIVER arrivals for case 1.

Flight	IAF time	Route	Entry time	V initial	Leg time	CDA time	Finaltime	V leg	Fuel initial	Fuel leg	Fuel CDA	Aircraft
COA58	0.00	SUGOL	41.58	290.92	0.00	582.80	624.38	0.00	60.45	0.00	404.42	A330
DAL238	130.00	SUGOL	171.59	290.92	0.00	582.80	754.39	0.00	60.45	0.00	404.42	A330
EZS3DC	269.00	RIVER	311.24	286.40	0.00	605.30	916.54	0.00	26.28	0.00	235.54	A319
DAL230	355.00	SUGOL	398.92	275.46	12.37	582.80	994.10	290.92	61.82	17.99	404.42	A330
BCY5200	455.00	RIVER	497.39	285.41	41.35	575.60	1114.35	261.16	23.00	21.27	202.02	B717
CKS329	605.00	SUGOL	646.59	290.92	0.00	559.50	1206.09	0.00	77.87	0.00	543.65	B772
KLM1736	671.00	RIVER	721.99	237.29	28.75	575.60	1326.34	250.41	25.70	14.66	202.02	B717
AWE798	864.00	SUGOL	905.59	290.92	0.00	582.80	1488.39	0.00	60.45	0.00	404.42	A330
KLM1486	1114.00	SUGOL	1155.59	290.92	0.00	560.70	1716.29	0.00	22.48	0.00	182.08	B717
KLM92Z	1195.00	SUGOL	1236.59	290.92	0.00	555.80	1792.39	0.00	27.85	0.00	248.14	B738
KLM1502	1267.00	SUGOL	1308.59	290.92	0.00	560.70	1869.29	0.00	22.48	0.00	182.08	B717
DAL244	1334.00	SUGOL	1375.59	290.92	0.00	582.80	1958.39	0.00	60.45	0.00	404.42	A330
KLM1034	1402.00	SUGOL	1447.53	265.75	70.41	560.70	2078.64	255.64	23.23	35.62	182.08	B717
KLM1530	1498.00	SUGOL	1548.29	240.58	41.80	560.70	2150.79	258.38	25.10	21.19	182.08	B717
KLM783	1574.00	SUGOL	1621.34	255.57	39.70	559.50	2220.54	272.03	85.52	72.40	543.65	B772
KLM32W	1613.00	SUGOL	1708.63	265.16	66.14	568.50	2343.26	272.17	26.68	39.38	230.36	B737
KLM54S	1670.00	SUGOL	1780.29	240.58	74.42	560.70	2415.41	241.86	25.10	37.20	182.08	B717
KLM90J	1810.00	SUGOL	1858.95	247.17	67.91	560.70	2487.56	265.05	24.58	34.63	182.08	B717
RAE482	1871.00	RIVER	1917.21	261.84	66.91	575.60	2559.71	269.03	23.78	35.02	202.02	B717
KLM1046	1930.00	SUGOL	1980.29	240.58	90.87	560.70	2631.86	277.31	25.10	47.64	182.08	B717
AZA118	1987.00	RIVER	2038.93	232.97	72.10	605.30	2716.34	249.64	27.99	40.39	235.54	A319
EIN60A	2035.00	SUGOL	2086.93	232.97	134.73	571.20	2792.86	240.48	31.08	81.27	221.83	A320
KLM1276	2102.00	SUGOL	2147.22	267.57	158.64	555.80	2861.65	272.32	29.05	102.33	248.14	B738
EZY887W	2170.00	SUGOL	2221.93	232.97	133.90	590.30	2946.13	241.98	27.69	72.80	212.18	A319
KLM1058	2246.00	SUGOL	2296.29	240.58	161.29	560.70	3018.28	290.17	25.10	87.04	182.08	B717
KLM952	2314.00	SUGOL	2358.43	272.32	173.24	555.80	3087.47	290.92	28.65	116.03	248.14	B738
EZY215D	2390.00	SUGOL	2440.53	239.41	152.07	568.50	3161.11	260.40	28.84	88.51	230.36	B737
KLM40M	2472.00	SUGOL	2522.53	239.41	143.70	568.50	3234.74	250.51	28.84	82.88	230.36	B737
KLM1618	2548.00	RIVER	2592.95	269.13	140.38	570.20	3303.53	282.10	29.30	93.93	274.61	B738
KLM1314	2764.00	RIVER	2806.24	286.40	0.00	575.60	3381.84	0.00	22.97	0.00	202.02	B717
RAE364	2851.00	RIVER	2893.24	286.40	0.00	575.60	3468.84	0.00	22.97	0.00	202.02	B717
KLM48Y	2923.00	RIVER	2965.24	286.40	0.00	582.90	3548.14	0.00	26.52	0.00	254.78	B737
KLM24H	2990.00	RIVER	3033.33	279.25	13.41	570.20	3616.94	268.41	28.82	8.74	274.61	B738
EIN84L	3067.00	SUGOL	3108.59	290.92	13.78	571.20	3693.57	261.26	27.39	8.49	221.83	A320

Table D.1: Flight results of the SUGOL and RIVER arrivals for case 1.

Flight	IAF time	Route	Entry time	V initial	Leg time	CDA time	Finaltime	V leg	Fuel initial	Fuel leg	Fuel CDA	Aircraft
SMX5110	3264.00	RIVER	3306.24	286.40	0.00	586.00	3892.24	0.00	28.03	0.00	247.41	A320
UAL908	3326.00	SUGOL	3373.35	255.49	13.64	582.80	3969.80	263.88	64.64	18.75	404.42	A330
KLM88T	3389.00	RIVER	3433.78	270.20	80.47	570.20	4084.45	268.41	29.25	52.42	274.61	B738
EZS1041	3657.00	RIVER	3699.24	286.40	0.00	605.30	4304.54	0.00	26.28	0.00	235.54	A319
EZY7905	3782.00	RIVER	3824.24	286.40	0.00	605.30	4429.54	0.00	26.28	0.00	235.54	A319
KLM1000	3931.00	SUGOL	3972.59	290.92	0.00	555.80	4528.39	0.00	27.85	0.00	248.14	B738
KLM1260	4027.00	RIVER	4069.24	286.40	0.00	575.60	4644.84	0.00	22.97	0.00	202.02	B717
BMI77H	4042.00	SUGOL	4092.53	239.41	57.44	568.50	4718.48	250.68	28.84	33.13	230.36	B737
KLM98C	4118.00	RIVER	4164.75	258.81	50.28	575.60	4790.63	286.40	23.99	27.35	202.02	B717
BMI13P	4171.00	SUGOL	4214.09	280.81	81.67	568.50	4864.26	264.46	26.22	47.72	230.36	B737
KLM1596	4291.00	RIVER	4337.71	258.99	25.14	570.20	4933.05	286.40	30.22	16.96	274.61	B738
KLM50G	4454.00	RIVER	4496.24	286.40	0.00	575.60	5071.84	0.00	22.97	0.00	202.02	B717
KLM1722	4536.00	RIVER	4578.24	286.40	0.00	575.60	5153.84	0.00	22.97	0.00	202.02	B717
AFR240F	4617.00	RIVER	4659.24	286.40	0.00	586.00	5245.24	0.00	28.03	0.00	247.41	A320
EZY300J	4723.00	SUGOL	4764.59	290.92	0.00	590.30	5354.89	0.00	25.72	0.00	212.18	A319
EXS201	4829.00	SUGOL	4870.59	290.92	0.00	568.50	5439.09	0.00	25.95	0.00	230.36	B737
KLM1400	4857.00	RIVER	4907.99	237.29	27.65	575.60	5511.24	260.37	25.70	14.21	202.02	B717
VLG8300	4949.00	RIVER	4991.24	286.40	12.57	586.00	5589.81	286.40	28.03	8.34	247.41	A320
BAW78TE	5078.00	SUGOL	5119.59	290.92	0.00	568.50	5688.09	0.00	25.95	0.00	230.36	B737
EZY700A	5251.00	SUGOL	5292.59	290.92	0.00	590.30	5882.89	0.00	25.72	0.00	212.18	A319
EZY2725	5265.00	RIVER	5316.93	232.97	45.13	605.30	5967.36	239.30	27.99	24.69	235.54	A319
DAL232	5410.00	SUGOL	5451.59	290.92	12.37	582.80	6046.76	290.92	60.45	17.99	404.42	A330
AFR1340	5419.00	RIVER	5462.60	277.47	125.70	586.00	6174.30	286.40	28.36	83.44	247.41	A320
DAL234	5774.00	SUGOL	5815.59	290.92	0.00	582.80	6398.39	0.00	60.45	0.00	404.42	A330
AFR3480	6014.00	RIVER	6056.24	286.40	0.00	575.60	6631.84	0.00	22.97	0.00	202.02	B717

Table D.2: Flight results of the ARTIP arrivals for case 1.

Flight	IAF time	Route	Entry time	V initial	Leg time	CDA time	Finaltime	V leg	Fuel initial	Fuel leg	Fuel CDA	Aircraft
KLM554	0.00	ARTIP	85.14	290.92	0.00	573.20	658.34	0.00	159.44	0.00	569.20	B772
KLM1900	149.00	ARTIP	234.15	290.92	0.00	574.40	808.55	0.00	46.02	0.00	189.44	B717
KLM88J	303.00	ARTIP	388.15	290.92	0.00	574.40	962.55	0.00	46.02	0.00	189.44	B717
KLM1750	802.00	ARTIP	887.15	290.92	0.00	574.40	1461.55	0.00	46.02	0.00	189.44	B717
KLM30K	903.00	ARTIP	988.15	290.92	0.00	574.40	1562.55	0.00	46.02	0.00	189.44	B717
DLH2FM	1119.00	ARTIP	1204.15	290.92	0.00	574.40	1778.55	0.00	46.02	0.00	189.44	B717
KLM08V	1210.00	ARTIP	1295.15	290.92	0.00	582.20	1877.35	0.00	53.13	0.00	238.85	B737
KLM1178	1820.00	ARTIP	1905.15	290.92	0.00	574.40	2479.55	0.00	46.02	0.00	189.44	B717
DLH6HR	1964.00	ARTIP	2049.15	290.92	0.00	574.40	2623.55	0.00	46.02	0.00	189.44	B717
GIA88	2170.00	ARTIP	2255.15	290.92	0.00	596.50	2851.65	0.00	123.77	0.00	424.22	A330
KLM74M	2280.00	ARTIP	2372.75	267.08	24.75	574.40	2971.90	290.92	47.48	13.38	189.44	B717
KLM1184	2410.00	ARTIP	2495.15	290.92	0.00	582.20	3077.35	0.00	53.13	0.00	238.85	B737
KLM1762	2525.00	ARTIP	2610.15	290.92	0.00	574.40	3184.55	0.00	46.02	0.00	189.44	B717
KLM1610	2597.00	ARTIP	2683.84	285.24	0.00	569.50	3253.34	0.00	57.49	0.00	257.27	B738
KLM1172	2741.00	ARTIP	2826.15	290.92	0.00	574.40	3400.55	0.00	46.02	0.00	189.44	B717
KLM58H	2847.00	ARTIP	2932.15	290.92	0.00	574.40	3506.55	0.00	46.02	0.00	189.44	B717
ELL773	2972.00	ARTIP	3057.15	290.92	0.00	582.20	3639.35	0.00	53.13	0.00	238.85	B737
KLM22T	3087.00	ARTIP	3172.15	290.92	0.00	582.20	3754.35	0.00	53.13	0.00	238.85	B737
KLM445	3197.00	ARTIP	3282.15	290.92	0.00	596.50	3878.65	0.00	123.77	0.00	424.22	A330
KLM1164	3288.00	ARTIP	3391.46	239.41	27.70	582.20	4001.37	259.88	59.05	16.12	238.85	B737
AUI101	3423.00	ARTIP	3508.15	290.92	0.00	582.20	4090.35	0.00	53.13	0.00	238.85	B737
KLM1212	3504.00	ARTIP	3589.15	290.92	0.00	574.40	4163.55	0.00	46.02	0.00	189.44	B717
KLM1866	3562.00	ARTIP	3661.30	249.46	0.00	574.40	4235.70	0.00	49.96	0.00	189.44	B717
KLM1140	3692.00	ARTIP	3777.15	290.92	0.00	569.50	4346.65	0.00	57.02	0.00	257.27	B738
KLM1106	3802.00	ARTIP	3887.15	290.92	0.00	582.20	4469.35	0.00	53.13	0.00	238.85	B737
CSA4VP	3879.00	ARTIP	3964.15	290.92	0.00	584.90	4549.05	0.00	56.08	0.00	230.80	A320
KLM1372	3970.00	ARTIP	4055.15	290.92	0.00	582.20	4637.35	0.00	53.13	0.00	238.85	B737
SDM277	4080.00	ARTIP	4165.15	290.92	0.00	604.10	4769.25	0.00	52.67	0.00	220.66	A319
KLM1362	4191.00	ARTIP	4276.15	290.92	0.00	574.40	4850.55	0.00	46.02	0.00	189.44	B717
KLM1572	4359.00	ARTIP	4444.15	290.92	0.00	569.50	5013.65	0.00	57.02	0.00	257.27	B738
KLM1650	4512.00	ARTIP	4597.15	290.92	0.00	582.20	5179.35	0.00	53.13	0.00	238.85	B737
KLM1838	4599.00	ARTIP	4684.15	290.92	0.00	574.40	5258.55	0.00	46.02	0.00	189.44	B717
KLM26B	4709.00	ARTIP	4794.15	290.92	0.00	574.40	5368.55	0.00	46.02	0.00	189.44	B717
KLM1790	4892.00	ARTIP	4977.15	290.92	0.00	582.20	5559.35	0.00	53.13	0.00	238.85	B737

Table D.2: Flight results of the ARTIP arrivals for case 1.

Flight	IAF time	Route	Entry time	V initial	Leg time	CDA time	Finaltime	V leg	Fuel initial	Fuel leg	Fuel CDA	Aircraft
KLM32J	5016.00	ARTIP	5101.15	290.92	0.00	574.40	5675.55	0.00	46.02	0.00	189.44	B717
CAI1523	5218.00	ARTIP	5303.15	290.92	0.00	582.20	5885.35	0.00	53.13	0.00	238.85	B737
CAI1503	5396.00	ARTIP	5481.15	290.92	0.00	582.20	6063.35	0.00	53.13	0.00	238.85	B737
KLM462	5515.00	ARTIP	5600.15	290.92	0.00	569.50	6169.65	0.00	57.02	0.00	257.27	B738
DLH7MJ	5626.00	ARTIP	5711.15	290.92	0.00	584.90	6296.05	0.00	56.08	0.00	230.80	A320

Table D.3: Flight results of the SUGOL and RIVER arrivals for case 2.

Flight	IAF time	Route	Entry time	V initial	Leg time	CDA time	Finaltime	V leg	Fuel initial	Fuel leg	Fuel CDA	Aircraft
BAW440	0.00	SUGOL	41.58	290.92	0.00	571.20	612.78	0.00	27.39	0.00	221.83	A320
TRA6332	124.01	RIVER	166.24	286.40	0.00	582.90	749.14	0.00	26.52	0.00	254.78	B737
BMI77Z	163.01	SUGOL	213.44	239.86	40.84	568.50	822.78	264.46	28.80	23.86	230.36	B737
IBE32YY	211.01	RIVER	262.93	232.97	50.37	586.00	899.30	285.88	31.36	33.40	247.41	A320
EXS205	312.01	SUGOL	362.53	239.41	41.90	568.50	972.93	257.76	28.84	24.33	230.36	B737
KLM574	369.01	RIVER	420.10	236.75	43.56	582.90	1046.57	247.91	29.48	25.40	254.78	B737
KLM1204	489.01	SUGOL	534.81	264.10	24.75	555.80	1115.36	290.92	29.36	16.58	248.14	B738
ISS3423	729.01	RIVER	771.24	286.40	0.00	605.30	1376.54	0.00	26.28	0.00	235.54	A319
KLM1088	926.01	SUGOL	967.59	290.92	0.00	560.70	1528.29	0.00	22.48	0.00	182.08	B717
RAE262	1247.01	RIVER	1289.24	286.40	0.00	575.60	1864.84	0.00	22.97	0.00	202.02	B717
KLM48M	1296.01	SUGOL	1345.23	245.76	24.75	568.50	1938.48	290.92	28.26	15.45	230.36	B737
KLM64H	1368.01	SUGOL	1412.80	270.04	37.12	560.70	2010.63	290.92	23.09	20.07	182.08	B717
KLM30W	1440.01	SUGOL	1490.53	239.41	25.23	568.50	2084.26	285.42	28.84	15.53	230.36	B737
KLM1286	1574.01	SUGOL	1615.59	290.92	0.00	568.50	2184.09	0.00	25.95	0.00	230.36	B737
KLM52R	1656.01	SUGOL	1697.59	290.92	0.00	560.70	2258.29	0.00	22.48	0.00	182.08	B717
KLM1550	1717.01	SUGOL	1758.59	290.92	12.37	560.70	2331.66	290.92	22.48	6.69	182.08	B717
KLM1190	1757.01	SUGOL	1807.53	239.41	29.26	568.50	2405.30	246.05	28.84	16.81	230.36	B737
KLM82J	1824.01	SUGOL	1868.31	273.07	49.98	555.80	2474.09	288.10	28.60	33.28	248.14	B738
KLM1148	2068.01	SUGOL	2109.59	290.92	0.00	555.80	2665.39	0.00	27.85	0.00	248.14	B738
EZY7909	2116.01	RIVER	2158.24	286.40	0.00	605.30	2763.54	0.00	26.28	0.00	235.54	A319
KLM1498	2270.01	SUGOL	2311.59	290.92	0.00	560.70	2872.29	0.00	22.48	0.00	182.08	B717
KLM42G	2270.11	RIVER	2318.56	249.66	50.28	575.60	2944.44	286.40	24.68	27.35	202.02	B717
KLM1512	2491.01	SUGOL	2532.59	290.92	0.00	560.70	3093.29	0.00	22.48	0.00	182.08	B717
EZY6923	2587.01	SUGOL	2628.59	290.92	0.00	590.30	3218.89	0.00	25.72	0.00	212.18	A319
KLM1746	2587.11	RIVER	2632.73	265.14	82.71	575.60	3291.04	261.16	23.67	42.54	202.02	B717
KLM80T	2702.01	RIVER	2749.39	255.27	40.24	570.20	3359.83	268.41	30.57	26.21	274.61	B738
KLM1732	2784.01	RIVER	2831.24	256.10	25.14	575.60	3431.98	286.40	24.19	13.67	202.02	B717
KLM1628	2875.01	RIVER	2918.00	281.34	12.57	570.20	3500.77	286.40	28.72	8.48	274.61	B738
EZY877C	2908.01	SUGOL	2957.83	242.82	37.12	590.30	3585.25	290.92	27.13	22.97	212.18	A319
KLM1538	2990.01	SUGOL	3040.29	240.58	56.41	560.70	3657.40	255.27	25.10	28.52	182.08	B717
KLM44U	3081.01	RIVER	3128.81	253.06	25.14	575.60	3729.55	286.40	24.42	13.67	202.02	B717
KLM1042	3216.01	SUGOL	3257.59	290.92	0.00	560.70	3818.29	0.00	22.48	0.00	182.08	B717
AFR3484	3302.01	RIVER	3344.24	286.40	0.00	575.60	3919.84	0.00	22.97	0.00	202.02	B717
KLM1408	3532.01	RIVER	3574.24	286.40	0.00	575.60	4149.84	0.00	22.97	0.00	202.02	B717

Table D.3: Flight results of the SUGOL and RIVER arrivals for case 2.

Flight	IAF time	Route	Entry time	V initial	Leg time	CDA time	Finaltime	V leg	Fuel initial	Fuel leg	Fuel CDA	Aircraft
KLM68U	3628.01	RIVER	3670.24	286.40	0.00	570.20	4240.44	0.00	28.50	0.00	274.61	B738
RAE486	3772.01	RIVER	3814.24	286.40	0.00	575.60	4389.84	0.00	22.97	0.00	202.02	B717
KLM1656	3883.01	RIVER	3925.24	286.40	0.00	582.90	4508.14	0.00	26.52	0.00	254.78	B737
EIN844	3988.01	SUGOL	4029.59	290.92	0.00	571.20	4600.79	0.00	27.39	0.00	221.83	A320
KLM1694	4003.01	RIVER	4049.10	262.43	50.28	570.20	4669.58	286.40	29.89	33.93	274.61	B738
KLM74N	4108.01	RIVER	4153.56	265.54	12.57	575.60	4741.73	286.40	23.65	6.84	202.02	B717
KLM1022	4152.01	SUGOL	4199.41	255.21	55.32	555.80	4810.53	260.31	30.17	35.36	248.14	B738
KLM54M	4252.01	RIVER	4294.50	284.65	12.57	575.60	4882.67	286.40	23.03	6.84	202.02	B717
KLM12H	4348.01	RIVER	4390.24	286.40	0.00	570.20	4960.44	0.00	28.50	0.00	274.61	B738
KLM26W	4435.01	RIVER	4477.24	286.40	0.00	575.60	5052.84	0.00	22.97	0.00	202.02	B717
SWR734	4511.01	RIVER	4553.24	286.40	0.00	586.00	5139.24	0.00	28.03	0.00	247.41	A320
AFR224C	4598.01	RIVER	4640.24	286.40	0.00	586.00	5226.24	0.00	28.03	0.00	247.41	A320
TRA6224	4790.01	RIVER	4832.24	286.40	0.00	570.20	5402.44	0.00	28.50	0.00	274.61	B738
KLM1592	5006.01	RIVER	5048.24	286.40	0.00	575.60	5623.84	0.00	22.97	0.00	202.02	B717
RAM852	5135.01	RIVER	5177.24	286.40	0.00	570.20	5747.44	0.00	28.50	0.00	274.61	B738
EIN610	5174.01	SUGOL	5225.21	236.25	27.56	571.20	5823.97	261.26	30.75	16.98	221.83	A320
BCY240D	5299.01	SUGOL	5340.59	290.92	0.00	560.70	5901.29	0.00	22.48	0.00	182.08	B717
VLG8423	6192.01	RIVER	6234.24	286.40	0.00	586.00	6820.24	0.00	28.03	0.00	247.41	A320

Table D.4: Flight results of the ARTIP arrivals for case 2.

Flight	IAF time	Route	Entry time	V initial	Leg time	CDA time	Finaltime	V leg	Fuel initial	Fuel leg	Fuel CDA	Aircraft
QTR6055	0.00	ARTIP	85.14	290.92	0.00	596.50	681.64	0.00	123.77	0.00	424.22	A330
DLH3FW	533.00	ARTIP	618.15	290.92	0.00	574.40	1192.55	0.00	46.02	0.00	189.44	B717
JAE7443	739.00	ARTIP	824.15	290.92	0.00	573.20	1397.35	0.00	159.44	0.00	569.20	B772
KLM1180	873.00	ARTIP	958.15	290.92	0.00	574.40	1532.55	0.00	46.02	0.00	189.44	B717
EZY3808	1123.00	ARTIP	1208.15	290.92	0.00	604.10	1812.25	0.00	52.67	0.00	220.66	A319
KLM16V	1349.00	ARTIP	1434.15	290.92	0.00	582.20	2016.35	0.00	53.13	0.00	238.85	B737
KLM804	1368.00	ARTIP	1486.43	280.11	26.47	573.20	2086.10	272.03	163.06	48.27	569.20	B772
KLM60S	1704.00	ARTIP	1789.15	290.92	0.00	574.40	2363.55	0.00	46.02	0.00	189.44	B717
KLM866	1857.00	ARTIP	1942.15	290.92	0.00	573.20	2515.35	0.00	159.44	0.00	569.20	B772
KLM1576	2045.00	ARTIP	2130.15	290.92	0.00	569.50	2699.65	0.00	57.02	0.00	257.27	B738
SXS944	2155.00	ARTIP	2240.15	290.92	0.00	569.50	2809.65	0.00	57.02	0.00	257.27	B738
CSN345	2400.00	ARTIP	2485.15	290.92	0.00	573.20	3058.35	0.00	159.44	0.00	569.20	B772
KLM1758	2501.00	ARTIP	2591.82	272.74	12.37	574.40	3178.60	290.92	47.11	6.69	189.44	B717
KLM1772	2577.00	ARTIP	2676.35	249.33	0.00	574.40	3250.75	0.00	49.98	0.00	189.44	B717
KLM78C	2678.00	ARTIP	2763.15	290.92	0.00	574.40	3337.55	0.00	46.02	0.00	189.44	B717
KLM1116	2822.00	ARTIP	2907.15	290.92	0.00	569.50	3476.65	0.00	57.02	0.00	257.27	B738
KLM24J	3057.00	ARTIP	3142.15	290.92	0.00	574.40	3716.55	0.00	46.02	0.00	189.44	B717
SHY589	3129.00	ARTIP	3214.15	290.92	0.00	582.20	3796.35	0.00	53.13	0.00	238.85	B737
SHY1783	3211.00	ARTIP	3296.15	290.92	0.00	584.90	3881.05	0.00	56.08	0.00	230.80	A320
KLM50B	3293.00	ARTIP	3378.15	290.92	0.00	582.20	3960.35	0.00	53.13	0.00	238.85	B737
KLM36S	3360.00	ARTIP	3451.78	269.89	0.00	582.20	4033.98	0.00	54.33	0.00	238.85	B737
DLH8RT	3465.00	ARTIP	3550.15	290.92	0.00	582.20	4132.35	0.00	53.13	0.00	238.85	B737
KLM896	3561.00	ARTIP	3646.15	290.92	0.00	573.20	4219.35	0.00	159.44	0.00	569.20	B772
KLM904	3657.00	ARTIP	3751.28	262.73	13.22	569.50	4334.00	272.32	60.36	8.53	257.27	B738
PGT293	3734.00	ARTIP	3820.08	287.78	13.22	569.50	4402.80	272.32	57.28	8.53	257.27	B738
KLM1830	3816.00	ARTIP	3901.15	290.92	0.00	574.40	4475.55	0.00	46.02	0.00	189.44	B717
KLM96B	3893.00	ARTIP	3978.15	290.92	0.00	574.40	4552.55	0.00	46.02	0.00	189.44	B717
SAS553	4162.00	ARTIP	4247.15	290.92	0.00	574.40	4821.55	0.00	46.02	0.00	189.44	B717
KLM40E	4258.00	ARTIP	4343.15	290.92	0.00	582.20	4925.35	0.00	53.13	0.00	238.85	B737
KLM1396	4483.00	ARTIP	4568.15	290.92	0.00	582.20	5150.35	0.00	53.13	0.00	238.85	B737
KLM62R	4795.00	ARTIP	4880.15	290.92	0.00	582.20	5462.35	0.00	53.13	0.00	238.85	B737
CSA618	4896.00	ARTIP	4981.15	290.92	0.00	584.90	5566.05	0.00	56.08	0.00	230.80	A320
KLM1614	4968.00	ARTIP	5053.15	290.92	12.37	569.50	5635.02	290.92	57.02	8.29	257.27	B738
KLM66F	5064.00	ARTIP	5149.15	290.92	0.00	574.40	5723.55	0.00	46.02	0.00	189.44	B717

Table D.4: Flight results of the ARTIP arrivals for case 2.

Flight	IAF time	Route	Entry time	V initial	Leg time	CDA time	Finaltime	V leg	Fuel initial	Fuel leg	Fuel CDA	Aircraft
AUA375H	5150.00	ARTIP	5235.15	290.92	0.00	604.10	5839.25	0.00	52.67	0.00	220.66	A319
KLM70J	5241.00	ARTIP	5337.00	258.04	0.00	574.40	5911.40	0.00	48.65	0.00	189.44	B717
JAE7453	5352.00	ARTIP	5437.15	290.92	0.00	573.20	6010.35	0.00	159.44	0.00	569.20	B772
KLM56T	5424.00	ARTIP	5519.07	260.54	37.12	574.40	6130.60	290.92	48.29	20.07	189.44	B717
KLM1386	5505.00	ARTIP	5602.06	255.21	27.83	569.50	6199.39	258.69	61.78	17.77	257.27	B738
KAL543	5587.00	ARTIP	5683.57	256.51	12.37	573.20	6269.14	290.92	174.55	23.18	569.20	B772
MAH668	5659.00	ARTIP	5749.71	273.07	64.59	569.50	6383.80	278.70	58.56	42.19	257.27	B738
CAL6419	5745.00	ARTIP	5842.28	254.63	38.07	573.20	6453.55	283.67	175.65	70.57	569.20	B772
KLM862	5837.00	ARTIP	5934.28	254.63	39.08	573.20	6546.56	276.38	175.65	71.68	569.20	B772
KLM1834	6096.00	ARTIP	6181.15	290.92	0.00	582.20	6763.35	0.00	53.13	0.00	238.85	B737

Table D.5: Flight results of the ARTIP, SUGOL and RIVER arrivals for case 3.

Flight	IAF time	Route	Entry time	V initial	Leg time	CDA time	Finaltime	V leg	Fuel initial	Fuel leg	Fuel CDA	Aircraft
DAL234	0.01	SUGOL	41.59	290.92	0.00	582.80	624.39	0.00	60.45	0.00	404.42	A330
BEE6AB	221.01	SUGOL	262.59	290.92	0.00	560.70	823.29	0.00	22.48	0.00	182.08	B717
AFR3480	240.01	RIVER	282.67	283.52	25.14	575.60	883.41	286.40	23.06	13.67	202.02	B717
AUA371A	317.01	ARTIP	358.59	290.92	24.75	560.70	944.04	290.92	22.48	13.38	182.08	B717
LZB461	432.01	ARTIP	473.59	290.92	0.00	590.30	1063.89	0.00	25.72	0.00	212.18	A319
BAW42AM	447.01	SUGOL	494.59	254.25	61.87	571.20	1127.66	290.92	29.11	40.75	221.83	A320
DAL34	692.01	SUGOL	733.59	290.92	0.00	582.80	1316.39	0.00	60.45	0.00	404.42	A330
SWR724	711.01	RIVER	757.59	259.69	87.58	586.00	1431.17	246.62	29.06	53.79	247.41	A320
ADR434	816.01	ARTIP	862.69	259.15	67.91	560.70	1491.30	265.05	23.68	34.63	182.08	B717
SXS102	936.01	ARTIP	977.59	290.92	0.00	582.80	1560.39	0.00	60.45	0.00	404.42	A330
KZR903	1220.01	ARTIP	1261.59	290.92	0.00	582.80	1844.39	0.00	60.45	0.00	404.42	A330
VLG8356	1239.01	RIVER	1285.18	261.96	87.99	586.00	1959.17	286.40	28.97	58.41	247.41	A320
SAS2551	1344.01	ARTIP	1390.16	262.09	61.87	568.50	2020.53	290.92	26.90	38.61	230.36	B737
EZY6921	1383.01	SUGOL	1431.73	248.26	68.90	590.30	2090.93	261.26	26.84	38.99	212.18	A319
LOT265	1498.01	ARTIP	1548.29	240.58	42.07	560.70	2151.05	256.74	25.10	21.30	182.08	B717
KLM84F	1541.01	SUGOL	1591.29	240.58	59.19	560.70	2211.18	243.28	25.10	29.62	182.08	B717
FIN841Q	1589.01	ARTIP	1630.59	290.92	74.25	571.20	2276.04	290.92	27.39	48.90	221.83	A320
KLM90G	2069.01	ARTIP	2110.59	290.92	0.00	560.70	2671.29	0.00	22.48	0.00	182.08	B717
MAH660	2386.01	ARTIP	2427.59	290.92	0.00	555.80	2983.39	0.00	27.85	0.00	248.14	B738
BCY210E	2444.01	SUGOL	2485.59	290.92	0.00	560.70	3046.29	0.00	22.48	0.00	182.08	B717
SAS821	2458.01	ARTIP	2499.59	290.92	40.84	568.50	3108.93	264.46	25.95	23.86	230.36	B737
KLM12P	2745.01	RIVER	2787.24	286.40	0.00	582.90	3370.14	0.00	26.52	0.00	254.78	B737
TFL344	2760.01	SUGOL	2810.78	238.24	41.19	582.80	3434.77	262.21	68.37	56.53	404.42	A330
MAS6170	3802.01	ARTIP	3843.59	290.92	0.00	559.50	4403.09	0.00	77.87	0.00	543.65	B772
MPH636	4008.01	SUGOL	4049.59	290.92	0.00	582.80	4632.39	0.00	60.45	0.00	404.42	A330
EZY8873	4191.01	SUGOL	4232.59	290.92	0.00	590.30	4822.89	0.00	25.72	0.00	212.18	A319
CAL065	4200.01	ARTIP	4247.27	255.95	74.25	559.50	4881.02	290.92	85.41	139.05	543.65	B772
DLH5HH	4325.01	ARTIP	4373.47	249.62	49.50	568.50	4991.47	290.92	27.92	30.89	230.36	B737
BAW430	4344.01	SUGOL	4395.93	232.97	88.10	571.20	5055.24	245.16	31.08	53.40	221.83	A320
ELY337	4488.01	ARTIP	4530.32	285.86	26.44	555.80	5112.56	272.32	28.05	17.05	248.14	B738
DLH9WY	4637.01	ARTIP	4678.59	290.92	0.00	560.70	5239.29	0.00	22.48	0.00	182.08	B717
DAL260	4656.01	SUGOL	4697.59	290.92	24.75	582.80	5305.14	290.92	60.45	35.98	404.42	A330
KLM644	4748.01	SUGOL	4789.59	290.92	39.70	559.50	5388.79	272.03	77.87	72.40	543.65	B772
BCY216D	5141.01	SUGOL	5182.59	290.92	0.00	560.70	5743.29	0.00	22.48	0.00	182.08	B717

Table D.5: Flight results of the ARTIP, SUGOL and RIVER arrivals for case 3.

Flight	IAF time	Route	Entry time	V initial	Leg time	CDA time	Finaltime	V leg	Fuel initial	Fuel leg	Fuel CDA	Aircraft
CTN450	5223.01	ARTIP	5264.59	290.92	0.00	571.20	5835.79	0.00	27.39	0.00	221.83	A320
DAL264	5424.01	SUGOL	5465.59	290.92	0.00	582.80	6048.39	0.00	60.45	0.00	404.42	A330
KLM24P	5429.01	RIVER	5471.24	286.40	113.13	570.20	6154.57	286.40	28.50	76.34	274.61	B738
KLM592	5688.01	RIVER	5730.24	286.40	0.00	573.80	6304.04	0.00	79.17	0.00	625.91	B772
THY1951	5847.01	ARTIP	5888.59	290.92	0.00	571.20	6459.79	0.00	27.39	0.00	221.83	A320
SAS1553	6226.01	ARTIP	6267.59	290.92	0.00	568.50	6836.09	0.00	25.95	0.00	230.36	B737
MPH665	6288.01	SUGOL	6329.59	290.92	0.00	582.80	6912.39	0.00	60.45	0.00	404.42	A330
KLM678	6380.01	SUGOL	6425.73	264.58	0.00	582.80	7008.53	0.00	62.89	0.00	404.42	A330
TRA5582	6518.01	RIVER	6560.24	286.40	0.00	582.90	7143.14	0.00	26.52	0.00	254.78	B737
KLM1002	6629.01	SUGOL	6670.59	290.92	0.00	555.80	7226.39	0.00	27.85	0.00	248.14	B738
KLM1856	6783.01	ARTIP	6824.59	290.92	0.00	560.70	7385.29	0.00	22.48	0.00	182.08	B717
DAL248	7080.01	SUGOL	7121.59	290.92	0.00	582.80	7704.39	0.00	60.45	0.00	404.42	A330
DAL156	7229.01	SUGOL	7270.59	290.92	0.00	582.80	7853.39	0.00	60.45	0.00	404.42	A330
KLM1692	7234.01	RIVER	7278.95	269.13	107.42	570.20	7956.58	268.10	29.30	69.96	274.61	B738
KLM1196	7306.01	SUGOL	7347.59	290.92	111.37	555.80	8014.76	290.92	27.85	74.59	248.14	B738
AMC396	7335.01	RIVER	7381.34	261.09	111.19	586.00	8078.53	259.01	29.00	69.30	247.41	A320

E

Comparison between FCFS and CPS2

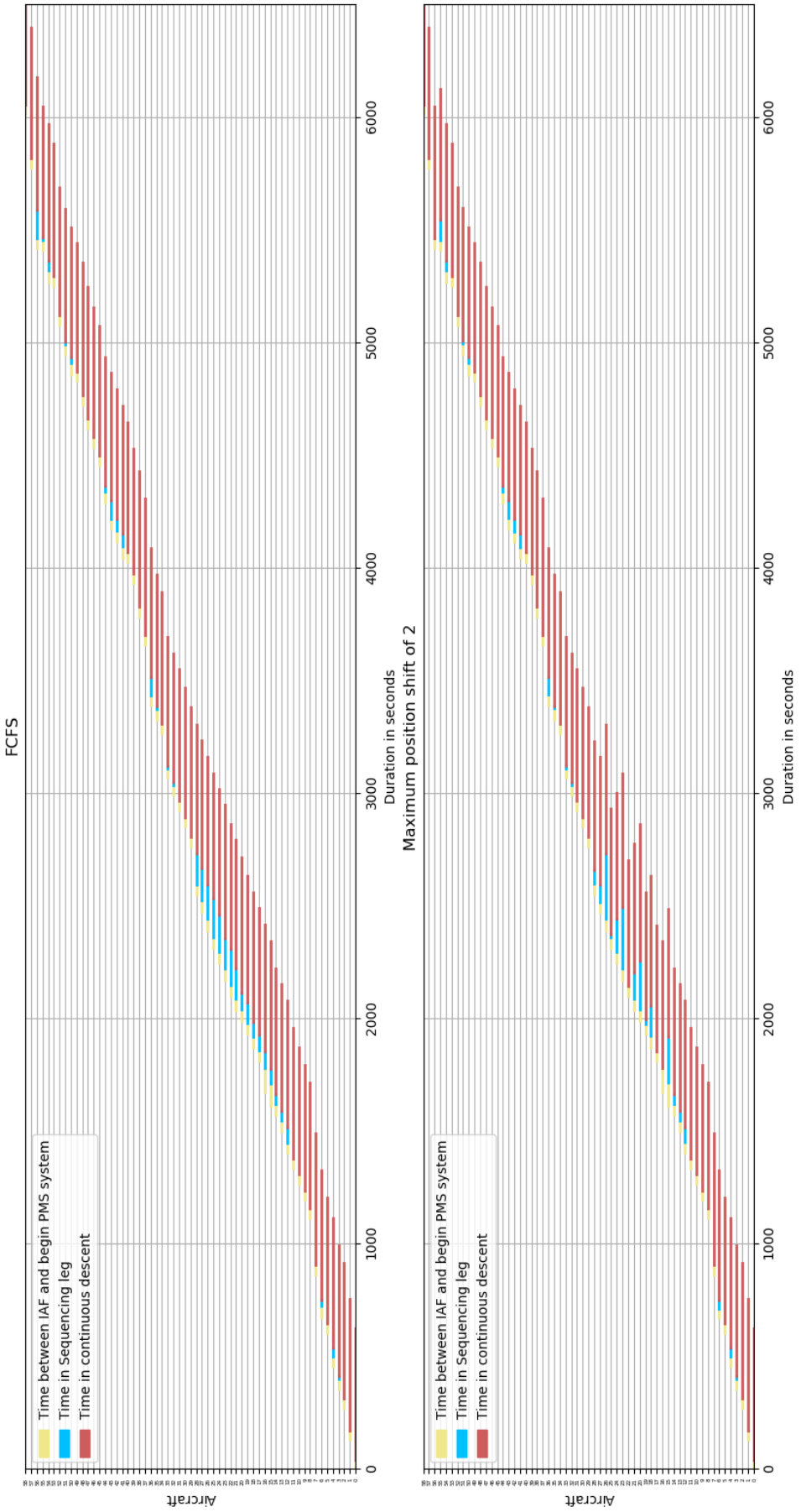

Figure E.1: Effect of the maximum allowed positions shift on the times in the sequencing leg for case 1.

Bibliography

[1] AIS. Integrated Aeronautical Information Package Netherlands (AIP). www.ais-netherlands.nl/, 2017. Accessed: 01-12-2017.

[2] S. Alam, M. H. Nguyen, H. A. Abbass, C. Lokan, M. Ellejmi, and S. Kirby Eurocontrol. A dynamic continuous descent approach methodology for low noise and emission. *AIAA/IEEE Digital Avionics Systems Conference - Proceedings*, 2010. ISSN 0021-8669. doi: 10.1109/DASC.2010.5655502.

[3] Pasquale Avella, Maurizio Boccia, Carlo Mannino, and Igor Vasilyev. Time-Indexed Formulations for the Runway Scheduling Problem. (October), 2017.

[4] AVINOR. Aeronautical Information Package Norway, 2018. URL https://ais.avinor.no/en/AIP/View/33/aip/ad/engm/engm{_}en.html.

[5] Hamsa Balakrishnan and Bala Chandran. Scheduling aircraft landings under constrained position shifting. *Collection of Technical Papers - AIAA Guidance, Navigation, and Control Conference 2006*, 4:2175–2197, 2006. doi: 10.2514/6.2006-6320. URL http://www.scopus.com/inward/record.url?eid=2-s2.0-33845734148{&}partnerID=tZOtx3y1.

[6] E. M L Beale and J. J H Forrest. Global optimization using special ordered sets. *Mathematical Programming*, 10(1):52–69, 1976. ISSN 00255610. doi: 10.1007/BF01580653.

[7] J E Beasley, M Krishnamoorthy, Y M Sharaiha, and D Abramson. Scheduling Aircraft Landings—The Static Case. *Transportation Science*, 34(2):180–197, 2000. ISSN 0041-1655. doi: 10.1287/trsc.34.2.180.12302. URL http://pubsonline.informs.org/doi/abs/10.1287/trsc.34.2.180.12302.

[8] Peter Belobaba. *The Global Airline Industry*. 2009. ISBN 9780470740774. doi: 10.1002/9780470744734.ch4.

[9] Alberto Bemporad and Manfred Morari. Control of systems integrating logic, dynamics, and constraints. *Automatica*, 35(3):407–427, 1999. ISSN 00051098. doi: 10.1016/S0005-1098(98)00178-2.

[10] Julia A Bennell, Mohammad Mesgarpour, and Chris N Potts. Airport runway scheduling. *Annals of Operations Research*, 204(1):249–270, 2013. ISSN 02545330. doi: 10.1007/s10479-012-1268-1.

[11] Lucio Bianco, Paolo Dell'Olmo, and Stefano Giordani. Scheduling models for air traffic control in terminal areas. *Journal of Scheduling*, 9(3):223–253, 2006. ISSN 10946136. doi: 10.1007/s10951-006-6779-7.

[12] Eric R Boeker, Eric Dinges, Bill He, and Gregg Fleming. INM Technical Manual. Technical report, Office of Environment and Energy, Cambridge, MA, 2008.

[13] Ludovic Boursier, Bruno Favennec, Eric Hoffman, Aymeric Trzmiel, François Vergne, and Karim Zeghal. Merging Arrival Flows Without Heading Instructions. *USA/Europe Air Traffic Management Research and Development Seminar*, (July):1–8, 2007. URL http://www.eurocontrol.int/eec/gallery/content/public/document/eec/conference/paper/2007/011{_}Merging{_}arrival{_}flows.pdf.

[14] Brian J Capozzi and Stephen C Atkins. Towards Optimal Routing and Scheduling of Metroplex Operations. *9th AIAA Aviation Technology, Integration, and Operations Conference (ATIO)*, (September), 2009.

[15] IBM corp. IBM ILOG CPLEX Optimization Studio CPLEX User's Manual Version 12 Release 7, 2017.

[16] Jasper de Wilde. Point-Merge Air Traffic Sequencing System. Technical report, 2017.

[17] Jitamitra Desai and Rakesh Prakash. An optimization framework for terminal sequencing and scheduling: The single runway case. *Advances in Intelligent Systems and Computing*, 426:195–207, 2016. ISSN 21945357. doi: 10.1007/978-3-319-29643-2_15.

[18] Angela Errico, Vittorio Di Vito, and Luigi Federico. Study on Continuous Descent Operation for Efficient Air Transport System. *16th AIAA Aviation Technology, Integration, and Operations Conference*, (June):1–14, 2016. doi: 10.2514/6.2016-3157. URL http://arc.aiaa.org/doi/10.2514/6.2016-3157.

[19] EUROCONTROL. RNAV Application in Terminal Airspace - an Atc Operational Perspective. 1999.

[20] EUROCONTROL. Guidance Material for the Design of Terminal Procedures for DME / DME and GNSS Area Navigation. (December), 1999.

[21] EUROCONTROL. Volume 2 EUROCONTROL Manual For Airspace Planning. 2, 2003.

[22] Eurocontrol. Eurocontrol Airspace Planning Manual. (2.0), 2005.

[23] EUROCONTROL. European Airspace Concept Handbook for PBN Implementation. (Edition 3.0), 2013.

[24] Eurocontrol. Base of Aircraft Data Factsheet, 2015. URL http://www.eurocontrol.int/sites/default/files/publication/files/bada-factsheet.pdf.

[25] EUROCONTROL. USER MANUAL FOR THE BASE OF AIRCRAFT DATA (BADA) REVISION 3.12. Technical report, 2104. URL http://scholar.google.com/scholar?hl=en{&}btnG=Search{&}q=intitle:REvisiting+the+Swiss+Cheese+model+of+accidents{#}0.

[26] EUROPEAN CIVIL AVIATION CONFERENCE. Report on Standard Method of Computing Noise Contours around Civil Airports. 1(4th Edition), 2016.

[27] Bruno Favennec, Eric Hoffman, Aymeric Trzmiel, François Vergne, and Karim Zeghal. The Point Merge Arrival Flow Integration Technique: Towards More Complex Environments and Advanced Continuous Descent. *9th AIAA Aviation Technology, Integration, and Operations Conference (ATIO)*, (September):1–12, 2009. doi: 10.2514/6.2009-6921. URL http://arc.aiaa.org/doi/10.2514/6.2009-6921.

[28] Bruno Favennec, François Vergne, and Karim Zeghal. Point merge integration of arrival flows enabling extensive RNAV application and CDA–operational services and environment definition. *Eurocontrol Experimental Center, Version*, (April):1–89, 2010. URL http://scholar.google.com/scholar?hl=en{&}btnG=Search{&}q=intitle:Point+Merge+Integration+of+Arrival+Flows+Enabling+Extensive+RNAV+Application+and+CDA+Operational+Services+and+Environment+Definition{#}0.

[29] FlightAware. Live Flight Tracking. URL https://flightaware.com/.

[30] Sander Hartjes, Vinh Ho-Huu, Hendrikus Visser, and Richard Curran. An Efficient Application of the MOEA/D Algorithm for Designing Noise Abatement Departure Trajectories. *Aerospace*, 4(4):54, 2017. ISSN 2226-4310. doi: 10.3390/aerospace4040054. URL http://www.mdpi.com/2226-4310/4/4/54.

[31] Hellenic Civil Aviation Authority. Introduction of precision RNAV in Greek terminal area. pages 1–6, 2006.

[32] Frederick S. Hillier and Gerald J. Lieberman. *Introduction to Operations research, Ninth Edition*. Number 9. McGraw-Hill, New York, ninth edit edition, 2010. ISBN 978-0-07-337629-5. doi: 10.1097/00000542-199707000-00046. URL http://content.wkhealth.com/linkback/openurl?sid=WKPTLP:landingpage{&}an=00000542-199707000-00046.

[33] Eric Hoffman. Point merge: improving and harmonising arrival operations. https://www.eurocontrol.int/services/point-merge-concept, 2017. Accessed: 06-12-2017.

[34] Youkyung Hong, Byunghun Choi, Somang Lee, Keumjin Lee, and Youdan Kim. Optimal and Practical Aircraft Sequencing and Scheduling for Point Merge System. *IFAC-PapersOnLine*, 50(2007):15209–15214, 2017. ISSN 24058963. doi: 10.1016/j.ifacol.2017.08.1904. URL https://doi.org/10.1016/j.ifacol.2017.08.1904.

[35] Youkyung Hong, Keumjin Lee, Youdan Kim, and Byunghun Choi. Optimal Scheduling Algorithm for Air Traffic Point Merge System Using MILP. *EuroGNC*, 2017.

[36] Xiao Bing Hu and Wen Hua Chen. Genetic algorithm based on receding horizon control for arrival sequencing and scheduling. *Engineering Applications of Artificial Intelligence*, 18(5):633–642, 2005. ISSN 09521976. doi: 10.1016/j.engappai.2004.11.012.

[37] ICAO. *Continuous Descent Operations (CDO) Manual*. 2010. ISBN 9789292316402.

[38] International Civil Aviation Organization. Doc 4444 - Air Traffic Management. (June):1–323, 2001.

[39] International Civil Aviation Organization. *Recommended Method for Computing Noise Contours Around Airports*. ICAO, 2008. ISBN 9789292312251.

[40] Irish Aviation Authority. Aeronautical Information Package Ireland, 2018. URL http://iaip.iaa.ie/iaip/aip{_}eidw{_}charts.htm.

[41] Hanbong Lee and Hamsa Balakrishnan. A Study of Tradeoffs in Scheduling Terminal-Area Operations. *Proceedings of the IEEE*, 96(12):2081–2095, 2008. ISSN 15582256. doi: 10.1109/JPROC.2008.2006145.

[42] Somang Lee, Youkyung Hong, and Youdan Kim. Optimal Scheduling Algorithm in Point Merge System Including Holding Pattern Based on MILP. pages 1–10, 2017. doi: 10.13009/EUCASS2017-137.

[43] Man Liang. Aircraft Route Network Optimization in Terminal Maneuvering Area. 2018.

[44] Man Liang, Daniel Delahaye, and Pierre Marechal. A Framework of Point Merge-based Autonomous System for Optimizing Aircraft Scheduling in Busy TMA To cite this version. (December): 1–8, 2015. ISSN 07701268.

[45] Mohammad Mesgarpour, Chris N Potts, and Julia A Bennell. Models for aircraft landing optimization. *Proceedings of the 4th international conference on research in air transportation (ICRAT2010)*, pages 1–4, 2010.

[46] Ministerie van Infrastructuur en Milieu. Luchtruimvisie - Bijlagerapprot 1 - Huidige inrichting en beheer van het Nederlandse luchtruim. Bijlagerap, 2012.

[47] Ministerie van Infrastructuur en Milieu and Ministerie van Defensie. Luchtruimvisie. 2012.

[48] E Mooij and Z Papp. Simulation , Verification and Validation. Lecture Notes. Technical Report February, 2015.

[49] National Air Traffic Services (NATS). United Kingdom Aeronautical Information Service, 2018. URL http://www.nats-uk.ead-it.com/public/index.php{%}3Foption=com{_}content{&}task=blogcategory{&}id=92{&}Itemid=141.html.

[50] Richard De Neufville and Amedeo R. Odoni. *Airport Systems. Planning, Design, and Management*. 2013. ISBN 978-0071770583.

[51] Doris Novak, Tino Bucak, and Tomislav Radišić. Development, design and flight test evaluation of continuous descent approach procedure in fir zagreb. *Promet - Traffic - Traffico*, 21(5):319–329, 2009. ISSN 03535320.

[52] Office of Civil Aviation. Aeronautical Information Publication Republic of Korea, 2018. URL http://aim.koca.go.kr/eaipPub/Package/2017-06-08/html/eAIP/KR-AD-2.RKSI-en-GB.html.

[53] Jérémy Omer. A space-discretized mixed-integer linear model for air-conflict resolution with speed and heading maneuvers. *Computers and Operations Research*, 58:75–86, 2015. ISSN 03050548. doi: 10.1016/j.cor.2014.12.012. URL http://dx.doi.org/10.1016/j.cor.2014.12.012.

[54] H Pinol and J E Beasley. Scatter Search and Bionomic Algorithms for the aircraft landing problem. *European Journal of Operational Research*, 171(2):439–462, 2006. ISSN 03772217. doi: 10.1016/j.ejor.2004.09.040.

[55] G.J.J. Ruijgrok. *Elements of Aviation Acoustics*. 1993. ISBN 90-6275-899-1.

[56] Schiphol Group. Gebruiksprognose 2018. (november 2017), 2017. URL http://mijksenaar.com/projects-quicktour/16-amsterdam-airport-schiphol.html.

[57] R Sopjes, P.M.A. de Jong, C Borst, and M.M. van Paassen. Continuous Descent Approaches with Variable Flight-Path Angles under Time Constraints. (August), 2011. doi: 10.2514/6.2011-6219.

[58] H. Van Der Plas and H. G. Visser. Trajectory optimisation of an aerobatic air race. *Aeronautical Journal*, 113(1139):1–8, 2009. ISSN 00019240. doi: 10.1017/S0001924000002724.

[59] H G Visser. Terminal area traffic management. *Progress in Aerospace Sciences*, 28:323–368, 1992.